

2-25-2016 12:00 AM

## Enhanced Solar Photocatalytic Hydrogen Generation and Water Treatment Using Hetero-Structure Photocatalysts

Ghodsieh Malekshoar, *The University of western ontario*

Supervisor: Dr. Ajay Ray, *The University of Western Ontario*

A thesis submitted in partial fulfillment of the requirements for the Doctor of Philosophy degree  
in Chemical and Biochemical Engineering

© Ghodsieh Malekshoar 2016

Follow this and additional works at: <https://ir.lib.uwo.ca/etd>

 Part of the [Catalysis and Reaction Engineering Commons](#)

---

### Recommended Citation

Malekshoar, Ghodsieh, "Enhanced Solar Photocatalytic Hydrogen Generation and Water Treatment Using Hetero-Structure Photocatalysts" (2016). *Electronic Thesis and Dissertation Repository*. 3518.  
<https://ir.lib.uwo.ca/etd/3518>

This Dissertation/Thesis is brought to you for free and open access by Scholarship@Western. It has been accepted for inclusion in Electronic Thesis and Dissertation Repository by an authorized administrator of Scholarship@Western. For more information, please contact [wlsadmin@uwo.ca](mailto:wlsadmin@uwo.ca).

## Abstract

Among different approaches to overcome current environmental concerns, heterogeneous photocatalysis is recognized as a promising one. While there are various applications of photocatalysis including water splitting and water treatment, the overall efficiency of this process is still fairly low due to the two dominant drawbacks of current semiconductors, namely wide band gap and fast recombination of photo-generated charges, which restrict the photocatalytic reactions. Designing a hybrid photocatalyst composed of semiconductor hetero-junctions is a viable approach to address these challenges.

The objective of this research project is developing efficient photocatalysts via simple and practical synthesis methods in order to enhance the solar photocatalytic water splitting and water treatment. In this regard, hetero-structure photocatalysts from various groups are synthesized and characterized. Furthermore, the performance of such photocatalysts for photocatalytic reactions are evaluated and compared with single semiconductors.

The experiments presented in this study use solar simulator as the light source. Platinum is loaded on  $\text{TiO}_2$  photocatalyst by solar photo-deposition method.  $\text{Pt/TiO}_2$  as a metal-semiconductor hetero-structure is used for sacrificial photocatalytic hydrogen generation and Formaldehyde acts as sacrificial agent. The performance of the Pt loaded  $\text{TiO}_2$  is shown to be superior to that of the pure  $\text{TiO}_2$ . Furthermore, a detailed parametric study is carried out on photocatalytic hydrogen generation using  $\text{Pt/TiO}_2$  and formaldehyde and it is shown that the solution pH, platinum content (wt %) on  $\text{TiO}_2$ , catalyst concentration, light intensity, and initial formaldehyde concentration all affect the process.

In order to study the performance of a noble metal-free co-catalyst-semiconductor hetero-structure for photocatalytic hydrogen generation, molybdenum sulfide is grown on  $\text{TiO}_2$  by applying the in-situ solar photo-deposition method in a dye-sensitized photocatalytic system. It is observed that the presence of molybdenum sulfide in the system improves the solar photocatalytic hydrogen generation. A systematic statistical analysis is performed to investigate the effect of different reaction parameters as well as their interaction effects and to maximize the hydrogen generation under solar light irradiation.

Graphene-based  $\text{TiO}_2$  and  $\text{ZnO}$  are synthesized by hydrothermal method and their performances for photocatalytic water treatment are studied. Optical and structural properties of the composites are obtained using XRD, XPS, Raman spectroscopy, UV-vis spectroscopy, TEM, and SEM. Due to the beneficial effects of graphene, using the two composites results in better degradation of photocatalytic phenol. The parametric study for optimizing the reaction conditions is also presented.

The study conducted in this research thesis establishes that the efficiency of solar photocatalytic is greatly enhanced by using a hybrid photocatalyst, since such photocatalyst can significantly suppress the recombination of photo-generated charge carries and absorb the wider range of solar light

## Keywords

Heterogeneous photocatalysis, water splitting, water treatment, solar, hydrogen, hetero-structure, co-catalyst

## Co-Authorship Statement

The following thesis contains materials that are published, or in preparation for publication in technical journals as listed below.

**Chapter 3:** Sacrificial Hydrogen Generation from Formaldehyde with Pt/TiO<sub>2</sub> Photocatalyst in Solar Radiation.

A version of this chapter was published as:” Chowdhury, P.\*; **Malekshoar, G.\***; Ray, M. B.; Zhu, J.; Ray, A. K. Sacrificial Hydrogen Generation from Formaldehyde with Pt/TiO<sub>2</sub> Photocatalyst in Solar Radiation. *Ind. Eng. Chem. Res.* **2013**, 52 (14), 5023.”

\* First and second authors contributed equally to this paper

Experimental work, data analysis and writing of the manuscript were done by Ghodsieh Malekshoar and Pankaj Chowdhury under the supervision of Dr. M.B. Ray, Dr. J.Zhu and Dr. A.K. Ray. The written manuscript was reviewed and revised by Dr. M.B. Ray and Dr. A.K. Ray.

**Chapter 4:** In-situ Grown Molybdenum Sulfide on TiO<sub>2</sub> for Solar Photocatalytic Hydrogen Generation.

An article based on this chapter was submitted to Chemical Engineering Science.

Experimental work, data analysis and writing of the manuscript were done by Ghodsieh Malekshoar under the supervision of Dr. A. K. Ray. The written manuscript was reviewed and revised by Dr. A. K. Ray.

**Chapter 5:** Enhanced Solar Photocatalytic Degradation of Phenol with Coupled Graphene-Based Titanium Dioxide and Zinc Oxide.

A version of this chapter was published as:”**Malekshoar, G.**; Pal, K.; He, Q.; Yu, A.; Ray, A. K. Enhanced Solar Photocatalytic Degradation of Phenol with Coupled Graphene-Based Titanium Dioxide and Zinc Oxide. *Ind. Eng. Chem. Res.* **2014**, 53, 18824.”

Experimental work, data analysis and writing of the manuscript were done by Ghodsieh Malekshoar. Some of the experiments were performed by K. Pal under the supervision of the first author. Dr. Q. He, Dr. A.Yu, and Dr. A. K. reviewed and revised the written manuscript.

## Acknowledgments

First, I would like to express my sincere gratitude to my supervisor Dr. Ajay K. Ray for his technical support, insightful guidance and encouragement during my research. His persistent understanding, kindness and patience are highly appreciated. I am greatly privileged to have this opportunity to work with him.

My appreciation also goes to Dr. Mita Ray and Dr. Jesse Zhu for the technical and financial support during OCE project. I am also grateful to Dr. Aiping Yu from University of Waterloo for her help and advice in part of my research.

I would like to thank my current and former friends and colleagues: Naeimeh, Noshin, Gloria, Manoli, Malini, and Nil for all the discussions, exchanges of knowledge and skills, and for all the fun we have had in the last four years. In particular, I am grateful to Pankaj, Sophia and Ferdinando for their invaluable advice and guidance.

I would like to extend my thanks to technical staffs: Fate Hashem, Pastor Solano, Jose Munoz, Souheil Afara, and Ying Zhang who were always ready to offer technical assistance during my experimental work.

Special thanks to my dear friends: Mahta, Mahdiyeh, Fatemeh, and Nasrin for their support, encouragements and all the pleasurable moments that they have made for me.

I doubt that I will ever be able to fully convey my appreciation to my parents for their unconditional support, patience, and love, without which I would not have been able to succeed. I thank you for being beside me through my entire life. I am also grateful to my parents-in-law for their care and encouragement. I am fortunate to have you all in my life.

Finally, my deepest appreciation and sincere gratitude are extended to my husband, Mohammad, for his endless love, support, kindness and encouragement in all the time that we have been together.

## Dedication

To my beloved parents,

To my dear husband and little baby,

Mohammad and Narges!

# Table of Contents

Abstract .....	i
Co-Authorship Statement.....	iii
Acknowledgments.....	v
Dedication .....	vi
Table of Contents .....	vii
List of Tables .....	xi
List of Figures .....	xii
Nomenclature .....	xv
Chapter 1 .....	1
1 Introduction .....	1
1.1 Background & Motivation .....	1
1.2 Thesis Objective.....	5
1.3 Thesis structure .....	6
1.4 References.....	8
Chapter 2.....	11
2 Literature Review .....	11
2.1 Introduction.....	11
2.2 Photocatalysis: Fundamentals.....	11
2.3 Principles of Photocatalytic Water Splitting.....	14
2.3.1 Co-catalyst .....	16
2.3.2 Sacrificial agent .....	17
2.4 Principles of Photocatalytic Water Treatment .....	17
2.5 Properties of Photocatalyst .....	19



2.5.1	Proper band gap .....	19
2.5.2	Efficient charge carrier transfer and electron conductivity.....	20
2.5.3	Stability .....	20
2.5.4	Surface active sites.....	21
2.6	Hetero-structure photocatalysts .....	21
2.6.1	Metal–semiconductor.....	22
2.6.2	Noble metal-free co-catalysts- semiconductor.....	23
2.6.3	Heterojunctions on 2-D nanomaterials .....	24
2.6.4	Semiconductor-semiconductor .....	25
2.7	References .....	27
Chapter 3	.....	38
3	Sacrificial Hydrogen Generation from formaldehyde with Pt/ TiO <sub>2</sub> Photocatalyst in Solar Radiation.....	38
3.1	Introduction.....	38
3.2	Materials and Methods.....	40
3.2.1	Photocatalyst Preparation.....	40
3.2.2	Photocatalyst Characterizations .....	40
3.2.3	Photocatalytic Reaction .....	41
3.3	Results and Discussion .....	42
3.3.1	Characterization .....	42
3.3.2	Effect of platinum deposition on the photocatalytic activity of TiO <sub>2</sub> .....	44
3.3.3	Effect of catalyst concentration .....	46
3.3.4	Effect of initial pH of formaldehyde solution.....	47
3.3.5	Effect of initial concentration of formaldehyde.....	49
3.3.6	Effect of light intensity .....	51
3.4	Stability of Pt/ TiO <sub>2</sub> Photocatalyst for H <sub>2</sub> Generation .....	52

3.5 Reaction Mechanism.....	52
3.6 Apparent Quantum Yield.....	54
3.7 Conclusion .....	54
3.8 References.....	55
Chapter 4.....	61
4 In-situ Grown Molybdenum Sulfide on TiO <sub>2</sub> for Solar Photocatalytic Hydrogen Generation .....	61
4.1 Introduction.....	61
4.2 Materials and Methods.....	63
4.2.1 Photocatalyst Preparation.....	63
4.2.2 Photocatalyst Characterizations .....	64
4.2.3 Photocatalytic Reaction .....	64
4.2.4 Experimental Design and Statistical Analysis .....	65
4.3 Results and Discussion .....	66
4.3.1 Characterization .....	66
4.3.2 Photocatalytic Performance of TiO <sub>2</sub> -MoS <sub>x</sub> -EY-TEOA reaction system .	69
4.3.3 Statistical Analysis.....	71
4.4 Mechanism.....	83
4.5 Apparent Quantum Yield.....	85
4.6 Conclusion .....	86
4.7 References.....	87
Chapter 5.....	92
5 Enhanced Solar Photocatalytic Degradation of Phenol with Coupled Graphene-based Titanium Dioxide and Zinc Oxide .....	92
5.1 Introduction.....	92
5.2 Materials and Methods.....	95
5.2.1 Photocatalyst Preparation.....	95

5.2.2 Photocatalyst Characterizations .....	95
5.2.3 Photocatalytic Reaction .....	96
5.3 Results and Discussion .....	97
5.3.1 Characterization .....	97
5.3.2 Photocatalytic Performance .....	103
5.3.3 Parametric Study .....	106
5.4 Conclusion .....	112
5.5 References .....	113
Chapter 6 .....	119
6 Conclusions and Recommendations .....	119
6.1 Major Conclusions .....	120
6.2 Recommendations .....	121
6.3 References .....	122
Appendices .....	123
Curriculum Vitae .....	125

## List of Tables

Table 2.1 Aqueous organic pollutants mineralized by photocatalysis.....	18
Table 3.1 Effect of Pt deposition on TiO <sub>2</sub> P25 under full solar light (UV+visible) .....	46
Table 4.1 Independent variables and their levels chosen for full factorial design.....	65
Table 4.2 Full factorial design matrix for four factors.....	72
Table 4.3 ANOVA for the proposed model (Full Factorial) .....	73
Table 4.4 Experimental design of the steepest ascent and the results .....	78
Table 4.5 Independent variables and their levels chosen for central composite design .....	78
Table 4.6 CCD matrix for two factors and the corresponding responses .....	79
Table 4.7 ANOVA for Quadratic Model (CCD) .....	80
Table 5.1 The peak area (A) ratios of the oxygen-containing bonds to the CC bonds of the TiO <sub>2</sub> -G and ZnO-G samples reduced by hydrothermal method. ....	101

## List of Figures

Figure 1.1 Global energy systems transition.....	2
Figure 2.1 Materials Band Structure .....	11
Figure 2.2 Different pathways for photo-generated charges .....	13
Figure 2.3 Fujishima's Photoelectrochemical cell (PEC).....	14
Figure 2.4 Types of photocatalytic reactions .....	15
Figure 2.5 Band positions of some semiconductors. ....	16
Figure 2.6 (a) Schottky junction with energy level alignment and (b) electron transfer across the metal–semiconductor junction. ....	22
Figure 3.1 XRD for TiO <sub>2</sub> and Pt/TiO <sub>2</sub> photocatalysts .....	42
Figure 3.2 DRS for TiO <sub>2</sub> and Pt/TiO <sub>2</sub> photocatalysts .....	43
Figure 3.3 TEM image of Pt/TiO <sub>2</sub> photocatalyst .....	44
Figure 3.4 Effect of platinum weight percent on TiO <sub>2</sub> on hydrogen generation rate. Experimental conditions: [HCHO] = 0.1332 M, pH 6.7, [TiO <sub>2</sub> /Pt] = 1 g L <sup>-1</sup> , I <sub>Solar</sub> = 100 mW cm <sup>-2</sup> , N <sub>2</sub> saturated, pre-sonicated). ....	45
Figure 3.5 Effect of catalyst concentration on the rate of hydrogen generation and rate per unit mass of catalyst. Experimental conditions: [HCHO] = 0.1332 M, pH 6.7, Pt (on TiO <sub>2</sub> ) = 0.25%, I <sub>Solar</sub> = 100 mW cm <sup>-2</sup> , N <sub>2</sub> saturated, pre-sonicated.....	47
Figure 3.6 Photocatalytic reaction of formaldehyde on Pt/TiO <sub>2</sub> surface .....	48

Figure 3.7 Effect of initial pH of formaldehyde solution on the rate of hydrogen generation. Experimental conditions: [HCHO] = 0.1332 M, [Pt/ TiO <sub>2</sub> (0.25%)] = 1 g L <sup>-1</sup> , I <sub>Solar</sub> = 100 mW cm <sup>-2</sup> , N <sub>2</sub> saturated, pre-sonicated).	49
Figure 3.8 Effect of initial concentration of formaldehyde on the rate of hydrogen generation. Experimental conditions: pH 6.7-7.2, [Pt/TiO <sub>2</sub> ] = 1 g L <sup>-1</sup> , I <sub>Solar</sub> = 100 mW cm <sup>-2</sup> , N <sub>2</sub> saturated, pre-sonicated.	50
Figure 3.9 Effect of light intensity on the rate of hydrogen generation. Experimental conditions: [HCHO] = 0.1332 M, pH 6.7, [Pt/ TiO <sub>2</sub> (0.25%)] = 1 g L <sup>-1</sup> , I <sub>Solar</sub> = 100 mW cm <sup>-2</sup> , N <sub>2</sub> saturated, pre-sonicated).	51
Figure 3.10 Short term performance analysis for Pt/TiO <sub>2</sub> photocatalyst in repeated uses. Experimental conditions: [HCHO] = 0.1332 M, pH 6.7, [TiO <sub>2</sub> /Pt (0.25%)] = 1 g L <sup>-1</sup> , I <sub>Solar</sub> = 100 mW cm <sup>-2</sup> , N <sub>2</sub> saturated, pre-sonicated).	52
Figure 4.1 XRD Patterns of TiO <sub>2</sub> and TiO <sub>2</sub> -MoS <sub>x</sub> .	67
Figure 4.2 XPS Spectrum of TiO <sub>2</sub> -MoS <sub>x</sub> (a), High resolution XPS spectra of Mo (b) and S 2p (c).	68
Figure 4.3 UV- Vis absorption spectra of TiO <sub>2</sub> and TiO <sub>2</sub> -MoS <sub>x</sub> .	69
Figure 4.4 Time course of hydrogen generation from (a) four components system:TiO <sub>2</sub> (100 mg), EY(7.8× 10 <sup>-4</sup> M), TEOA( 10 v%), (NH <sub>4</sub> ) <sub>2</sub> MoS <sub>4</sub> (2.27× 10 <sup>-4</sup> M),I <sub>Solar</sub> =100 mW/cm <sup>2</sup> (b) without EY , (c) without (NH <sub>4</sub> ) <sub>2</sub> MoS <sub>4</sub> , (d) without EY and (NH <sub>4</sub> ) <sub>2</sub> MoS <sub>4</sub> , (e) without TEOA, (f) Recovered TiO <sub>2</sub> -MoS <sub>x</sub> obtained by in situ photo-deposition	70
Figure 4.5 Pareto Chart for full factorial design	74
Figure 4.6 Predicted vs. Actual square root values of response (H <sub>2</sub> : μmol/g <sub>cat</sub> ).	75
Figure 4.7 Normal probability plot of the studentized residuals	76
Figure 4.8 Box-Cox plot for power transform	77
Figure 4.9 Predicted vs. Actual values of response for CCD (H <sub>2</sub> : μmol/g <sub>cat</sub> ).	81

Figure 4.10 Normal probability plot of the studentized residuals (CCD).....	82
Figure 4.11 Response Surface and Contour plot of the quadratic model .....	84
Figure 4.12 Proposed mechanism for H <sub>2</sub> generation in an in-situ photo-deposition method to grow MoS <sub>x</sub> as a co-catalyst.....	85
Figure 5.1 XRD patterns of (a) GO, (b) TiO <sub>2</sub> , (c) TiO <sub>2</sub> -G, (d) ZnO and (e) ZnO-G.....	97
Figure 5.2 (A) Absorbance spectra, (B) Tauc plot for band gap estimation.....	99
Figure 5.3 High-resolution XPS spectra of C 1s for (a) ZnO-G, (b) TiO <sub>2</sub> -G, (c) GO .....	100
Figure 5.4 Raman Spectra of (A) TiO <sub>2</sub> -G (a), GO (b) and ZnO-G (c), (B) TiO <sub>2</sub> -G, (C) ZnO-G .....	102
Figure 5.5 SEM images for ZnO-G, TiO <sub>2</sub> -G (a, c), TEM images for ZnO-G, TiO <sub>2</sub> -G (b, d). .....	103
Figure 5.6 Photocatalytic degradation of phenol using different photocatalysts. Experimental conditions: [photocatalyst] = 1 g/L, [phenol] = 40 ppm, I <sub>solar</sub> = 100 mW/cm <sup>2</sup> , pH = 7, O <sub>2</sub> saturated. ....	104
Figure 5.7 Phenol degradation rate constants using coupled system at different weight ratio Experimental conditions: [photocatalyst] = 1 g/L, [phenol] = 40 ppm, I <sub>solar</sub> = 100 mW/cm <sup>2</sup> , pH = 7, O <sub>2</sub> saturated.....	105
Figure 5.8 Effect of catalyst loading .....	107
Figure 5.9 Effect of initial concentration of phenol. Experimental conditions: [ZnO-G/TiO <sub>2</sub> -G] = 1.25 g/L, [phenol] = 20-100 ppm, I <sub>solar</sub> = 100 mW/cm <sup>2</sup> , pH = 7, O <sub>2</sub> saturated.....	108
Figure 5.10 Effect of solution pH on degradation rate of phenol. Experimental conditions: [ZnO-G/TiO <sub>2</sub> -G] = 1.25 g/L, [phenol] = 40 ppm, I <sub>solar</sub> = 100 mW/cm <sup>2</sup> , O <sub>2</sub> saturated. ....	110
Figure 5.11 Apparent degradation rate constant at different light intensities.....	111

## Nomenclature

$C_0$	initial concentration (ppm)
$C$	concentration at time $t$ (ppm)
$e^-$	electron
EY	Eosin Y dye
$EY^+$	oxidized form of Eosin Y dye
GO	graphene Oxide
G	graphene
$h^+$	hole
$I_{\text{Solar}}$	intensity of solar light ( $\text{mWcm}^{-2}$ )
$k$	reaction rate constant ( $\text{mol min}^{-1}$ )
$k(I)$	kinetic rate constant as a function of light intensity ( $\text{mol min}^{-1}$ )
$K$	adsorption constant ( $\text{M}^{-1}$ )
$\text{OH}^\bullet$	hydroxyl radical
$\text{pH}_{\text{PZC}}$	point of zero charge
$r_1$	rate of degradation per unit volume of the reaction liquid ( $\text{mg/L}\cdot\text{min}$ )
$r_2$	rate of degradation per unit mass of the catalyst ( $\text{mg/g}_{\text{cat}}\cdot\text{min}$ )
TEOA	triethanolamine

### *Greek letters*

$\lambda$	wavelength of radiation (nm)
-----------	------------------------------



$\phi_{H_2}$                       apparent quantum yield for hydrogen generation

$\Delta G$                         change in Gibb's free energy

$\Delta H$                         change in enthalpy

*Abbreviations*

AOP                        advanced oxidation process

ANOVA                    analysis of variance

CB                         conduction band

CCD                        central composite design

DRS                        diffuse reflectance spectra

GHG                        green house gas

GC                         gas chromatography

LOF                        Lack of fit

PEC                        photoelectrochemical cell

VB                         valence band

XRD                        x-ray diffraction

XPS                        x-ray photoelectron spectroscopy

## Chapter 1

### 1 Introduction

#### 1.1 Background & Motivation

Growing energy demand, reducing conventional energy resources along with increasing environmental pollution and climate change are the world main challenges and concerns that make the use of renewable energy resources more imperative.<sup>1</sup> Due to the world population growth, the expected energy demand is increased, which causes the higher rate of fossil fuels consumption than the rate of their production.<sup>1</sup> The global energy consumption is predicted to be increased by more than 50% until 2030.<sup>2</sup> Therefore, incorporation of alternative fuels is strongly required to overcome the energy shortage in near future.

In addition, the pollution and emission rise in the environment by conventional use of energy is another challenge, which the world has difficulty to conquer with. Despite Canada's continuous endeavour to lower its greenhouse gas (GHG) emissions, the oil and gas economic sector accounted for the largest contribution of GHG emissions in 2012. Since 2005, GHG emissions from the oil and gas sector have increased from 159 Mt to 173 Mt in 2012.<sup>3</sup> Therefore, it is of great interest and demand to search for alternative sources of energy, which are clean and renewable.

Hydrogen is known as the simplest, lightest and the most abundant element in the universe and it has captured the world's attention as an energy carrier.<sup>4</sup> It helps the current transition from the limited non-renewable energy sources to unlimited renewable sources. Moreover, hydrogen plays an essential role in the "decarbonisation" of the global energy system. A view of energy history represents that there has been slow shift in energy from solids to liquids to gases as shown in Figure 1.1.<sup>4</sup> Likewise, this move involves the process of "decarbonisation", meaning that the ratio of hydrogen (H) to carbon(C) in the molecule of each new source has increased. In this trend, which favours hydrogen atom over carbon, hydrogen will be the next logical fuel.<sup>4</sup> It is clean, abundant,

the lightest fuel and richest in energy per unit mass.<sup>1</sup> Owing to these properties it is known as a viable source of energy for future.

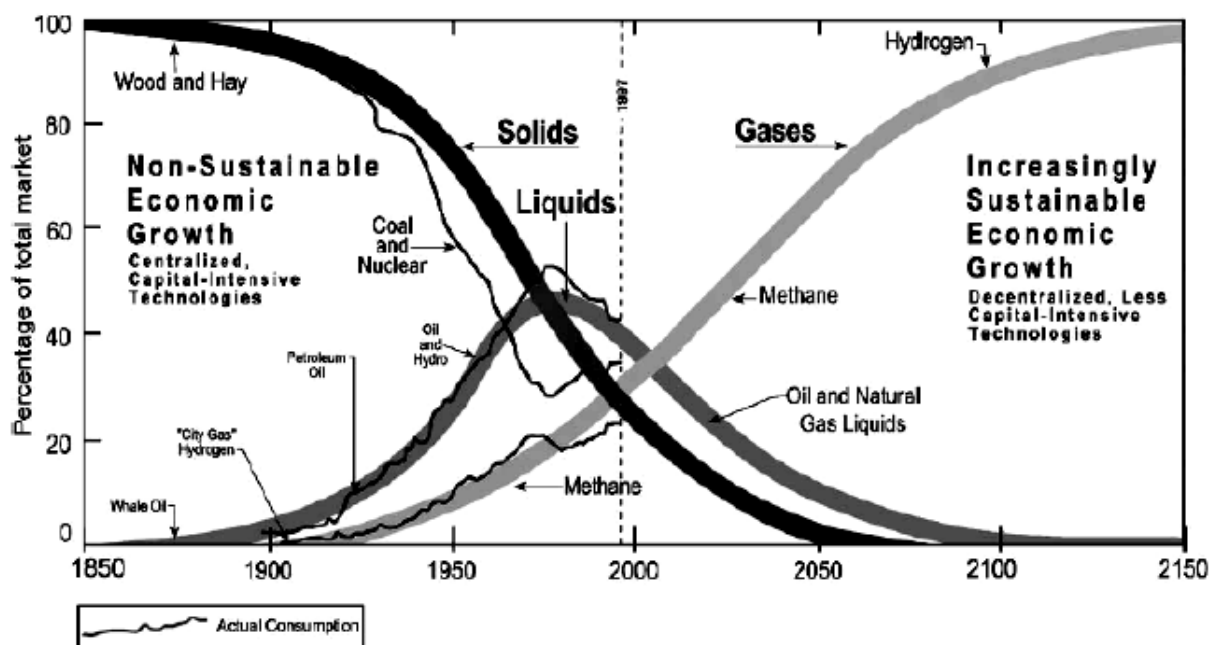


Figure 1.1 Global energy systems transition.<sup>4</sup>

In general, hydrogen can be produced from fossil resources such as natural gas and coal or renewable resources such as water and biomass with application of renewable energy resources such as solar and wind energy.<sup>5</sup> Natural gas reforming, gasification of coal, water electrolysis, biomass gasification, photoelectrolysis and photocatalysis are known processes to produce hydrogen.<sup>2</sup>

Currently, global hydrogen production is extensively based on fossil fuels. Steam reforming of natural gas is the most common and least expensive method to produce hydrogen; however, it has a great contribution in the greenhouse gas emissions.<sup>4</sup> Electrolysis is cost effective for production of extremely pure hydrogen in small scale and it is expensive at large scale. Solar and wind power based electrolysis are less expensive than the conventional process; however, they are still in developing stage.<sup>4</sup> Considering all the environmental and economical aspects, photocatalytic water splitting from renewable water and solar energy is the most promising approach for hydrogen

generation. Solar energy is certainly the most abundant source of energy. The amount of solar irradiation receiving by earth surface is  $3 \times 10^{24}$  J/year, which is  $10^4$  times higher than annual world consumption rate.<sup>6</sup> However, its current contribution in the global energy production is less than 1%. Hence, great efforts are required to use the substantial potential of this renewable energy resource in order to fulfill unlimited future global energy demands.

The first demonstration of water splitting in a photo-electrochemical system was reported by Fujishima and Honda<sup>7</sup> in the early 70's. It was shown that photo-generated charge-carriers (electron and hole) on  $\text{TiO}_2$  and Pt electrode were able to split water into oxygen and hydrogen gas. After that semiconductor photocatalysis was introduced by Bard<sup>8</sup>, since then, the interest in photocatalysis has grown significantly and various applications for that including air purification, disinfection, self-cleaning, and more importantly water treatment and water splitting have been found and studied.<sup>9-13</sup>

Water treatment was mentioned as one of the important applications of heterogeneous photocatalysis. Although, the access to the safe drinking water is a high priority issue for the life of human being, water resources are continuously contaminated due to population growth, over-use and wastage. According to The World Health Organization (WHO), many people are forced to rely on microbiologically unsafe sources of water, which significantly increase the risk of waterborne disease including typhoid, hepatitis and cholera.<sup>13</sup> The water contaminations include both organic and inorganic compounds. The most common organic water pollutants are herbicides, pesticides, textile dye, alcohols, carboxylic acids, aromatic compounds, detergent, and surfactants and compounds like heavy metals, mercury, nickel and silver are considering as inorganic water pollutants.<sup>14,15</sup>

Therefore, the removal of harmful compounds from wastewater and detoxification of pollutants in surface water and ground water is a challenging issue in the world. In order to meet the regulations for water contamination, Advanced Oxidation Processes (AOPs) including  $\text{O}_3/\text{UV}$ ,  $\text{H}_2\text{O}_2/\text{UV}$ ,  $\text{O}_3/\text{H}_2\text{O}_2/\text{UV}$  and photocatalysis (semiconductor/UV) have

emerged to remove those compounds that cannot be effectively treated by conventional methods.<sup>16–18</sup>

Photocatalysis can be carried out under ambient condition, the oxidant is strong enough for complete mineralization, and the photocatalysts are less expensive, non-hazardous and reusable.<sup>19</sup> Owing to these properties, photocatalysis has recently received great attention as a promising alternative for pollutant degradation. However, it is quite imperative to replace the commercial UV lamps with renewable solar energy in order to make this technology economically more viable.

Herein, the main focus is on two main applications of heterogeneous photocatalysis; solar photocatalytic water splitting and water treatment. Heterogeneous photocatalysis relies on a class of materials known as semiconductors due to their particular electronic structure. Their structure comprises of a filled valence band (VB) and an empty conduction band (CB). When a photon strikes the semiconductor with energy equal or greater than the semiconductor's band gap ( $E_g$ ), an electron ( $e^-$ ) is excited from the valence band into the conduction band, leaving a hole ( $h^+$ ) in the valence band.<sup>11</sup> These photo-generated charges will initiate the redox reaction with adsorbed species. The electron is involved in a reduction process, while the hole will act as an oxidizer in an oxidation process.

The photo-activity of the semiconductor is majorly determined by the future fate of the photo-generated electron and hole. If the charges are able to migrate separately to the surface of the semiconductor, then they can interact with the surface species. However, the excited charges often have strong tendency to recombine and generate heat, which restricts the photocatalytic reactions resulting in low efficiency of the process. In addition, commonly used semiconductors possess wide band gap, which limit their application to the narrow wavelength range of solar spectrum (UV range). The UV light wavelength range corresponds to only 4-5% of full solar spectrum, while visible light wavelength range covers about 46% of that.<sup>20</sup> Hence, to combat the aforementioned challenges, the research on modifying the current photocatalysts and on developing efficient material are growing continuously.

Coupling two materials to form a hetero-junction has been recognized to be a viable approach to address the challenges, which make a single semiconductor to be barely efficient for photocatalytic processes. Designing a hybrid photocatalyst made of semiconductor hetero-junctions significantly suppresses the recombination of photo-generated charge carriers and also extends the solar light-response range, leading to substantial enhancement of solar photocatalytic efficiency.<sup>21,22</sup>

Depending on the material compositions that form the hetero-structure photocatalysts, they can be categorized into different groups. Metal-semiconductor, semiconductor on 2-D nanomaterial, semiconductor-semiconductor, noble metal-free co-catalyst-semiconductor are the most widely investigated categories.<sup>21</sup> However, more complex hetero-structures composed of multiple components can also be obtained.

## 1.2 Thesis Objective

The general objective of this thesis is to investigate the merits of different hetero-structure photocatalysts over a single semiconductor for solar photocatalytic reactions. These hetero-structures are including i) metal-semiconductor, ii) semiconductor on 2-D nanomaterial, iii) semiconductor-semiconductor, and iv) noble metal-free co-catalyst-semiconductor. The main focus is on development of efficient photocatalysts that can be used to enhance the photocatalytic water splitting and water treatment under full solar light illumination.

The specific research objectives are:

- 1) To develop and characterize Pt loaded  $\text{TiO}_2$  photocatalyst.
- 2) To employ  $\text{TiO}_2$ -Pt for sacrificial solar hydrogen generation using formaldehyde as electron donor.
- 3) To explore the effect of various operational parameters such as catalyst amount, solution pH, light intensity and formaldehyde concentration on solar hydrogen generation.
- 4) To apply in-situ photo-deposition method in order to synthesis the noble-metal-free co-catalyst (Molybdenum sulfide) grown on  $\text{TiO}_2$  ( $\text{MoS}_x\text{-TiO}_2$ ) and perform the characterization.

- 5) To apply  $\text{MoS}_x$ - $\text{TiO}_2$  as a photocatalyst for solar hydrogen generation in a dye-sensitized reaction system.
- 6) To perform a systematic statistical analysis to investigate the effect of different operational parameters in synthesis procedure of  $\text{MoS}_x$ - $\text{TiO}_2$  and optimize them to maximize in-situ solar hydrogen generation.
- 7) To synthesis and characterize graphene based semiconductors ( $\text{TiO}_2$ -G and  $\text{ZnO}$ -G).
- 8) To employ  $\text{TiO}_2$ -G and  $\text{ZnO}$ -G for solar photo-degradation of phenol as water pollutant model compound and compare the developed hetero-structure photocatalysts with single semiconductors ( $\text{TiO}_2$  and  $\text{ZnO}$ ).
- 9) To perform the parametric study in order to understand the effect of various operational parameters such as catalyst amount, solution pH, light intensity and phenol concentration on solar photo- degradation of phenol.

### 1.3 Thesis structure

This thesis is written in an article-integrated format as specified by the School of Graduate and Postdoctoral studies of the University of Western Ontario. It is composed of 6 chapters.

Chapter 1 provides a brief introduction and background for photocatalytic process as well as the goal and scope of the research for this thesis

Chapter 2 is a brief overview of the fundamentals of photocatalytic processes, in particular, photocatalytic water splitting and water treatment. The advances in hetero-structure photocatalysts is discussed in detail focusing on main categories: metal-semiconductor, semiconductor-semiconductor, semiconductor on 2-D nanomaterial, and noble metal-free co-catalyst- semiconductor.

Chapter 3 is a research article entitled “Sacrificial hydrogen generation from formaldehyde with  $\text{Pt/TiO}_2$  photocatalyst in solar radiation” published in Industrial & Engineering Chemistry Research.  $\text{Pt/TiO}_2$  was developed and characterized and was applied for sacrificial hydrogen generation in full solar light. Formaldehyde was used as

an electron donor. Parametric studies were performed for the platinum content on  $\text{TiO}_2$ , catalyst loading, solution pH, initial formaldehyde concentration, and solar light intensity.  $\text{Pt/TiO}_2$  is an example of metal-semiconductor hetero-structure photocatalyst.

Chapter 4 entitled “In-situ grown molybdenum sulfide on  $\text{TiO}_2$  for solar photocatalytic hydrogen generation”. In this chapter the effect of molybdenum sulfide as a co-catalyst was investigated. Molybdenum sulfide was loaded on  $\text{TiO}_2$  by an in-situ solar photo-deposition method over a dye synthesized photocatalytic process using Eosin Y (EY) as a photo-sensitizer and tri-ethanolamine (TEOA) as an electron donor.  $(\text{NH}_4)_2\text{MoS}_4$  was also used as a precursor. A systematic statistical analysis was applied to explore the impact of various factors and to optimize the photocatalytic hydrogen production. The possible mechanism for the in-situ solar photo-deposition method was also proposed. This chapter shows the benefits of noble metal-free co-catalyst- semiconductor structure.

Chapter 5 is a research article entitled “Enhanced solar photocatalytic degradation of phenol with coupled graphene based titanium dioxide and zinc oxide” published in Industrial & Engineering Chemistry Research. In this chapter Graphene-base semiconductors ( $\text{TiO}_2\text{-G}$ ,  $\text{ZnO-G}$ ) were synthesized and characterized. The photocatalytic activity of the coupled composites was investigated for phenol degradation in full solar light. Parametric studies of catalyst amount, initial phenol concentration, solution pH and light intensity were carried out using coupled  $\text{ZnO-G/TiO}_2\text{-G}$ . The beneficial effect of photocatalysts with the general hetero-structure of semiconductor on 2-D nanomaterial and coupled semiconductors is discussed in this chapter.

Chapter 6 summarizes the key conclusions of this thesis together with suggestions for the future studies.



## 1.4 References

- (1) Jain, I. P. Hydrogen the Fuel for 21st Century. *Int. J. Hydrogen Energy* **2009**, *34* (17), 7368.
- (2) Ball, M.; Wietschel, M. The Future of Hydrogen – Opportunities and Challenges. *Int. J. Hydrogen Energy* **2009**, *34* (2), 615.
- (3) Canada, E. *Canada ' S Emissions Trends*; 2014.
- (4) Dunn, S. Hydrogen Futures: Toward a Sustainable Energy System. *Int. J. Hydrogen Energy* **2002**, *27* (3), 235.
- (5) Guo, L. J.; Zhao, L.; Jing, D. W.; Lu, Y. J.; Yang, H. H.; Bai, B. F.; Zhang, X. M.; Ma, L. J.; Wu, X. M. Solar Hydrogen Production and Its Development in China. *Energy* **2009**, *34* (9), 1073.
- (6) Gratzel, M. Photoelectrochemical Cells. *Nature* **1995**, *414* (6861), 338.
- (7) Fujishima, a; Honda, K. Electrochemical Photolysis of Water at a Semiconductor Electrode. *Nature* **1972**, *238* (5358), 37.
- (8) Allen J.Bard. Photoelectrochemistry and Heterogeneous Photo-Catalysis at Semiconductors. *J. Photochem.* **1979**, *10*, 59.
- (9) Mills, A.; Lee, S. A Web-Based Overview of Semiconductor Photochemistry-Based Current Commercial Applications. *J. Photochem. Photobiol. A Chem.* **2002**, *152*, 233.
- (10) Herrmann, J. Heterogeneous Photocatalysis : Fundamentals and Applications to the Removal of Various Types of Aqueous Pollutants. *Catal. Today* **1999**, *53*, 115.
- (11) Hoffmann, M. R.; Martin, S. T.; Choi, W.; Bahnemannt, D. W. Environmental Applications of Semiconductor Photocatalysis. *Chem. Rev.* **1995**, *95* (1), 69.

- (12) Maeda, K.; Domen, K. Photocatalytic Water Splitting: Recent Progress and Future Challenges. *J. Phys. Chem. Lett.* **2010**, *1* (18), 2655.
- (13) Byrne, J. A.; Fernandez-Ibañez, P. A.; Dunlop, P. S. M.; Alrousan, D. M. A.; Hamilton, J. W. J. Photocatalytic Enhancement for Solar Disinfection of Water: A Review. *International Journal of Photoenergy*. **2011**, 1–12.
- (14) Alfano, O. .; Bahnemann, D.; Cassano, A. .; Dillert, R.; Goslich, R. Photocatalysis in Water Environments Using Artificial and Solar Light. *Catalysis Today*. **2000**, *58*, 199.
- (15) Vidal, A. Developments in Solar Photocatalysis for Water Purification. *Chemosphere* **1998**, *36* (12), 2593.
- (16) Smith, D. W. Advanced Technologies in Water and Wastewater Treatment. *J. Environ. Eng. Sci.* **2002**, *1* (4), 247.
- (17) Li, D.; Qu, J. The Progress of Catalytic Technologies in Water Purification: A Review. *J. Environ. Sci.* **2009**, *21* (6), 713.
- (18) Legrini, O.; Oliveros, E.; Braun, a M. Photochemical Processes for Water Treatment. *Chem. Rev.* **1993**, *93* (2), 671.
- (19) Chong, M. N.; Jin, B.; Chow, C. W. K.; Saint, C. Recent Developments in Photocatalytic Water Treatment Technology: A Review. *Water Res.* **2010**, *44* (10), 2997.
- (20) Gueymard, C. a. The Sun's Total and Spectral Irradiance for Solar Energy Applications and Solar Radiation Models. *Sol. Energy* **2004**, *76* (4), 423.
- (21) Yuan, Y.; Ruan, L.; Barber, J.; Chye, S.; Loo, J.; Xue, C. Hetero-Nanostructured Suspended Photocatalysts for Solar-to-Fuel Conversion. *Energy Environ. Sci.* **2014**, *7*, 3934.

- (22) Liu, G.; Wang, L.; Yang, H. G.; Cheng, H.-M.; (Max) Lu, G. Q. Titania-Based Photocatalysts—crystal Growth, Doping and Heterostructuring. *J. Mater. Chem.* **2010**, 20 (5), 831.

## Chapter 2

### 2 Literature Review

#### 2.1 Introduction

This chapter provides the fundamental aspects of the heterogeneous photocatalysis. The mechanism and the elementary steps of photocatalytic water splitting as well as water treatment are discussed. It presents the challenges of photocatalysis and the possible approaches to overcome these challenges with the main focus on developing hetero-structure materials. It outlines the advances in this particular research area.

#### 2.2 Photocatalysis: Fundamentals

Photocatalysis refers to a set of chemical reactions that are occurred by using a light activated catalyst. Photocatalysts activate upon light absorption and subsequently photo-generated electron and hole are produced, and captured by other species to complete the secondary reactions. Photocatalysts are chosen from a class of material called semiconductors. Semiconductors have a unique energy band structure that is beneficial for photocatalysis.

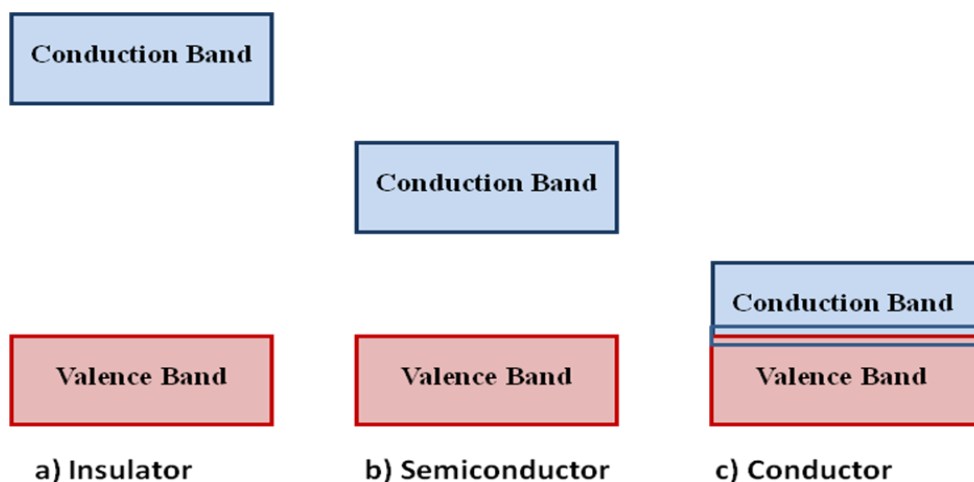


**Figure 2.1** Materials Band Structure

Materials can be classified into three different groups based on their band structure, as shown in Figure 2.1. Conductors are class of material that their conduction band (CB) and the valence band (VB) are overlapped, so electrons can simply move. Insulators have a very large band gap, avoiding electron movement. Electronic band gap is the gap between two energy states where no electron can exist, and is the amount of energy required to excite an electron from the valence band to the conduction band.<sup>1,2</sup>

Semiconductors have relatively small band gap, and they are not conductive as their valence band is filled with electrons and so the electrons are not mobile within the material.<sup>3</sup> However, in presence of external energy source electrons can be excited to the conduction band which was previously empty, thereby provides partial conductivity of the semiconductor. There would be an electron vacancy in the valence band after the electron excitation to the conduction band. This vacancy is referred to an imaginary particle with a positive charge - i.e., a hole.

The process of light absorption and electron-hole generation are the first elementary steps for heterogeneous photocatalytic process to take place. Once these steps are completed, electron-hole pairs as the active charge-carriers must be separated and migrate to an active site for reaction. However, several pathways are possible for the photo-generated charge carriers as shown in figure 2.2. Electrons have a tendency to decrease their potential energy whereas the holes are leaning to increase their potential energy. Therefore, electron and hole pairs are more favoured to recombine rather than to separate.

The charge carrier recombination is unfavourable as it strongly competes with the desired charge carrier separation and transfer process to the surface and thus declines the efficiency of a photocatalytic process.<sup>5</sup> Energy will dissipate in the form of heat (non-radiative) or photon emission (radiative) due to the charge carrier recombination. It is difficult to quantify the amount of non-radiative recombination, but the radiative recombination can be measured with photoluminescence studies.<sup>6</sup> This study is performed to evaluate charge carrier dynamics and to estimate the lifetime of the charge carriers of the photocatalyst.<sup>7</sup>

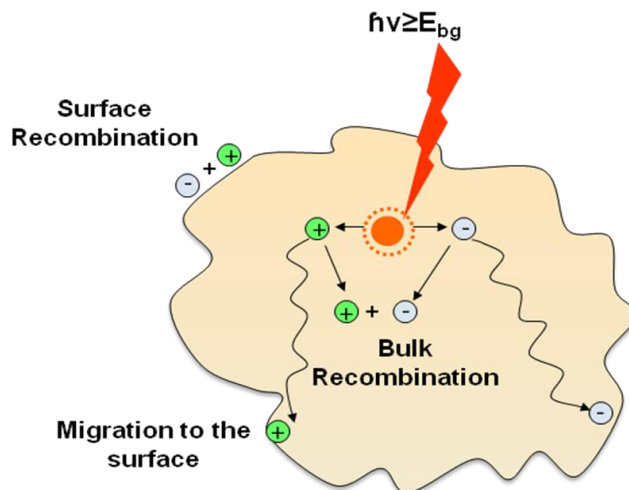


**Figure 2.2** Different pathways for photo-generated charges <sup>4</sup>

Once the migration of the charge carriers to the active sites successfully achieved, the last step of the photocatalysis process, which is redox reactions, will be accomplished. Redox reactions are chemical reactions, in which the oxidation state of an atom is changed.<sup>8</sup> Redox reactions involve two types of electron transfer processes: reduction and oxidation. The important step for the redox reactions to occur is the transfer of the charge carriers between the surface of the photocatalyst and the adsorbed chemical species-i.e., interfacial charge transfer. This charge carrier transfer across the interface strongly depends on the energy level positions of the semiconductor and the adsorbed species. In order to have electron transfer from the conduction band to the acceptor species and the photo-reduction process to occur, the position of conduction band of the semiconductor should be higher than the reduction potential of the acceptor. Similarly, for the hole transfer from the valence band to the donor species and photo-oxidation to take place, the position of the valence band should be lower than the oxidation potential of the adsorbed donor.

In summary, all the steps that can describe the mechanism of the heterogeneous photocatalytic process, are: (i) light absorption and photo-generation of electron and hole pairs, (ii) successful separation and movement of the charge –carriers to the active sites on the surface of the photocatalyst, and (iii) chemical redox reaction with adsorbed species at the surface.

Extensive research on heterogeneous photocatalysis has been conducted for a few decades. Photocatalysis can be applied for different purposes depending on the type of the reactions that are taken place. It can be classified into two main groups: (i) photo-oxidation processes such as pollutant degradation, oxygen evolution, and (ii) photo-reduction processes such as hydrogen production, metal reduction and carbon dioxide reduction.<sup>2</sup>

The main focus of this thesis will be on the two important applications; hydrogen generation via water splitting, and water pollutant degradation. In this chapter, the fundamentals of these two processes will be discussed in detail.

## 2.3 Principles of Photocatalytic Water Splitting

Decomposition of water into hydrogen and oxygen using an electro-chemical cell was first discovered by Fujishima and Honda.<sup>9,10</sup> It was reported that  $\text{TiO}_2$  and platinum can act as anode and cathode electrodes in an electro-chemical cell, as shown in figure 2.3. After UV light illumination, water oxidation and reduction reactions occurred at the  $\text{TiO}_2$  and Pt electrodes, respectively, resulting in oxygen and hydrogen production. Bard later applied this concept to propose a semiconductor-based photocatalytic process.<sup>11</sup> Since then, photocatalytic water splitting has been investigated extensively by different research groups.

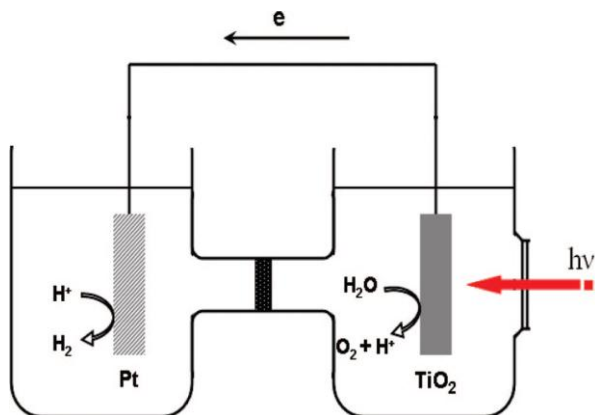
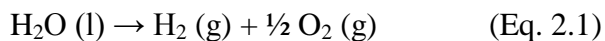


**Figure 2.3** Fujishima's Photoelectrochemical cell (PEC)<sup>9,10</sup>

Water splitting refers to the decomposition of water molecules to hydrogen and oxygen gases, according to Eq. 2.1.



This reaction has a large positive change in the Gibbs free energy ( $\Delta G^\circ = 237$  kJ/mol). Therefore, it is considered as an “uphill” reaction (as shown in Figure 2.4) meaning that this reaction is not spontaneous in nature.<sup>12</sup>

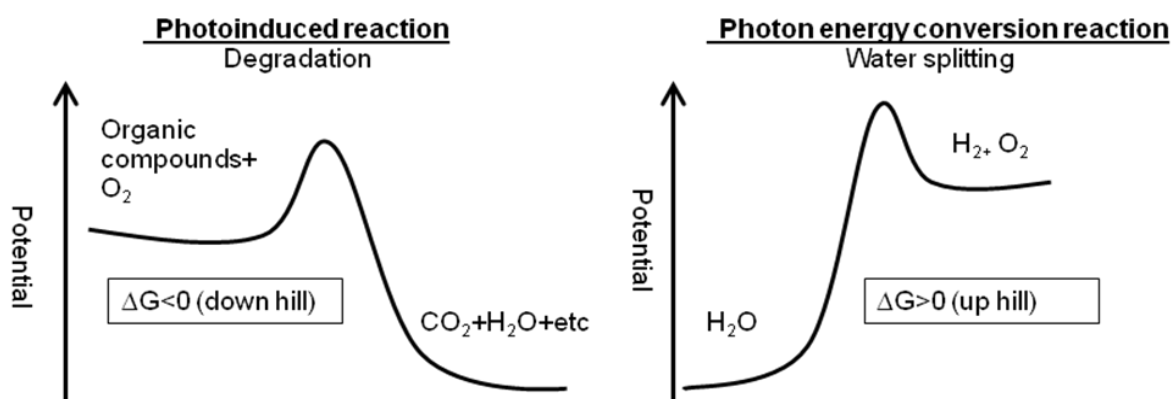


**Figure 2.4** Types of photocatalytic reactions<sup>13,14</sup>

As mentioned before, in a typical band structure of semiconductors the conduction band (CB) and the valence band (VB) are separated by band gap. Photons with higher energy than the band gap are required to excite a semiconductor resulting in generation of electrons and holes. The electrical potential corresponding to the Gibbs free energy change of water splitting is 1.23 eV. Therefore, the equivalent energy to the Gibbs free energy need to be provided by the incident photon's for this non-spontaneous reaction to be done. Therefore, minimum band gap of 1.23 eV is required for overall water splitting, theoretically.<sup>9</sup>

In water splitting, the electron in the CB is used to reduce  $\text{H}^+$  to  $\text{H}_2$ , while the hole in the VB is involved in oxidation reaction to produce oxygen. Another thermodynamic requirement for achieving water splitting is the match of the band gap and the potentials



for the conduction and the valence bands to facilitate both the reduction and the oxidation of  $\text{H}_2\text{O}$ . The bottom level of conduction band has to be more negative than the reduction potential of  $\text{H}^+/\text{H}_2$ , whereas the top level of valence band needs to be more positive than the oxidation potential of  $\text{O}_2/\text{H}_2\text{O}$ .<sup>15</sup> Figure 2.5 depicts the band position of some semiconductors. There are few semiconductors which can provide the band structure requirement for water splitting and their electronic structures match well with redox potential of water. Among them  $\text{TiO}_2$  is the first reported photocatalyst for water splitting and still is considered as the most suitable photocatalyst due to its high activity, chemical inertness, low cost and nontoxicity.<sup>8</sup>

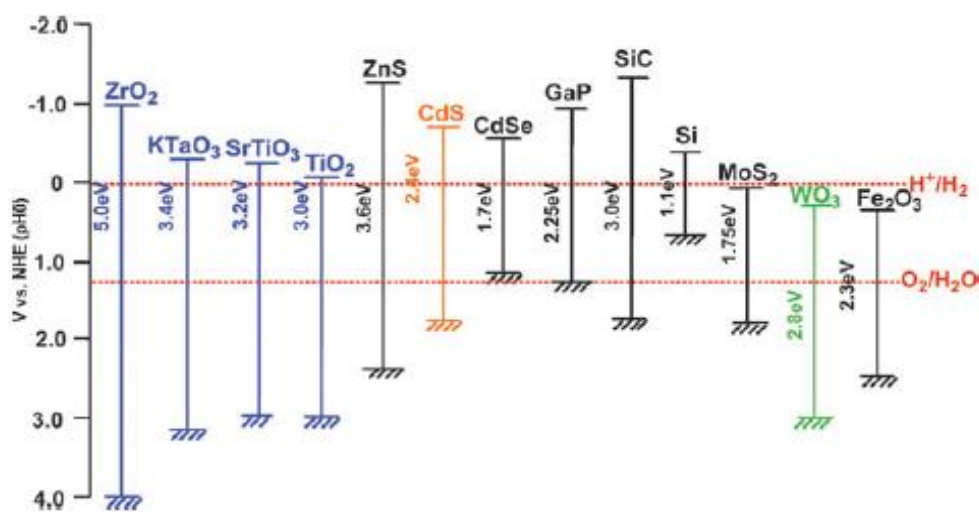


**Figure 2.5** Band positions of some semiconductors.<sup>14</sup>

### 2.3.1 Co-catalyst

In addition to active semiconductors, the presence of other important components is strongly required for efficient photocatalytic water splitting. Co-catalyst is one important element that is mostly incorporated in photocatalysis in order to improve the separation of photo-generated charges. Moreover, co-catalysts generally exhibit smaller over potential compared to semiconductors, facilitating the water oxidation or reduction reaction. Various materials can be chosen as co-catalyst. This concept will be explained more in detail in section 2.6.

### 2.3.2 Sacrificial agent

Adding sacrificial agent to the solution can substantially suppress electron-hole recombination.<sup>9,16</sup> Sacrificial agent (electron donor) reacts irreversibly with the photo-generated holes and/or oxygen, thereby, increasing the rate of hydrogen generation.

Taking into account that water splitting is an uphill reaction, addition of sacrificial agent is needed to increase the efficiency of hydrogen production. Thus, sacrificial agents (electron donors or hole scavengers) are oxidized by photo-generated holes, and water reduction is facilitated by photo-generated electrons in the conduction band. Inorganic compounds such as sulphide ion and organic compounds such as alcohols have been used as electron donors for photocatalytic hydrogen generation. By using organic pollutants as sacrificial agent, bi-functional photocatalytic system can be developed, in which photocatalytic production of hydrogen with simultaneous degradation of organic pollutant is achieved.<sup>16</sup> To date different kinds of model compounds, azo dyes, oxalic acid, formic acid, acetic acid, EDTA, TEA, etc. were used as electron donor to develop the bi-functional photocatalytic systems. The results are encouraging for development of photocatalytic systems to have simultaneous enhancement of the H<sub>2</sub> production rate and the pollutant degradation in water, however, the limited works have been done in this area and more explorations are required.

## 2.4 Principles of Photocatalytic Water Treatment

Heterogeneous photocatalysis is one of the advanced oxidation processes (AOPs) that is known as a promising approach for water purification. Heterogeneous photocatalysis employing semiconductor catalysts (TiO<sub>2</sub>, ZnO, Fe<sub>2</sub>O<sub>3</sub>, CdS, GaP and ZnS) has demonstrated its efficiency in degrading a wide range of organics into readily biodegradable compounds, and eventually mineralized them to harmless carbon dioxide and water.<sup>17,18</sup> Ollis et al.<sup>19</sup> first conducted research on photo-mineralization of halogenated hydrocarbon contaminants in water, including trichloroethylene, dichloromethane, chloroform, and carbon tetrachloride by TiO<sub>2</sub>. This process is capable of mineralizing many toxic organic species present in water without producing any harmful compounds.<sup>20</sup>

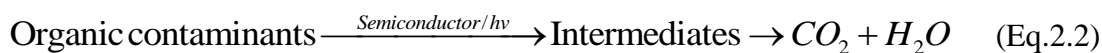
The semiconductor photocatalysis has the number of advantages over other advanced oxidation process for water treatment, including: (i) the reactions can take place in ambient operating temperature and pressure, (ii) the mineralization of many organic pollutants to less harmful effluents such as carbon dioxide, water, and mineral acid is possible, (iii) dissolved oxygen is sufficient and no expensive and hazardous oxidizing chemicals such as  $O_3$  or  $H_2O_2$  is required, (iv)  $TiO_2$ , the most widely used semiconductor is active, inexpensive, nontoxic and stable, and (v) it is possible to modify the system to use solar light as an alternative for UV light.<sup>17,21</sup>

Table 2.1 provides a list of organic pollutants that can be mineralized by photocatalysis.<sup>22</sup>

**Table 2.1** Aqueous organic pollutants mineralized by photocatalysis<sup>22</sup>

Class of organics	Examples
Aldehydes	Acetaldehyde, Formaldehyde
Alkanes	isobutane, pentane, heptane, cyclohexane, paraffin
Aliphatic alcohols	Methanol, ethanol, propanol, glucose
Aliphatic carboxylic acids	Formic, ethanoic, propanoic, oxalic, butyric, malic acids
Alkenes	Propene, cyclohexene
Haloalkenes	1,2-dichloroethylene, 1,1,2-trichloroethylene
Aromatics	Benzene, naphthalene
Phenolic compounds	Phenol, hydroquinone, catechol, methylcatechol, resorcinol, <i>O</i> -, <i>M</i> -, <i>P</i> -cresol, nitrophenols
Aromatic carboxylic acids	Benzoic, 4-aminobenzoic, phthalic, salicylic, <i>M</i> - and <i>P</i> -hydroxybenzoic, chlorohydroxybenzoic and chlorobenzoic acids
Dyes	Rhodamine B, methylene blue, methyl orange, fluorescein, acid orange 8 and acid red1, chrysoidine Y, acridine orange and ethidium bromide, indigo carmine, Chicago sky blue, mixed dye (mixture of the four dyes)
Ethers	Methyl <i>tert</i> -butyl ether (MBTE), mixture of 4-chlorophenol, 2,4-dichlorophenol, 2,4,6-trichlorophenol, and pentachlorophenol
Pesticides	DDT, parathion, lindane, tetrachlorvinphos, phenitrothion
Surfactants	Sodium dodecylsulphate, polyethylene glycol, sodium dodecyl benzene sulphonate, trimethyl phosphate

The overall process can be summarized as (Eq.2.2) <sup>17</sup> and the overall photocatalysis reaction described by this equation can be divided into five steps as follow <sup>17,22</sup> :



- (i) Mass transfer of the organic contaminant in the liquid phase to the semiconductor surface.
- (ii) Adsorption of the organic contaminant onto the light activated semiconductor surface.
- (iii) Photocatalysis reaction for the adsorbed compound on the semiconductor surface
- (iv) Desorption of the intermediate(s) from the semiconductor surface.
- (v) Mass transfer of the intermediate from the interface region to the bulk fluid.

Many studies demonstrated that Langmuir-Hinshelwood can be used to describe the pollutant degradation rate, which is expressed in terms of degradation of compounds or the formation of CO<sub>2</sub>. The kinetic of photo-mineralization is governed by various operation parameters such as catalyst dosage, initial concentration of pollutants, light intensity, dissolved oxygen, and pH of the solution.<sup>20</sup> These parameters affect the oxidation rates and efficiency of the photocatalytic system.

## 2.5 Properties of Photocatalyst

Photocatalytic materials as the core element of the photocatalysis should meet essential requirements that are described as follow.

### 2.5.1 Proper band gap

One of the main requirements for a good photocatalyst is the capability of light absorption in a wide range of solar spectrum. Band gap is a semiconductor's property, which determines light absorption range. Smaller band gap facilitates wider range of light that can be absorbed. However, the challenge associated with the current semiconductors is their wide band gap, which limits their application within only 5% of full solar

spectrum (UV range).<sup>9</sup> For example, the anatase phase of  $\text{TiO}_2$  has a band gap of 3.2 eV and can only absorb light within the UV range. Therefore, many strategies have been applied to shift the light absorption into the visible region, including metal or non-metal doping, dye sensitization and hetero-structuring a large band gap material with a small band gap material, etc.

In addition to band gap, the CB and VB positions must be appropriate for the desired redox reaction as described in section 3. In general, higher CB of the semiconductor thermodynamically favors for reduction reaction, whereas low VB has better potential for oxidation reaction.

### 2.5.2 Efficient charge carrier transfer and electron conductivity

Efficient charge carriers' transfer is crucial for a successful photocatalysis. If the electrons and holes migrate to the surface of the catalyst quickly and react with the adsorbed species, the charge recombination is greatly suppressed.

Electrons can flow easily in a material with high electron conductivity such as metals due to their Fermi levels which exists within their energy band. Therefore, energy levels near the Fermi level can easily be occupied by electrons.<sup>1</sup> However, semiconductors that are used as photocatalyst have low conductivity. Therefore, it is required to improve their conductivity by fabricating a hybrid material composed of semiconductor and a conductive material such as metals, and carbonaceous material.<sup>18</sup> This approach has been widely reported in literatures to assist electron and hole separation.

### 2.5.3 Stability

Another important property of photocatalysts is chemical stability and photo-corrosion resistance to avoid its decomposition during reaction. Otherwise, a photocatalyst should be replaced with new catalyst and hazardous products will be formed due to the decomposition.<sup>23</sup>

For instance, CdS is a good photocatalyst with high activity in visible light owing to its narrow band gap of 2.39 eV. However, it suffers from low photo-corrosion resistance

because of the oxidation of  $S^{2-}$ . In order to overcome this drawback of unstable catalysts such as CdS, a hole scavenger or a co-catalyst should be added to the system to accept the hole and diminish the rate of self-oxidation.<sup>24</sup>

#### 2.5.4 Surface active sites

The number of active sites is an important property that should be taken into account in photocatalysis. In heterogeneous photocatalysis, reactants adsorb on these active sites and then their reactions with photo-generated charges take place. Photo-generated charges tend to recombine even after their migration to the surface of the catalyst. Therefore, adequate active sites must be present at the surface for the redox reactions to be completed before the charges recombination. In this regard, surface area of the photocatalyst has an important role in determining the number of active sites.<sup>25</sup> Therefore, a high specific surface area ( $m^2/g$ ) is required for photocatalysts to be effective. In order to improve this property of photocatalyst, various strategies have been studied and developed such as Incorporation of co-catalyst, surface defect control, surface-doping, etc.

## 2.6 Hetero-structure photocatalysts

Single semiconductors are proved to be hardly efficient for solar photocatalysis due to some intrinsic restrictions, including: light-harvesting capability, electron-hole recombination, CB and VB levels and surface reaction rate.<sup>26</sup> Many transition metal oxides such as  $TiO_2$ ,  $SrTiO_3$ ,  $Nb_2O_5$ ,  $Ta_2O_5$ , etc. have a wide band gap, making them only active in UV region and not able to employ visible light.<sup>9</sup>

In order to cope with these limitations, design of hybrid (hetero-structure) photocatalyst made of two or more functional components has been proposed to be a viable approach. The hetero-structure photocatalyst significantly decreases the recombination of photo-generated charge carriers. In addition, it extends the solar light absorption. Therefore, substantial enhancement of solar photocatalytic efficiency is achieved by taking the advantage of hetero-structure photocatalyst.<sup>27–30</sup>

The interface between the different components is the main parameter in hetero-structure materials. Various charge carrier pathways are expected depending on type of materials that form different hetero-structures.<sup>25</sup> Therefore, hetero-structures can be classified into several modes. In this chapter the main focus is on four important structures including hetero-junctions of metal-semiconductor, noble-metal free co-catalyst- semiconductor, 2D nanomaterial-semiconductor and semiconductor-semiconductor.

### 2.6.1 Metal-semiconductor

Different studies have demonstrated that incorporation of metals on semiconductors improve the photocatalytic activity.<sup>31–36</sup> The key concept in metal-semiconductor structure is Schottky junction that is created due to the close contact of a metal and n-type semiconductor. Particular energy level alignment in a Schottky junction provides a potential barrier to prevent electron and holes from passing through them.<sup>37–39</sup> The energy band diagram of a metal-semiconductor Schottky junction is depicted in Figure 2.6. In this figure,  $\Phi_b$  represents the height of the potential barrier, which depends on the band bending of the semiconductor and the Fermi level of metal.<sup>37</sup>

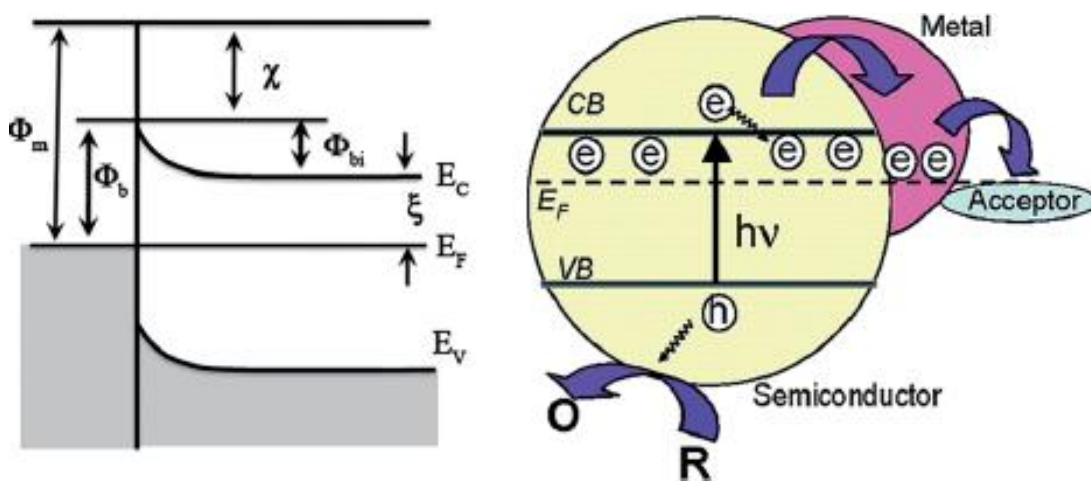


**Figure 2.6** (a) Schottky junction with energy level alignment and (b) electron transfer across the metal-semiconductor junction.<sup>26,39</sup>

Schottky junction facilitates the transfer of photo-generated electrons to the contacting metal, as shown in figure 2.6.<sup>26,38–40</sup> In this process, metal acts as an electron trap center and accelerate the separation of photo-generated charges. Thereby, hole will have more time to react as an oxidizer on the semiconductor surface. Moreover, the metal surface provides active sites for reduction reaction.<sup>41</sup> It has been recognized that the Fermi level of the incorporated metal should be lower than the semiconductor CB. In this manner, various noble metals have been used to construct metal-semiconductor hetero-structure. Metals in this structure are often known as co-catalyst. The most commonly used metals are Pt,<sup>42</sup> Pd,<sup>43,44</sup> Au,<sup>45</sup> Rh,<sup>46</sup> and Ru,<sup>47</sup>. Among them, Pt is the most popular one owing to its low Fermi level and it has been considered to be effective in inhibiting photo-generated charges recombination.<sup>41,48</sup>

## 2.6.2 Noble metal-free co-catalysts- semiconductor

Although it is common to deposit noble metals as co-catalyst on semiconductors to improve their photocatalytic performance, the scarcity and high cost of these metals is an issue. Therefore, extensive research has been conducted to use noble-metal free co-catalyst as an alternative for noble metals.

Some transition metal oxides, sulfides and complexes have been reported to be effective co-catalysts. Photo-generated electrons are able to transfer from the semiconductor to the co-catalyst impeding the charges recombination. However, transition metal sulfides have shown more activity for hydrogen production compared to metal oxides.<sup>29,49</sup> MoS<sub>2</sub> is an important example of noble metal-free co-catalyst. Zong et al. reported the great potential of MoS<sub>2</sub> to act as co-catalyst on CdS.<sup>50</sup> It was demonstrated that MoS<sub>2</sub>-loaded on CdS had a 36 times higher hydrogen production rate compared to pure CdS. This enhancement is ascribed to the close contact of MoS<sub>2</sub> and CdS, which facilitates the electron transfer from CdS to MoS<sub>2</sub>.<sup>51</sup> MoS<sub>2</sub> have been reported as co-catalyst in different semiconductor hetero-structures such as MoS<sub>2</sub>-C<sub>3</sub>N<sub>4</sub>,<sup>52</sup> MoS<sub>2</sub>-CdSe,<sup>53</sup> MoS<sub>2</sub>-TiO<sub>2</sub>.<sup>54–56</sup> For example, Gao et al.<sup>56</sup> could fabricate a MoS<sub>2</sub> quantum dots-graphene-TiO<sub>2</sub> with improved photocatalytic properties.



However, the synthesis methods to obtain these photocatalysts based on MoS<sub>2</sub> mostly require high temperature process, long-term hydrothermal process and also presence of H<sub>2</sub>S, which prevent these methods to be applicable.<sup>57–59</sup> Recently, photo-deposition method has been proposed to load MoS<sub>2</sub> on semiconductors.<sup>60–62</sup> Zong et al.<sup>63</sup> reported an in-situ photo-reduction process in a noble metal-free organic dye (EB) sensitized system to obtain MoS<sub>x</sub>. This simple method exhibited high efficiency for photocatalytic hydrogen generation. Xu et al.<sup>64</sup> in their recent work loaded MoS<sub>x</sub> on g-C<sub>3</sub>N<sub>4</sub> with an in-situ approach during the photocatalytic hydrogen production. (NH<sub>4</sub>)<sub>2</sub>MoS<sub>4</sub> and EB were used as precursor and sensitizer, respectively. EB-sensitized MoS<sub>x</sub>-g-C<sub>3</sub>N<sub>4</sub> (EB-MoS<sub>x</sub>-g-C<sub>3</sub>N<sub>4</sub>) exhibited the higher activity and stability than both EB-sensitized g-C<sub>3</sub>N<sub>4</sub> (EB-g-C<sub>3</sub>N<sub>4</sub>) and EB-sensitized MoS<sub>x</sub> (EB-MoS<sub>x</sub>).<sup>64</sup> Kanda et al.<sup>65</sup> applied a photo-deposition technique to form MoS<sub>2</sub> nano-crystals on TiO<sub>2</sub> and ethanol was used as a reducing agent. In aqueous solution of formic acid the MoS<sub>2</sub>/TiO<sub>2</sub> system exhibited a high photocatalytic activity for hydrogen generation.

### 2.6.3 Heterojunctions on 2-D nanomaterials

In order to improve the photocatalytic efficiency, composites consisting of carbonaceous materials have been extensively studied.<sup>66</sup> Among various carbon nanomaterials, graphene is quite popular owing to its remarkable properties.<sup>67</sup> It was first discovered by Novoselov et al.<sup>68</sup> in 2004 and since then, vast applications of graphene in nano-electronics, sensors, catalysts and energy conversion have been observed.

Graphene has a two-dimensional (2D) sp<sup>2</sup> hybridized carbon network.<sup>69,70</sup> It possesses unique characteristics such as a large theoretical specific surface area (2600 m<sup>2</sup>/g), high thermal conductivity (3000 W/mK), and high intrinsic electron mobility (15,000 m<sup>2</sup>/Vs).<sup>71</sup> These characteristics make graphene one of the strongest and most conductive materials currently known.

Many efforts have been devoted to take advantage of graphene's superior properties by constructing graphene-semiconductors hetero-structures. Several graphene-semiconductor composites have been reported such as TiO<sub>2</sub>-graphene,<sup>72,73</sup> ZnO-graphene,<sup>74</sup> CdS-graphene.<sup>75</sup>

The 2D structure of graphene together with the large surface area makes it an excellent platform for supporting semiconductors. In addition, the work function of graphene is  $-4.42\text{eV}$ , which is higher than that of the reduction potential of hydrogen.<sup>76,77</sup> Therefore, if the CB position of a deposited semiconductor is properly matching with graphene, the injection of photo-generated electrons from the semiconductor to graphene would be thermodynamically favored.<sup>26</sup> Furthermore, due to an excellent electronic conductivity and high mobility of charge carriers; the injected electrons can easily move along the graphene surface and complete the reduction reaction.<sup>78,72</sup>

The improvement in photocatalytic hydrogen generation as well as water treatment has been demonstrated by using graphene-based hetero- structures.<sup>73,76,79</sup> For example, Zhang et al. reported the deposition of  $\text{TiO}_2$  particles onto RGO surfaces, and the resulting  $\text{TiO}_2/\text{RGO}$  composite showed a higher hydrogen generation rate than pristine  $\text{TiO}_2$  and P25.<sup>80</sup>

Various methods have been studied in order to synthesize single-layer or bi-layer graphene. These methods are including micromechanical cleavage of highly oriented pyrolytic graphite, epitaxial growth, chemical vapour deposition, and arc discharge of graphite<sup>81</sup> However, these methods are not applicable for large scale production of graphene. Another approach to produce graphene is to reduce chemically exfoliated graphene oxide (GO)<sup>82</sup>, which is currently known as the most popular method. Hummers method was first introduced by Hummers as the simple large scale method to produce GO.<sup>83</sup> In general, the Hummers method is based on the exfoliation and oxidation of graphite in order to obtain graphene oxide. Graphene oxide is basically a non-conductive and hydrophilic graphene sheet containing functionalities such as epoxides, alcohols, ketone carbonyls, and carboxylic groups.<sup>1</sup> The modified version of this method has been studied in order to improve the quality of the synthesized GO and also be able to control the process more safely and easily.<sup>84</sup>

#### 2.6.4 Semiconductor-semiconductor

Hetero-structure of two semiconductors has been extensively investigated for photocatalysis. This type of photocatalyst composite has shown improved performance for photocatalysis compared to individual semiconductors.  $\text{ZnO}/\text{SnO}_2$  has been reported

to be more active than pure ZnO or SnO<sub>2</sub> for decolorization of methyl orange.<sup>85-88</sup> Serpone et al.<sup>89</sup> explained this improvement by proposing an interparticle electron-transfer process (IPET) within the coupled semiconductors due to their different redox energy levels corresponding to their conduction and valence bands. Wu<sup>90</sup> compared the photodegradation efficiency of single semiconductor and coupled semiconductor systems using TiO<sub>2</sub>, ZnO, and SnO<sub>2</sub> to degrade two azo dyes. The reaction rate constant of Procion red MX-5B was reported to be larger for the TiO<sub>2</sub>/ZnO couple than that of pure ones at pH 7. Many other composites such as hybrid of TiO<sub>2</sub> and CdS,<sup>91,92</sup> CdSe<sup>93</sup> and Cu<sub>2</sub>O<sup>94</sup> have been also studied. This enhancement is due to absorbing a wider spectral range of light by two different semiconductors. Furthermore, by choosing appropriate semiconductors in order to have proper band energy alignment between the two semiconductors, the separation of photo-generated charges is also improved.<sup>85,95</sup>

## 2.7 References

- (1) Lui, G. Graphene-Wrapped Hierarchical TiO<sub>2</sub> Nanoflower Composites with Enhanced Photocatalytic Performance, University of Waterloo, 2014.
- (2) Xing, Z. Development of New Layer-Structured Materials as Photocatalysts for Water Splitting, 2014.
- (3) Kiyoshi Takahashi, Akihiko Yoshikawa, A. S. *Wide Bandgap Semiconductors: Fundamental Properties and Modern Photonic and Electronic Devices*; Springer, 2007.
- (4) Mills, A.; Lee, S. A Web-Based Overview of Semiconductor Photochemistry-Based Current Commercial Applications. *J. Photochem. Photobiol. A Chem.* **2002**, *152*, 233.
- (5) Linsebigler, A. L.; Linsebigler, A. L.; Yates Jr, J. T.; Lu, G.; Lu, G.; Yates, J. T. Photocatalysis on TiO<sub>2</sub> Surfaces: Principles, Mechanisms, and Selected Results. *Chem. Rev.* **1995**, *95* (3), 735.
- (6) Henderson, M. a. A Surface Science Perspective on TiO<sub>2</sub> Photocatalysis. *Surf. Sci. Rep.* **2011**, *66* (6-7), 185.
- (7) Sellappan, R. Mechanisms of Enhanced Activity of Model TiO<sub>2</sub>/Carbon and TiO<sub>2</sub>/Metal Nanocomposite Photocatalysts, Chalmers University of Technology, 2013.
- (8) B. Viswanathan, S. Sivasanker, A. V. R. *Catalysis : Principles and Applications*; New Delhi : Narosa, 2002.
- (9) Chen, X.; Shen, S.; Guo, L.; Mao, S. S. Semiconductor-Based Photocatalytic Hydrogen Generation. *Chem. Rev.* **2010**, *110* (11), 6503.
- (10) Fujishima, a; Honda, K. Electrochemical Photolysis of Water at a Semiconductor Electrode. *Nature* **1972**, *238* (5358), 37.

- (11) Allen J. Bard. Photoelectrochemistry and Heterogeneous Photo-Catalysis at Semiconductors. *J. Photochem.* **1979**, 10, 59.
- (12) Maeda, K.; Domen, K. Solid Solution of GaN and ZnO as a Stable Photocatalyst for Overall Water Splitting under Visible Light <sup>†</sup>. *Chem. Mater.* **2010**, 22 (3), 612.
- (13) Kudo, A.; Kato, H.; Tsuji, I. Strategies for the Development of Visible-Light-Driven Photocatalysts for Water Splitting. *Chem. Lett.* **2004**, 33 (12), 1534.
- (14) Kudo, A.; Miseki, Y. Heterogeneous Photocatalyst Materials for Water Splitting. *Chem. Soc. Rev.* **2009**, 38 (1), 253.
- (15) Osterloh, F. E. Inorganic Materials as Catalysts for Photochemical Splitting of Water. *Chem. Mater.* **2008**, 20 (1), 35.
- (16) Patsoura, A.; Kondarides, D. I.; Verykios, X. E. Photocatalytic Degradation of Organic Pollutants with Simultaneous Production of Hydrogen. *Catal. Today* **2007**, 124 (3-4), 94.
- (17) Chong, M. N.; Jin, B.; Chow, C. W. K.; Saint, C. Recent Developments in Photocatalytic Water Treatment Technology: A Review. *Water Res.* **2010**, 44 (10), 2997.
- (18) Vidal, A.; Alarc, D.; Malato, S.; Maldonado, M. I.; Julia, C.; Gernjak, W. Applied Studies in Solar Photocatalytic Detoxification : An Overview. *Sol. Energy* **2003**, 75, 329.
- (19) David F. Ollis, Chen-Yung Hsiao, Lely Budiman, C.-L. L. Heterogeneous Photoassisted Catalysis: Conversions of Perchloroethylene, Dichloroethane, Chloroacetic Acids, and Chlorobenzenes. *J. Catal.* **1984**, 88 (1), 89.
- (20) Chen, D.; Ray, A. K. Photocatalytic Kinetics of Phenol and Its Derivatives over UV Irradiated TiO<sub>2</sub>. *Appl. Catal. B Environ.* **1999**, 23 (2-3), 143.

- (21) Mehrotra, K.; Yablonsky, G. S.; Ray, A. K. Kinetic Studies of Photocatalytic Degradation in a TiO<sub>2</sub> Slurry System : Distinguishing Working Regimes and Determining Rate Dependences. *Ind. Eng. Chem. Res.* **2003**, 42 (11), 2273.
- (22) Herrmann, J. Heterogeneous Photocatalysis : Fundamentals and Applications to the Removal of Various Types of Aqueous Pollutants. *Catal. Today* **1999**, 53, 115.
- (23) D. Murzin, T. S. *Catalytic Kinetics*; Elsevier Science, 2005.
- (24) Davis, A. P.; Huang, C. P. The Photocatalytic Oxidation of Sulfur-Containing Organic Compounds Using Cadmium Sulfide and the Effect on CdS Photocorrosion. *Water Res.* **1991**, 25 (10), 1273.
- (25) Liu, G.; Wang, L.; Yang, H. G.; Cheng, H.-M.; (Max) Lu, G. Q. Titania-Based Photocatalysts—crystal Growth, Doping and Heterostructuring. *J. Mater. Chem.* **2010**, 20 (5), 831.
- (26) Yuan, Y.; Ruan, L.; Barber, J.; Chye, S.; Loo, J.; Xue, C. Hetero-Nanostructured Suspended Photocatalysts for Solar-to-Fuel Conversion. *Energy Environ. Sci.* **2014**, 7, 3934.
- (27) Mayer, M. T.; Lin, Y.; Yuan, G.; Wang, D. Forming Heterojunctions at the Nanoscale for Improved Photoelectrochemical Water Splitting by Semiconductor Materials: Case Studies on Hematite. *Acc. Chem. Res.* **2013**, 46 (7), 1558.
- (28) Jang, J. S.; Kim, H. G.; Lee, J. S.; Suk, J.; Gyu, H.; Sung, J. Heterojunction Semiconductors: A Strategy to Develop Efficient Photocatalytic Materials for Visible Light Water Splitting. *Catal. Today* **2012**, 185 (1), 270.
- (29) Wang, Y.; Wang, Q.; Zhan, X.; Wang, F.; Safdar, M.; He, J. Visible Light Driven Type II Heterostructures and Their Enhanced Photocatalysis Properties: A Review. *Nanoscale* **2013**, 5 (18), 8326.

- (30) Fan, W.; Zhang, Q.; Wang, Y. Semiconductor-Based Nanocomposites for Photocatalytic H<sub>2</sub> Production and CO<sub>2</sub> Conversion. *Phys. Chem. Chem. Phys.* **2013**, *15* (8), 2632.
- (31) Choi, W.; Termin, A.; Hoffmann, M. R. The Role of Metal Ion Dopants in Quantum-Sized TiO<sub>2</sub>: Correlation between Photoreactivity and Charge Carrier Recombination Dynamics. *J. Phys. Chem.* **1994**, *98* (51), 13669.
- (32) Karakitsou, K. E.; Verykios, X. E. Effects of Altrivalent Cation Doping of Titania on Its Performance as a Photocatalyst for Water Cleavage. *J. Phys. Chem.* **1993**, *97* (6), 1184.
- (33) Soria, J.; Conesa, J. Dinitrogen Photoreduction to Ammonia over Titanium Dioxide Powders Doped with Ferric Ions. *J. Phys. Chem.* **1991**, No. 6, 274.
- (34) Mogyorósi, K.; Kmetykó, Á.; Czirbus, N.; Veréb, G.; Sipos, P.; Dombi, A. Comparison of the Substrate Dependent Performance of Pt-, Au- and Ag-Doped TiO<sub>2</sub> Photocatalysts in H<sub>2</sub>-Production and in Decomposition of Various Organics. *React. Kinet. Catal. Lett.* **2009**, *98* (2), 215.
- (35) Bahruji, H.; Bowker, M.; Davies, P. R.; Pedrono, F. New Insights into the Mechanism of Photocatalytic Reforming on Pd/TiO<sub>2</sub>. *Appl. Catal. B Environ.* **2011**, *107* (1-2), 205.
- (36) Connelly, K. a.; Idriss, H. The Photoreaction of TiO<sub>2</sub> and Au/TiO<sub>2</sub> Single Crystal and Powder Surfaces with Organic Adsorbates. Emphasis on Hydrogen Production from Renewables. *Green Chem.* **2012**, *14* (2), 260.
- (37) Potje-Kamloth, K. Semiconductor Junction Gas Sensors. *Chem. Rev.* **2008**.
- (38) Jakob, M.; Levanon, H.; Kamat, P. V. Charge Distribution between UV-Irradiated TiO<sub>2</sub> and Gold Nanoparticles: Determination of Shift in the Fermi Level. *Nano Lett.* **2003**, *3* (3), 353.

- (39) Subramanian, V.; Wolf, E. E.; Kamat, P. V. Catalysis with TiO<sub>2</sub>/Gold Nanocomposites. Effect of Metal Particle Size on the Fermi Level Equilibration. *J. Am. Chem. Soc.* **2004**, *126* (15), 4943.
- (40) Wood, A.; Giersig, M.; Mulvaney, P. Fermi Level Equilibration in Quantum Dot-Metal Nanojunctions. *J. Phys. Chem. B* **2001**, *105* (37), 8810.
- (41) Yang, J.; Wang, D.; Han, H.; Li, C. A. N. Roles of Cocatalysts in Photocatalysis and Photoelectrocatalysis. *Acc. Chem. Res.* **2013**, *46* (8).
- (42) Lingampalli, S. R.; Gautam, U. K.; Rao, C. N. R. Highly Efficient Photocatalytic Hydrogen Generation by Solution-Processed ZnO/Pt/CdS, ZnO/Pt/Cd<sub>1-x</sub>Zn<sub>x</sub>S and ZnO/Pt/CdS<sub>1-x</sub>Se<sub>x</sub> Hybrid Nanostructures. *Energy Environ. Sci.* **2013**, *6* (12), 3589.
- (43) Wu, X.; Song, Q.; Jia, L.; Li, Q.; Yang, C.; Lin, L. Pd-Gardenia-TiO<sub>2</sub> as a Photocatalyst for H<sub>2</sub> Evolution from Pure Water. *Int. J. Hydrogen Energy* **2012**, *37* (1), 109.
- (44) Jin, S.; Shiraishi, F. Photocatalytic Activities Enhanced for Decompositions of Organic Compounds over Metal-Photodepositing Titanium Dioxide. *Chem. Eng. J.* **2004**, *97*, 203.
- (45) Chiarello, G. L.; Selli, E.; Forni, L. Photocatalytic Hydrogen Production over Flame Spray Pyrolysis-Synthesised TiO<sub>2</sub> and Au/TiO<sub>2</sub>. *Appl. Catal. B Environ.* **2008**, *84* (1-2), 332.
- (46) Pal, B.; Ikeda, S.; Kominami, H.; Kera, Y.; Ohtani, B. Photocatalytic Redox-Combined Synthesis of L-Pipecolinic Acid from L-Lysine by Suspended Titania Particles: Effect of Noble Metal Loading on the Selectivity and Optical Purity of the Product. *J. Catal.* **2003**, *217* (1), 152.
- (47) Navarro, R. M.; del Valle, F.; Fierro, J. L. G. Photocatalytic Hydrogen Evolution from CdS-ZnO-CdO Systems under Visible Light Irradiation: Effect of Thermal



- Treatment and Presence of Pt and Ru Cocatalysts. *Int. J. Hydrogen Energy* **2008**, *33* (16), 4265.
- (48) Sivalingam, G.; Nagaveni, K.; Hegde, M. S.; Madras, G. Photocatalytic Degradation of Various Dyes by Combustion Synthesized Nano Anatase TiO<sub>2</sub>. *Appl. Catal. B Environ.* **2003**, *45* (1), 23.
- (49) Obregón, S.; Colón, G. Improved H<sub>2</sub> Production of Pt-TiO<sub>2</sub>/g-C<sub>3</sub>N<sub>4</sub>-MnO<sub>x</sub> Composites by an Efficient Handling of Photogenerated Charge Pairs. *Appl. Catal. B Environ.* **2014**, *144*, 775.
- (50) Zong, X.; Yan, H.; Wu, G.; Ma, G.; Wen, F.; Wang, L.; Li, C. Enhancement of Photocatalytic H<sub>2</sub> Evolution on CdS by Loading MoS<sub>2</sub> as Cocatalyst under Visible Light Irradiation. *J. Am. Chem. Soc.* **2008**, *130* (23), 7176.
- (51) Jaramillo, T. F.; Jørgensen, K. P.; Bonde, J.; Nielsen, J. H.; Hørch, S.; Chorkendorff, I. Identification of Active Edge Sites for Electrochemical H<sub>2</sub> Evolution from MoS<sub>2</sub> Nanocatalysts. *Science* **2007**, *317* (July), 100.
- (52) Ge, L.; Han, C.; Xiao, X.; Guo, L. Synthesis and Characterization of Composite Visible Light Active Photocatalysts MoS<sub>2</sub>-G-C<sub>3</sub>N<sub>4</sub> with Enhanced Hydrogen Evolution Activity. *Int. J. Hydrogen Energy* **2013**, *38* (17), 6960.
- (53) Frame, F. A.; Osterloh, F. E. CdSe-MoS<sub>2</sub>: A Quantum Size-Confined Photocatalyst for Hydrogen Evolution from Water under Visible Light. *J. Phys. Chem. C* **2010**, *114* (23), 10628.
- (54) Zhou, W.; Yin, Z.; Du, Y.; Huang, X.; Zeng, Z.; Fan, Z.; Liu, H.; Wang, J.; Zhang, H. Synthesis of Few-Layer MoS<sub>2</sub> Nanosheet-Coated TiO<sub>2</sub> Nanobelt Heterostructures for Enhanced Photocatalytic Activities. *Small* **2013**, *9* (1), 140.
- (55) Hu, K. H.; Hu, X. G.; Xu, Y. F.; Sun, J. D. Synthesis of Nano-MoS<sub>2</sub>/TiO<sub>2</sub> Composite and Its Catalytic Degradation Effect on Methyl Orange. *J. Mater. Sci.* **2010**, *45* (10), 2640.

- (56) Gao, W.; Wang, M.; Ran, C.; Li, L. Facile One-Pot Synthesis of MoS<sub>2</sub> Quantum dots–graphene–TiO<sub>2</sub> Composites for Highly Enhanced Photocatalytic Properties. *Chem. Commun.* **2015**, 51 (9), 1709.
- (57) Pourabbas, B.; Jamshidi, B. Preparation of MoS<sub>2</sub> Nanoparticles by a Modified Hydrothermal Method and the Photo-Catalytic Activity of MoS<sub>2</sub>/TiO<sub>2</sub> Hybrids in Photo-Oxidation of Phenol. *Chem. Eng. J.* **2008**, 138 (1-3), 55.
- (58) Zhu, B.; Lin, B.; Zhou, Y.; Sun, P.; Yao, Q.; Chen, Y.; Gao, B. Enhanced Photocatalytic H<sub>2</sub> Evolution on ZnS Loaded with Graphene and MoS<sub>2</sub> Nanosheets as Cocatalysts. *J. Mater. Chem. A* **2014**, 2 (11), 3819.
- (59) Deng, Z. H.; Li, L.; Ding, W.; Xiong, K.; Wei, Z. D. Synthesized Ultrathin MoS<sub>2</sub> Nanosheets Perpendicular to Graphene for Catalysis of Hydrogen Evolution Reaction. *Chem. Commun.* **2015**, 51 (10), 1893.
- (60) Nguyen, M.; Tran, P. D.; Pramana, S. S.; Lee, R. L.; Batabyal, S. K.; Mathews, N.; Wong, L. H.; Graetzel, M. In Situ Photo-Assisted Deposition of MoS<sub>2</sub> Electrocatalyst onto Zinc Cadmium Sulphide Nanoparticle Surfaces to Construct an Efficient Photocatalyst for Hydrogen Generation. *Nanoscale* **2013**, 5 (4), 1479.
- (61) Meng, C.; Liu, Z.; Zhang, T.; Zhai, J. Layered MoS<sub>2</sub> Nanoparticles on TiO<sub>2</sub> Nanotubes by Photocatalytic Strategy as High-Performance Electrocatalysts for Hydrogen Evolution Reaction. *Green Chem.* **2015**.
- (62) Li, Y.; Wang, H.; Peng, S. Tunable Photodeposition of MoS<sub>2</sub> onto a Composite of Reduced Graphene Oxide and CdS for Synergic Photocatalytic Hydrogen Generation. *J. Phys. Chem. C* **2014**, 118 (34), 19842.
- (63) Zong, X.; Xing, Z.; Yu, H.; Bai, Y.; Lu, G. Q.; Wang, L. Photocatalytic Hydrogen Production in a Noble-Metal-Free System Catalyzed by in Situ Grown Molybdenum Sulfide Catalyst. *J. Catal.* **2014**, 310, 51.

- (64) Xu, J.; Li, Y.; Peng, S. Photocatalytic Hydrogen Evolution over Erythrosin B-Sensitized Graphitic Carbon Nitride with in Situ Grown Molybdenum Sulfide Cocatalyst. *Int. J. Hydrogen Energy* **2015**, *40* (1), 353.
- (65) Kanda, S.; Akita, T.; Fujishima, M.; Tada, H. Facile Synthesis and Catalytic Activity of MoS<sub>2</sub>/TiO<sub>2</sub> by a Photodeposition-Based Technique and Its Oxidized Derivative MoO<sub>3</sub>/TiO<sub>2</sub> with a Unique Photochromism. *J. Colloid Interface Sci.* **2011**, *354* (2), 607.
- (66) Leary, R.; Westwood, A. Carbonaceous Nanomaterials for the Enhancement of TiO<sub>2</sub> Photocatalysis. *Carbon N. Y.* **2011**, *49* (3), 741.
- (67) Castro Neto, a. H. .; Peres, N. M. R. .; Novoselov, K. S. .; Geim, a. K. .; Guinea, F.; Neto, A. The Electronic Properties of Graphene. *Rev. Mod. Phys.* **2009**, *81* (1), 109.
- (68) Novoselov, A. K. S.; Geim, A. K.; Morozov, S. V; Jiang, D.; Zhang, Y.; Dubonos, S. V; Firsov, A. A. Electric Field Effect in Atomically Thin Carbon Films  
Author(s): K. S. Novoselov, A. K. Geim, S. V. Morozov, D. Jiang, Y. Zhang, S. V. Dubonos, I. V. Grigorieva and A. A. Firsov Source: **2015**, *306* (5696), 666.
- (69) Zhang, X.; Tang, Y.; Li, Y.; Wang, Y.; Liu, X.; Liu, C.; Luo, S. Reduced Graphene Oxide and PbS Nanoparticles Co-Modified TiO<sub>2</sub> Nanotube Arrays as a Recyclable and Stable Photocatalyst for Efficient Degradation of Pentachlorophenol. *Appl. Catal. A Gen.* **2013**, *457*, 78.
- (70) Liu, Y.; Hu, Y.; Zhou, M.; Qian, H.; Hu, X. Microwave-Assisted Non-Aqueous Route to Deposit Well-Dispersed ZnO Nanocrystals on Reduced Graphene Oxide Sheets with Improved Photoactivity for the Decolorization of Dyes under Visible Light. *Appl. Catal. B Environ.* **2012**, *125*, 425.
- (71) Akhavan, O.; Ghaderi, E. Photocatalytic Reduction of Graphene Oxide Nanosheets on TiO<sub>2</sub> Thin Film for Photoinactivation of Bacteria in Solar Light Irradiation. **2009**, No. 50 mL, 20214.

- (72) Xiang, Q.; Yu, J.; Jaroniec, M. Graphene-Based Semiconductor Photocatalysts. *Chem. Soc. Rev.* **2012**, *41* (2), 782.
- (73) Zhang, H.; Lv, X.; Li, Y.; Wang, Y.; Li, J. P25-Graphene Composite as a High Performance Photocatalyst. *ACS Nano* **2010**, *4* (1), 380.
- (74) Li, B.; Cao, H. ZnO@graphene Composite with Enhanced Performance for the Removal of Dye from Water. *J. Mater. Chem.* **2011**, *21* (10), 3346.
- (75) Li, Q.; Guo, B.; Yu, J.; Ran, J.; Zhang, B.; Yan, H.; Gong, J. R. Highly Efficient Visible-Light-Driven Photocatalytic Hydrogen Production of CdS-Cluster-Decorated Graphene Nanosheets. *J. Am. Chem. Soc.* **2011**, *133* (28), 10878.
- (76) Zhang, J.; Xiong, Z.; Zhao, X. S. Graphene-metal-oxide Composites for the Degradation of Dyes under Visible Light Irradiation. *J. Mater. Chem.* **2011**, *21* (11), 3634.
- (77) Lee, J. S.; You, K. H.; Park, C. B. Highly Photoactive, Low Bandgap TiO<sub>2</sub> Nanoparticles Wrapped by Graphene. *Adv. Mater.* **2012**, *24* (8), 1084.
- (78) An, X.; Yu, J. C. Graphene-Based Photocatalytic Composites. *RSC Adv.* **2011**, *1* (8), 1426.
- (79) Fan, W.; Lai, Q.; Zhang, Q.; Wang, Y. Nanocomposites of TiO<sub>2</sub> and Reduced Graphene Oxide as Efficient Photocatalysts for Hydrogen Evolution. *J. Phys. Chem. C* **2011**, *115* (21), 10694.
- (80) Zhang, X.-Y.; Li, H.-P.; Cui, X.-L.; Lin, Y. Graphene/TiO<sub>2</sub> Nanocomposites: Synthesis, Characterization and Application in Hydrogen Evolution from Water Photocatalytic Splitting. *J. Mater. Chem.* **2010**, *20* (14), 2801.
- (81) Rao, C. N. R.; Sood, a. K.; Subrahmanyam, K. S.; Govindaraj, a. Graphene: The New Two-Dimensional Nanomaterial. *Angew. Chemie Int. Ed.* **2009**, *48* (42), 7752.

- (82) Dreyer, D. R.; Park, S.; Bielawski, C. W.; Ruoff, R. S. The Chemistry of Graphene Oxide. *Chem. Soc. Rev.* **2010**, 39 (1), 228.
- (83) William S. Hummers, J.; Offeman, R. E. Preparation of Graphitic Oxide. *J. Am. Chem. Soc.* **1958**, 80 (1937), 1339.
- (84) Marcano, D. C.; Kosynkin, D. V.; Berlin, J. M.; Sinitskii, A.; Sun, Z.; Slesarev, A.; Alemany, L. B.; Lu, W.; Tour, J. M. Improved Synthesis of Graphene Oxide. *ACS Nano* **2010**, 4 (8), 4806.
- (85) Chiang, Y. J.; Lin, C. C. Photocatalytic Decolorization of Methylene Blue in Aqueous Solutions Using Coupled ZnO/SnO<sub>2</sub> Photocatalysts. *Powder Technol.* **2013**, 246, 137.
- (86) Cun, W.; Jincai, Z.; Xinming, W.; Bixian, M.; Guoying, S.; Ping'an, P.; Jiamo, F. Preparation, Characterization and Photocatalytic Activity of Nano-Sized ZnO/SnO<sub>2</sub> Coupled Photocatalysts. *Appl. Catal. B Environ.* **2002**, 39 (3), 269.
- (87) Wang, C.; Wang, X.; Xu, B.-Q.; Zhao, J.; Mai, B.; Peng, P.; Sheng, G.; Fu, J. Enhanced Photocatalytic Performance of Nanosized Coupled ZnO/SnO<sub>2</sub> Photocatalysts for Methyl Orange Degradation. *J. Photochem. Photobiol. A Chem.* **2004**, 168 (1-2), 47.
- (88) Maolin Zhang; Guoying Sheng; Jiamo Fu; Taicheng An; Xinming Wang; Xiaohong Hu. Novel Preparation of Nanosized ZnO–SnO<sub>2</sub> with High Photocatalytic Activity by Homogeneous Co-Precipitation Method. *Mater. Lett.* **2005**, 59 (28), 3641.
- (89) Serpone, N.; Maruthamuthu, P.; Pichat, P.; Pelizzetti, E.; Hidaka, H. Exploiting the Interparticle Electron Transfer Process in the Photocatalysed Oxidation of Phenol, 2-Chlorophenol and Pentachlorophenol: Chemical Evidence for Electron and Hole Transfer between Coupled Semiconductors. *J. Photochem. Photobiol. A Chem.* **1995**, 85 (3), 247.

- (90) Wu, C.-H. Comparison of Azo Dye Degradation Efficiency Using UV/single Semiconductor and UV/coupled Semiconductor Systems. *Chemosphere* **2004**, 57 (7), 601.
- (91) Tada, H.; Mitsui, T.; Kiyonaga, T.; Akita, T.; Tanaka, K. All-Solid-State Z-Scheme in CdS–Au–TiO<sub>2</sub> Three-Component Nanojunction System. *Nat. Mater.* **2006**, 5 (10), 782.
- (92) Baker, D. R.; Kamat, P. V. Photosensitization of TiO<sub>2</sub> Nanostructures with CdS Quantum Dots: Particulate versus Tubular Support Architectures. *Adv. Funct. Mater.* **2009**, 19 (5), 805.
- (93) Yang, L.; Luo, S.; Li, Y.; Xiao, Y.; Kang, Q.; Cai, Q. High Efficient Photocatalytic Degradation of P-Nitrophenol on a Unique Cu<sub>2</sub>O/TiO<sub>2</sub> P-N Heterojunction Network Catalyst. *Environ. Sci. Technol.* **2010**, 44 (19), 7641.
- (94) Hensel, J.; Wang, G.; Li, Y.; Zhang, J. Z. Synergistic Effect of CdSe Quantum Dot Sensitization and Nitrogen Doping of TiO<sub>2</sub> Nanostructures for Photoelectrochemical Solar Hydrogen Generation. *Nano Lett.* **2010**, 10 (2), 478.
- (95) Liao, D. L.; Badour, C. a.; Liao, B. Q. Preparation of Nanosized TiO<sub>2</sub>/ZnO Composite Catalyst and Its Photocatalytic Activity for Degradation of Methyl Orange. *J. Photochem. Photobiol. A Chem.* **2008**, 194 (1), 11.

## Chapter 3

### 3 Sacrificial Hydrogen Generation from formaldehyde with Pt/ TiO<sub>2</sub> Photocatalyst in Solar Radiation

#### 3.1 Introduction

Hydrogen production from a renewable source is one of the most studied multi-disciplinary research areas in the contemporary world. Photocatalytic water splitting technique has the potential for renewable hydrogen production from water.<sup>1-6</sup> However water splitting is not an easy task because of two main reasons: (i) very high positive free energy change ( $\Delta G^0 = 237 \text{ KJ mol}^{-1}$ ), and (ii) rapid reverse reaction. Water splitting being an endothermic reaction demands the energy that is equal to enthalpy change ( $\Delta H$ ) required to split water into hydrogen and oxygen.<sup>7, 8</sup> Sacrificial agents can be used as electron donor during the photocatalytic reaction process, to achieve a much higher hydrogen production rate by reacting irreversibly with the oxygen formed, photo-induced hole, or OH<sup>•</sup> radicals, to prevent backward reaction between produced H<sub>2</sub> and O<sub>2</sub> and hindering the recombination of photo-induced electrons and holes.<sup>9-15</sup>

Instead of pure organic compounds, organic pollutants in water can perform the role of electron donor, thereby can reduce the hydrogen production costs due to dual processes of hydrogen production and water purification. The chosen sacrificial agent should be inexpensive compared to the hydrogen produced to make the process a feasible one. Organic pollutants in wastewater can be considered as suitable electron donors for this purpose. There are only few reports that demonstrate the involvement of organic pollutants as sacrificial electron donor for such a system.<sup>9, 16-19</sup>

Numerous organic compounds have been used as electron donors for photocatalytic hydrogen generation, namely, carboxylic acids, alcohols, carbohydrates, hydrocarbons, artificial high polymers.<sup>9, 20, 21</sup> Recently methanol has been widely used as a sacrificial electron donor in photocatalytic hydrogen generation because of its lower splitting energy demand ( $16.1 \text{ KJ mol}^{-1}$ ) compared to water. The reaction of hydrogen formation goes through the formation of formaldehyde. Therefore, formaldehyde as a sacrificial agent

would also serve the purpose which has even much lower splitting energy ( $-48 \text{ KJ mol}^{-1}$ ).<sup>22-24</sup> Formaldehyde is a major volatile organic compound commonly found in the indoor environment emitted from building, furnishing materials and consumer products. Formaldehyde can also be found in gas phase and wastewater as pollutant which can be oxidized under UV radiation with  $\text{TiO}_2$ .<sup>25-28</sup> Formaldehyde is used in many industries as adhesive and glue manufacturing, production of synthetic resin, chemical and petroleum industry, paper industry, textile and wood processing, disinfectant and preservative production etc.<sup>29-31</sup> These industries generate wastewater having variable concentration of formaldehyde in the range of 3 to 10  $\text{g L}^{-1}$ .<sup>31-35</sup> Formaldehyde is toxic and has several health problems for humans. Thus, formaldehyde can seriously harm human health and impose ecological problems on the environment.<sup>31</sup>

$\text{TiO}_2$  photocatalyst has inherent electron donation ability for hydrogen production. Hence, the electron donor should have higher electron donation efficiency and stability than  $\text{TiO}_2$ . In common photocatalytic oxidation reactions,  $\text{TiO}_2$  catalyst shows very good results under UV light.<sup>36</sup> In a photodegradation process with  $\text{TiO}_2$ ,  $\text{O}_2$  acts as an electron donor and produce superoxide ion, which finally produces  $\text{OH}^\bullet$  radical.<sup>37</sup> If oxygen is present during photocatalytic water splitting it would compete with  $\text{H}^+$  ion for electron. Therefore, presence of oxygen in water splitting system is not advisable.

$\text{TiO}_2$  can also produce hydrogen from water but the efficiency of the process is not significant with different sacrificial agents as the system has considerable electron/hole recombination problem. Noble metal co-catalyst in trace amount on  $\text{TiO}_2$  catalyst surface has been used to reduce the electro/hole recombination.<sup>20</sup> Platinum loaded  $\text{TiO}_2$  catalyst has the highest potential for hydrogen generation as shown by Li et al.<sup>9</sup>

There are very limited studies conducted on formaldehyde as sacrificial agent for hydrogen generation.<sup>38</sup> Moreover, all studies primarily use UV lamps as light sources. In this present work, simulated solar light was used for degradation and simultaneous hydrogen generation from formaldehyde. The photocatalytic activity of  $\text{Pt/TiO}_2$  catalyst produced by solar photo-deposition method was studied under both visible and full (UV + Visible) solar irradiation. Effect of different basic parameters such as platinum content



on  $\text{TiO}_2$ , solution pH, initial concentration of formaldehyde, catalyst concentration, and light intensity were systematically studied to understand the qualitative and quantitative effects as well as overall mechanism of the process.

## 3.2 Materials and Methods

### 3.2.1 Photocatalyst Preparation

All reagents were of analytical grade and used without further treatment. Aeroxide  $\text{TiO}_2$  P25 (80-20% anatase to rutile) from Evonik Degussa Corporation, USA, was used as the catalyst. Formaldehyde solution (36.5%) from Sigma-Aldrich was used as the sacrificial agent. Hydrogen hexachloroplatinate (IV) solution (8 wt%) was purchased from Sigma-Aldrich Canada Ltd. Ultra pure water (18 M $\Omega$ ) was prepared from an in-house EASYPure<sup>®</sup> RODI system (Thermo Scientific, Canada).

Platinum loading of the  $\text{TiO}_2$ -P25 catalyst was performed by solar photo-deposition method following a modified version of previously reported by Chowdhury et al.<sup>39</sup>  $\text{TiO}_2$  powder was mixed with required volume of 0.08% hexachloroplatinic acid solution (corresponding to 0.25%, 1%, 1.3%, 1.8% nominal loading) and ethanol, and then it was sonicated for 5 min. A 90:10 volume ratio of water and ethanol was taken. Ethanol was used to supply enough sacrificial agents as hole ( $\text{h}^+$ ) scavenger to ensure complete reduction of Pt (IV). Then, the reaction mixture was placed under the solar simulator (AM 1.5G filter, 1-Sun) for 3 h under vigorous stirring. As time progressed, the solution turned off-white color. After filtering and washing with water, the powder was dried at 150 °C for 2 h and milled in a mortar.

### 3.2.2 Photocatalyst Characterizations

Phase composition and the degree of crystallinity of the catalyst were determined by X-ray diffraction (XRD). The XRD data were obtained using a Rigaku–MiniFlex II, powder diffractometer (Japan), using  $\text{CuK}\alpha$  ( $\lambda$  for  $\text{K}\alpha = 1.54059 \text{ \AA}$ ) over the desired 2 $\theta$  range with step width of 0.05°. DRS (diffuse reflectance spectra) were recorded on a Shimadzu UV-VIS-NIR spectrophotometer (UV-3600) equipped with an integrating sphere using  $\text{BaSO}_4$  as reference. Both absorbance and diffuse reflectance spectra were

recorded for all samples. Brunauer-Emmett-Teller (BET) specific surface areas of the photocatalysts were quantified using the N<sub>2</sub> adsorption method on a Micromeritics ASAP 2010 instrument. Before the measurement, the sample was pretreated at 473 K under vacuum for 1 hour. Transmission electron microscopic (TEM) study was performed with a Hitachi H-7000 electron microscope operating at 100 kV. Platinum content in the photocatalyst was determined using Agilent 7500cx inductively coupled plasma mass spectrometer (ICP MS).

### 3.2.3 Photocatalytic Reaction

Experiments were performed under both solar and visible light. The simulated solar light was generated using solar simulator (Model: SS1KW, Sciencetech, ON, Canada with a 1000-W Xe arc lamp and an AM 1.5G filter). It produces identical simulated sunlight (1-Sun) of 100 mW cm<sup>-2</sup> at full power that matches the global solar spectrum at sea level, as reported by the supplier. To generate only visible light, a UV cut-off filter (Omega optical, USA:  $\lambda > 420$  nm) was used. Spectral analysis of the irradiation from solar simulator was performed with StellarNet EPP2000C-25LT16 spectrometer.

Photocatalytic reactions were carried out in a gas tight 530 mL pyrex glass reactor with a flat transparent window at the top for illumination (illumination through 6.5 cm diameter). The catalyst powder (Pt/TiO<sub>2</sub>) was suspended in 100 mL of formaldehyde solution (40 ppm to 4600 ppm initial concentration) after pH adjustment with either 1:1 HCl or 0.1 M NaOH solution. The catalyst suspension was dispersed for 5 min in an ultrasonic bath and then the system was degassed by bubbling ultra pure nitrogen for about 40 min. Continuous stirring was performed using a magnetic stirrer (500 rpm). The photocatalyst was irradiated from the top with a solar simulator.

The gas sampling port in the reactor was sealed with a silicone rubber septum, and sampling was made intermittently through the septum during the experiments. The gas mixture was analyzed by Shimadzu GC 2014 with HeyeSep D packed column: 10 m length, 2 mm ID, 2  $\mu$ m film thickness and thermal conductivity detector (TCD). Ultra pure N<sub>2</sub> gas was used as carrier gas.

### 3.3 Results and Discussion

#### 3.3.1 Characterization

The specific surface area of  $\text{TiO}_2$  and platinum loaded  $\text{TiO}_2$  were  $50 \text{ m}^2 \text{ g}^{-1}$  and  $54 \text{ m}^2 \text{ g}^{-1}$  respectively. Therefore, platinum incorporation did not significantly affect the photocatalyst surface area. Pore size distribution data confirmed a microporous structure of the photocatalyst.

The ICP-MS analysis was performed with 0.25% (nominal) platinum loaded  $\text{TiO}_2$ . Results showed that the actual loading of platinum on  $\text{TiO}_2$  was 0.17%. The residual platinum in the filtrate was also confirmed through ICP-MS.

XRD of bare  $\text{TiO}_2$  P25 and platinum loaded (0.25%)  $\text{TiO}_2$  is shown in Figure 3.1. Inclusion of platinum metal onto  $\text{TiO}_2$  P25 did not alter the phase composition of the  $\text{TiO}_2$ . The XRD pattern in term of position and width of the peaks was similar to the standard crystal structure of  $\text{TiO}_2$ .<sup>37</sup>

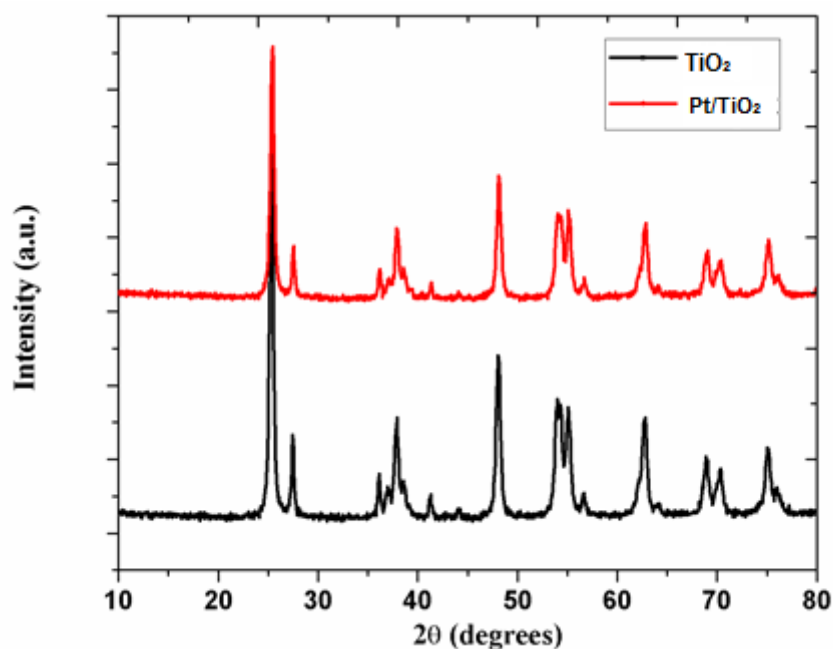


**Figure 3.1** XRD for  $\text{TiO}_2$  and  $\text{Pt/TiO}_2$  photocatalysts

Diffuse reflectance spectra (DRS) of  $\text{TiO}_2$  and platinum loaded  $\text{TiO}_2$  are shown in Figure 3.2. With the incorporation of Pt metal, the peak shifts slightly towards visible region, and the band-gap changed from 3.04 eV to 2.95 eV.

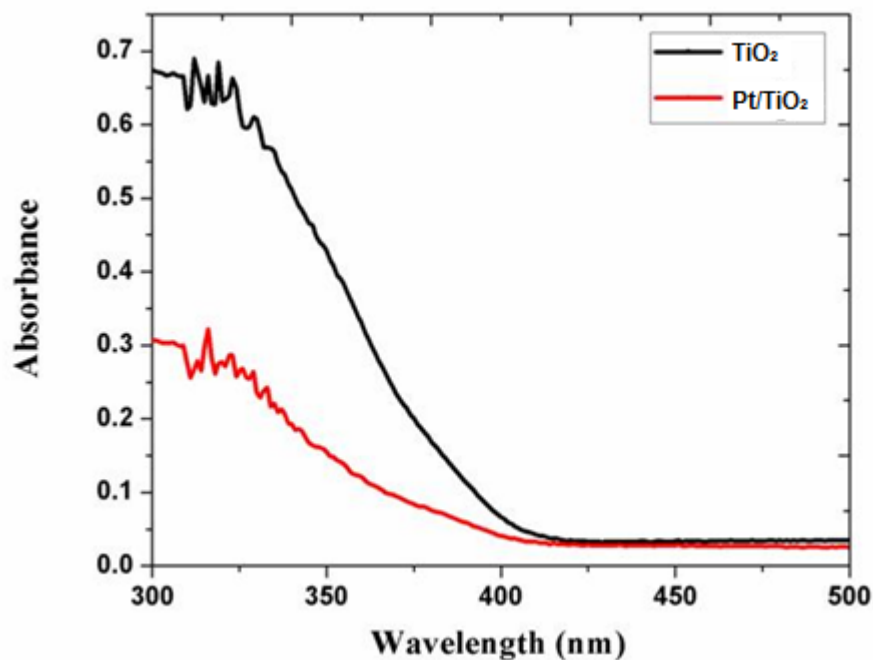


**Figure 3.2** DRS for  $\text{TiO}_2$  and  $\text{Pt/TiO}_2$  photocatalysts

TEM study of  $\text{Pt/TiO}_2$  indicated that platinum was mainly deposited on the surface of  $\text{TiO}_2$ . This was also confirmed by visual color change of the catalyst. Pure  $\text{TiO}_2$  has a milky white color, whereas  $\text{Pt/TiO}_2$  is gray colored. Figure 3.3 shows the dispersed Pt particles on  $\text{TiO}_2$  matrix.

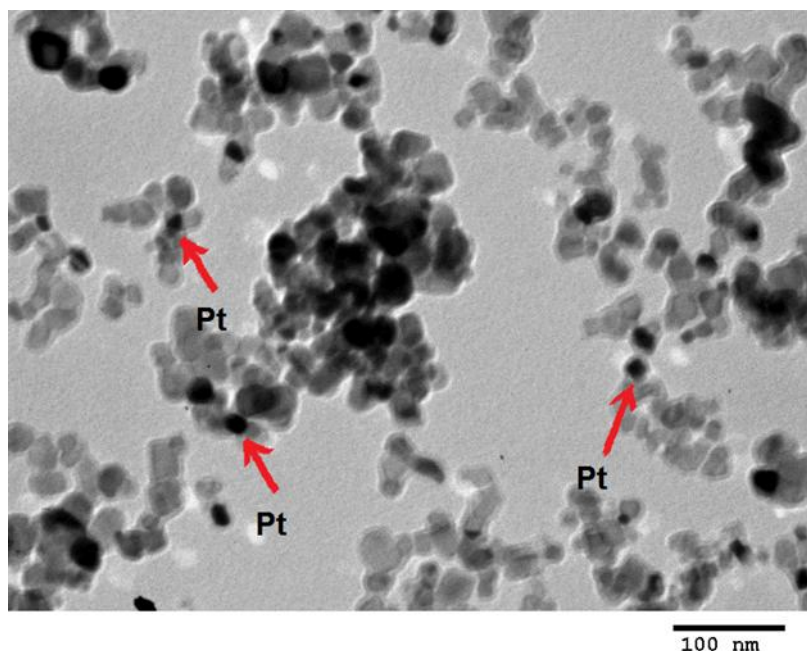


**Figure 3.3** TEM image of Pt/TiO<sub>2</sub> photocatalyst

### 3.3.2 Effect of platinum deposition on the photocatalytic activity of TiO<sub>2</sub>

Photocatalytic activity increased significantly with the incorporation of platinum metal on TiO<sub>2</sub> catalyst via solar photo-deposition method as shown in Figure 3.4. The rate of hydrogen generation increased from 0.34  $\mu\text{mol min}^{-1}$  to 2.28  $\mu\text{mol min}^{-1}$  with 1.0% nominal loading of platinum. In order to determine the optimum dose of platinum, the loading was varied between 0 and 1.8%. The rate of hydrogen generation increased rapidly up to 0.25% platinum loading but then gradually dropped with further increment. Although, platinum metal as a dopant slightly reduced the band-gap of TiO<sub>2</sub>, it could not initiate hydrogen generation under visible range of solar light. However, a significant enhancement of hydrogen generation was observed with the incorporation of platinum on TiO<sub>2</sub> surface under full solar light as shown in Table 3.1. Higher platinum loading beyond optimum dose (0.25%) showed negative effect on hydrogen generation due to the increases in  $e^-/h^+$  recombination sites.<sup>1</sup>

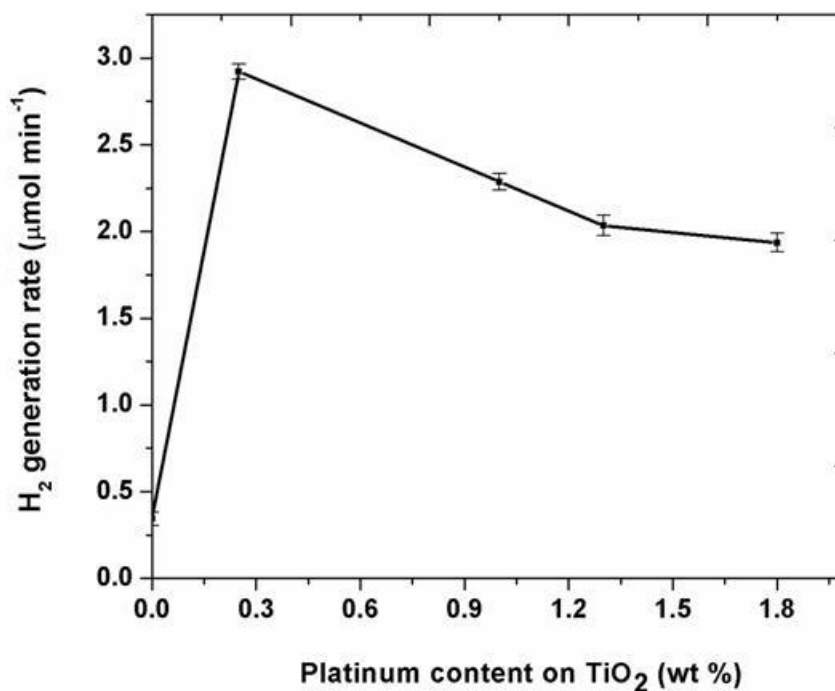


**Figure 3.4** Effect of platinum weight percent on TiO<sub>2</sub> on hydrogen generation rate. Experimental conditions: [HCHO] = 0.1332 M, pH 6.7, [TiO<sub>2</sub>/Pt] = 1 g L<sup>-1</sup>, I<sub>Solar</sub> = 100 mW cm<sup>-2</sup>, N<sub>2</sub> saturated, pre-sonicated).

According to Linsebigler et al.<sup>40</sup> dispersed Pt metal on TiO<sub>2</sub> surface forms a Schottky barrier at the metal/semiconductor interface. This actually reduces the electron/hole recombination rate, and thereby, improves charge separation efficiency. Platinum metal on TiO<sub>2</sub> surface basically “pumps” the photogenerated electron from TiO<sub>2</sub> to the adsorbed species, and thus hinders the possibility of their recombination with holes. In addition, platinum metal particle on TiO<sub>2</sub> improves reaction kinetics by decreasing the overpotential for hydrogen evolution.<sup>41, 42</sup>

**Table 3.1** Effect of Pt deposition on TiO<sub>2</sub> P25 under full solar light (UV+visible)

Photocatalyst	H <sub>2</sub> generation ( $\mu\text{mol min}^{-1}$ )
TiO <sub>2</sub> (P25)	$0.344 \pm 0.039$
Pt/ TiO <sub>2</sub> (0.25%)	$2.922 \pm 0.043$

### 3.3.3 Effect of catalyst concentration

To explore the effects of catalyst concentration on hydrogen generation, experiments were performed with Pt/TiO<sub>2</sub> (0.25%) catalyst, in which the catalyst loading was varied between 0.2 and 1.9 g L<sup>-1</sup>. In all cases, natural pH (6.7) was used and all other parameters such as initial concentration of formaldehyde, platinum content on TiO<sub>2</sub>, and light intensity were kept identical. Pt/TiO<sub>2</sub> has no visible light activity, and thus only solar-UV light was utilized during degradation of formaldehyde as well as generation of hydrogen. The rate of hydrogen production ( $r_1$ ) as a function of catalyst concentration (g L<sup>-1</sup>) is shown in Figure 3.5. The rate increased with increased catalyst concentration, but not linearly, in particular at low catalyst loadings, as would be expected.

The rate of hydrogen generation increased initially up to 1 g L<sup>-1</sup> then reached a plateau. At a low concentration of photocatalyst the photocatalytic reaction is mainly controlled by active sites which are accessible for adsorption of light and reactant.<sup>16, 43</sup> With gradual increment of photocatalyst slurry concentration, the solution turbidity increases, which thereby increases the UV light scattering. Moreover, the increased UV light scattering by suspended photocatalyst significantly reduces the UV transmission resulting in poor photocatalytic hydrogen generation. This observed phenomenon can be rationalized in terms of the availability of illuminated active sites on the TiO<sub>2</sub> surfaces, absorption and the penetration depths of light into the suspension. Hence, the rate of H<sub>2</sub> production per unit mass of catalyst ( $r_2$ ) decreases with the increase in catalyst loading<sup>44</sup>, as shown in Figure 3.5.

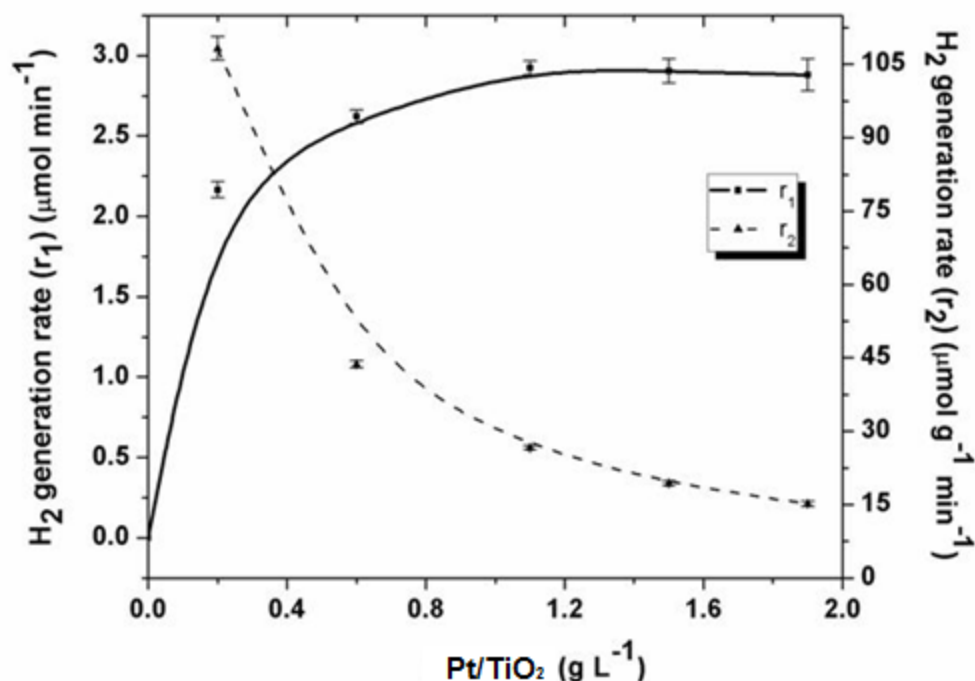
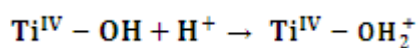
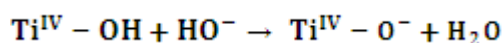


**Figure 3.5** Effect of catalyst concentration on the rate of hydrogen generation and rate per unit mass of catalyst. Experimental conditions: [HCHO] = 0.1332 M, pH 6.7, Pt (on TiO<sub>2</sub>) = 0.25%, I<sub>Solar</sub> = 100 mW cm<sup>-2</sup>, N<sub>2</sub> saturated, pre-sonicated.

### 3.3.4 Effect of initial pH of formaldehyde solution

Solution pH has a very significant influence in the photocatalytic reaction that takes place on Pt/TiO<sub>2</sub> surface. In aqueous slurry of TiO<sub>2</sub> the catalyst surface is embraced with plenty of hydroxyl groups and thus the ionization of TiO<sub>2</sub> is greatly affected by the solution pH.



The point of zero charge (pzc) of pure Degussa P25 TiO<sub>2</sub> is in between 5.6 and 6.8,<sup>37, 45</sup> which can be slightly altered by the presence of trace amount of platinum deposits as per Pichat.<sup>46</sup> Sun et al.<sup>47</sup> proposed plausible reaction mechanism for photocatalytic oxidation of gaseous formaldehyde in oxygen atmosphere where formation of superoxide anion or hydroxyl radical was mentioned as the heart of photo-oxidation process. In our case, the



reactions were performed in  $N_2$  atmosphere, which totally eliminates the possibility of formation of superoxide ions. Thus, the active species would be only hydroxyl radical produced by the reaction of positive hole ( $h^+$ ) with water and hydroxyl groups adsorbed on the  $TiO_2$  surface. During the photocatalytic oxidation of formaldehyde on the  $Pt/TiO_2$ , the formaldehyde is adsorbed on the hydroxyl groups on the catalyst surface via hydrogen bonding as shown in Figure 3.6. In presence of solar light irradiation, the formaldehyde is rapidly converted to formate species.

Under acidic pH, the degradation of formaldehyde producing hydrogen was lower compared to natural and alkaline pH (Figure 3.7). This could be explained by the fact of linkage of formaldehyde on  $TiO_2$  surface via hydrogen bonding, which was favored by negative surface charge of  $TiO_2$  at  $pH \geq 6.2$  (average point of zero charge of Degussa P25  $TiO_2$ ). The above phenomenon is quite opposite compared to the hydrogen generation from formic acid, acetic acid and oxalic acid,<sup>9</sup> where acidic pH is considered as the best pH for hydrogen generation.

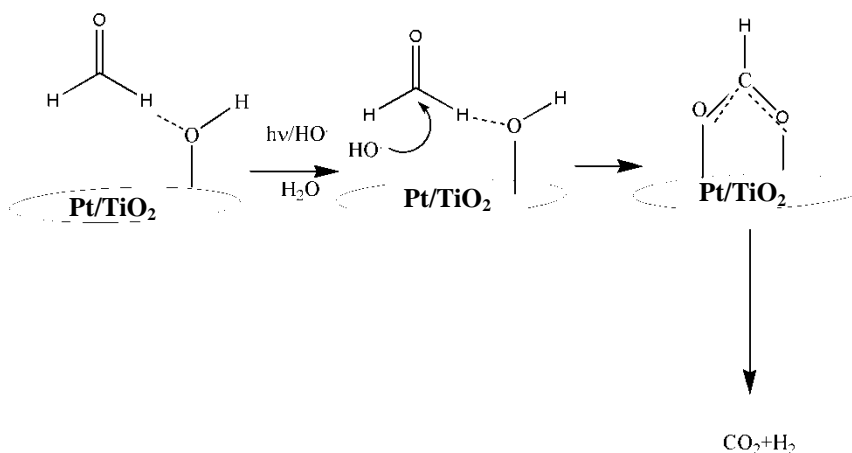


**Figure 3.6** Photocatalytic reaction of formaldehyde on  $Pt/TiO_2$  surface

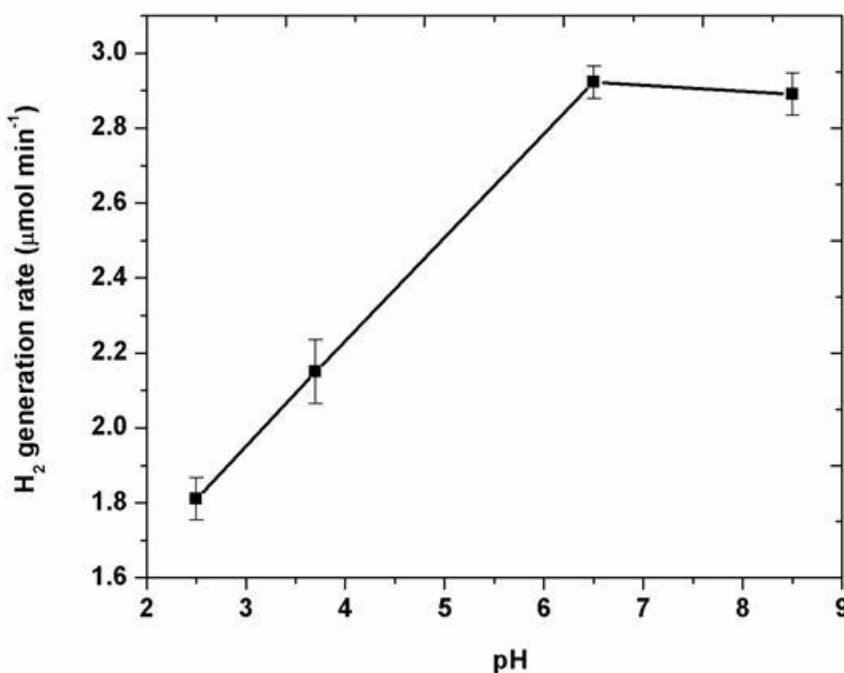


**Figure 3.7** Effect of initial pH of formaldehyde solution on the rate of hydrogen generation. Experimental conditions:  $[\text{HCHO}] = 0.1332 \text{ M}$ ,  $[\text{Pt}/\text{TiO}_2 (0.25\%)] = 1 \text{ g L}^{-1}$ ,  $I_{\text{Solar}} = 100 \text{ mW cm}^{-2}$ ,  $\text{N}_2$  saturated, pre-sonicated).

### 3.3.5 Effect of initial concentration of formaldehyde

Formaldehyde molecule reacts with the photo-generated hole and/or hydroxyl radical and degrades to different compounds. Thus, the concentration of formaldehyde continuously changes as reaction progresses. To determine the effect of initial concentration of formaldehyde on hydrogen generation, we have chosen 60 minutes time duration of experiment to compare the production of hydrogen as the change of reactant and/or product can be significant during this time interval. Figure 3.8 describes the effect of initial formaldehyde concentration on the rate of hydrogen evolution. A significant improvement of hydrogen generation was observed with an increase in the concentration of formaldehyde. However, the hydrogen generation rate was found almost independent beyond  $0.1332 \text{ M}$  ( $4000 \text{ mg L}^{-1}$ ) of formaldehyde concentration. The rate varied as a

function of formaldehyde concentration according to Langmuir-type equation as described below.<sup>9, 20</sup>

$$r = \frac{dC_{H_2}}{dt} = \frac{kKC_0}{1 + KC_0} \quad (\text{Eq.3.1})$$

Where,  $r$  is the initial rate of hydrogen generation,  $k$  is the reaction rate constant, and  $K$  is the adsorption constant of formaldehyde on to Pt/TiO<sub>2</sub> photocatalyst. By fitting the above equation with experimental data (Figure 3.8), the values obtained for  $k = 2.3598 \times 10^{-6}$  mol min<sup>-1</sup> and  $K = 17.73$  M<sup>-1</sup>.

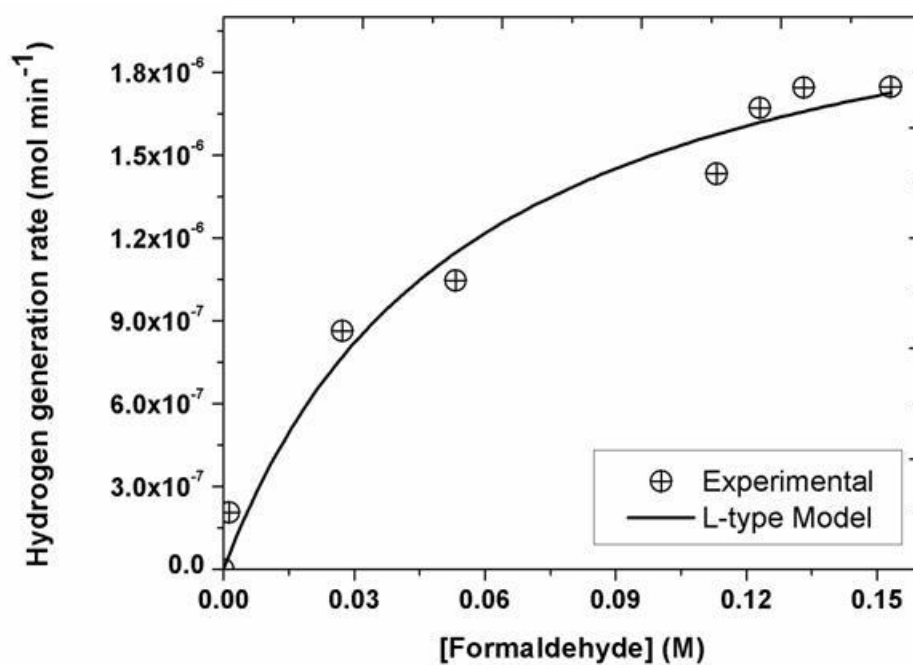


**Figure 3.8** Effect of initial concentration of formaldehyde on the rate of hydrogen generation. Experimental conditions: pH 6.7-7.2, [Pt/TiO<sub>2</sub>] = 1 g L<sup>-1</sup>,  $I_{\text{Solar}} = 100 \text{ mW cm}^{-2}$ , N<sub>2</sub> saturated, pre-sonicated.

### 3.3.6 Effect of light intensity

The main objective behind the optimization of different parameters such as photocatalyst dose, initial concentration of formaldehyde and/or the amount of noble metal (Pt) were to enhance the effective utilization of light energy. However, if the effect of light intensity on hydrogen is not wisely selected, a large fraction of photons will be wasted to heat up the system. This will also make a parameter optimization study ineffective.

We have studied the effect of solar light intensity in the range of  $30 \text{ mW cm}^{-2}$  to  $100 \text{ mW cm}^{-2}$ . The reaction rate constant  $k$ , followed power-law dependence on light intensities. The hydrogen generation rate constants were evaluated as a function of solar light intensity, keeping all other parameters fixed. In solar radiation, the data fitted well with the power law model ( $k(I) = aI^b$ ) with  $a = 1.4266 \times 10^{-6}$ ,  $b = 1.42$  and  $R^2 = 0.999$  (Figure 3.9). Therefore, there is a potential for further increase in the rate of hydrogen production with higher UV intensity. However, UV intensity in natural solar light is fixed and the upper bound of intensity was reached in our case.

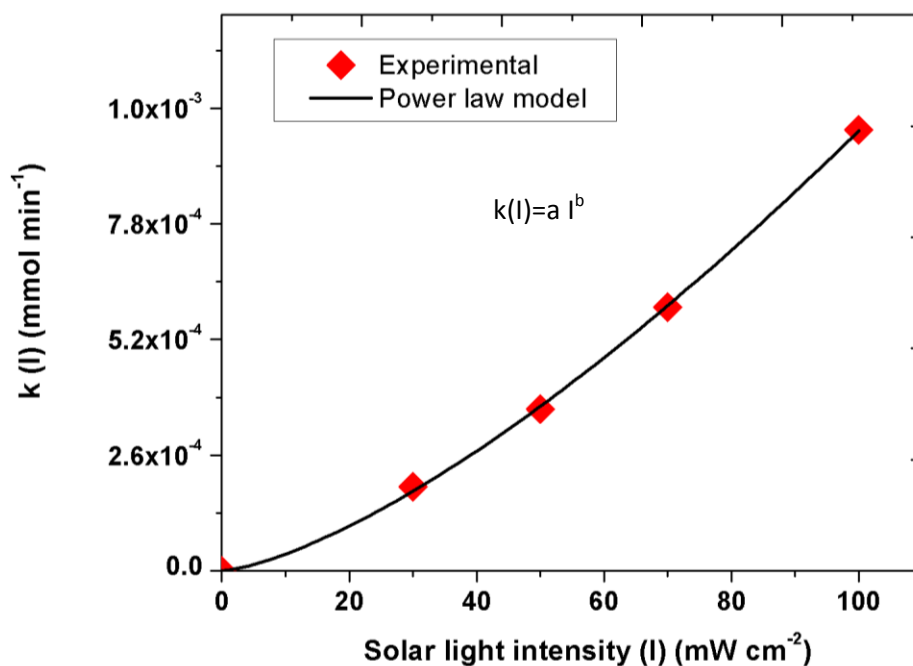


**Figure 3.9** Effect of light intensity on the rate of hydrogen generation. Experimental conditions:  $[\text{HCHO}] = 0.1332 \text{ M}$ ,  $\text{pH } 6.7$ ,  $[\text{Pt}/\text{TiO}_2 (0.25\%)] = 1 \text{ g L}^{-1}$ ,  $I_{\text{Solar}} = 100 \text{ mW cm}^{-2}$ ,  $\text{N}_2$  saturated, pre-sonicated).

### 3.4 Stability of Pt/ TiO<sub>2</sub> Photocatalyst for H<sub>2</sub> Generation

A short-term stability test was performed with TiO<sub>2</sub>/Pt photocatalyst under optimum reaction conditions. Experiments were conducted up to 12 h, and at every 3 h interval hydrogen gas was evacuated by nitrogen purging.<sup>48</sup> This enabled us to obtain the consecutive hydrogen generation rates (Figure 3.10). There was negligible change in hydrogen generation rate which implies reliable stability under the experimental periods.

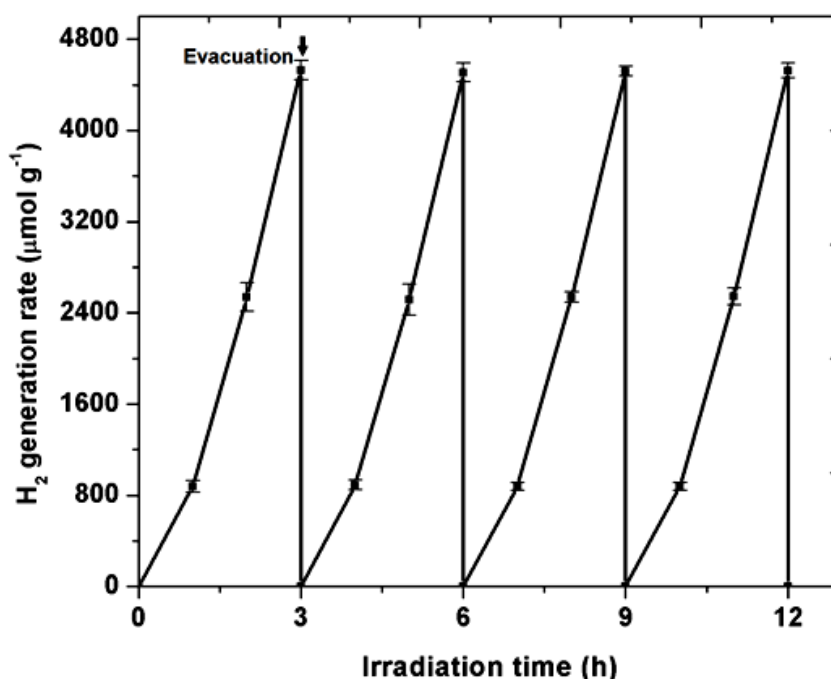
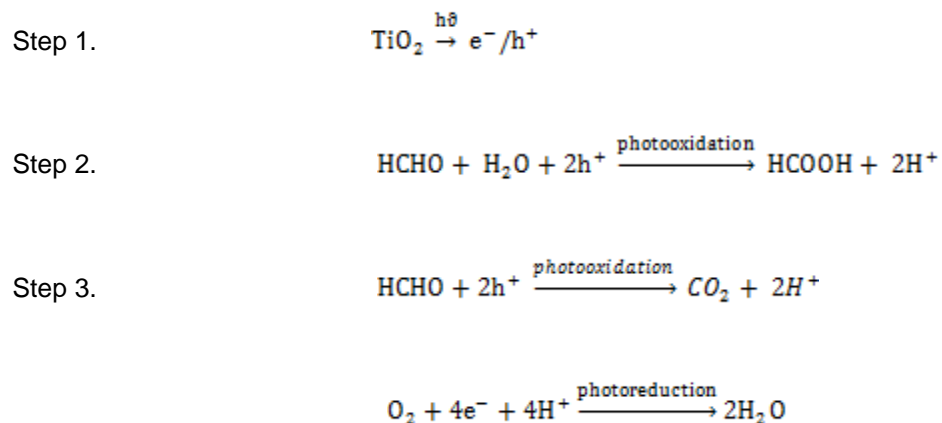


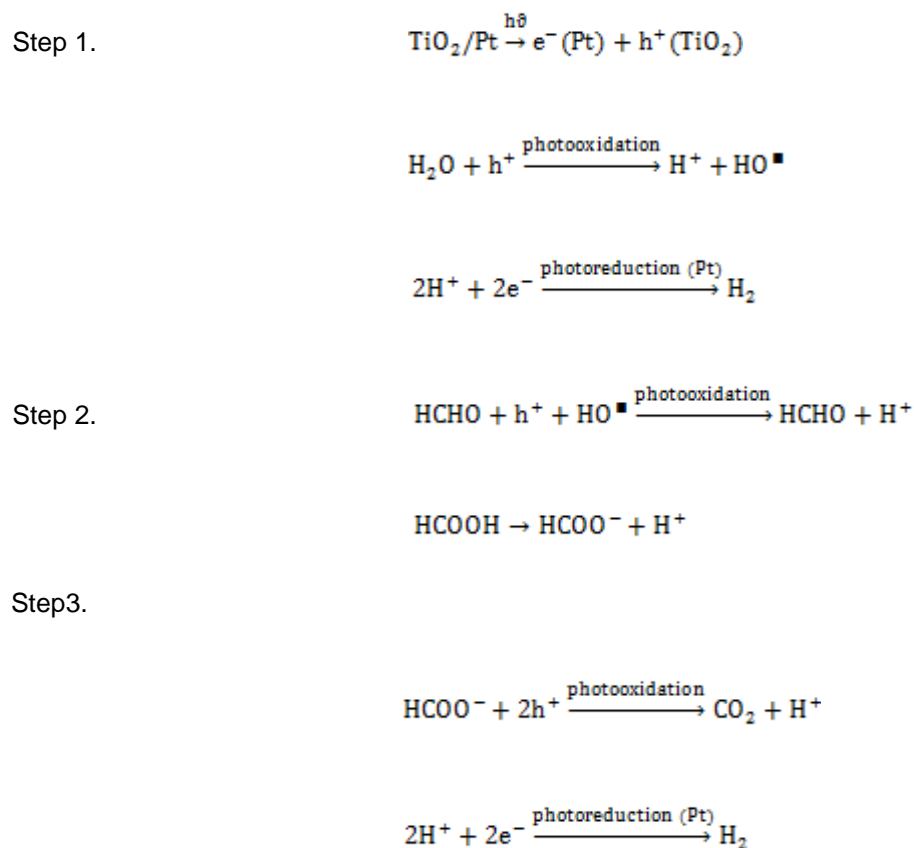
**Figure 3.10** Short term performance analysis for Pt/TiO<sub>2</sub> photocatalyst in repeated uses. Experimental conditions: [HCHO] = 0.1332 M, pH 6.7, [TiO<sub>2</sub>/Pt (0.25%)] = 1 g L<sup>-1</sup>, I<sub>Solar</sub> = 100 mW cm<sup>-2</sup>, N<sub>2</sub> saturated, pre-sonicated).

### 3.5 Reaction Mechanism

The major oxidative and reductive processes in the photodegradation of formaldehyde in aerated system with TiO<sub>2</sub> can be written as follows<sup>25</sup>:



In absence of -oxygen (nitrogen atmosphere) the reaction mechanism slightly differs with Pt/TiO<sub>2</sub> photocatalyst.<sup>49</sup>



### 3.6 Apparent Quantum Yield

Apparent quantum yield can be calculated using the formula stated by Shimidzu et al.<sup>50</sup>

$$\text{Apparent quantum yield, } \phi_{H_2}(\%) = \frac{(\text{number of reacted } e^- \text{ or } h^+)}{(\text{number of incident photons})} \times 100 \quad (\text{Eq.3.2})$$

Considering full solar spectrum (300-650 nm) the apparent quantum yield was 0.18 % and 1.24 % for TiO<sub>2</sub> and Pt/TiO<sub>2</sub> respectively. However, both the photocatalysts utilized only UV light range for photocatalytic reaction. Therefore, we recalculated the apparent quantum yield with only UV radiation portion (300-388) and found much higher apparent quantum yield of 1.6 % and 10.91 % for TiO<sub>2</sub> and Pt/TiO<sub>2</sub> respectively.

### 3.7 Conclusion

Results of the present study show that aqueous solution of formaldehyde under anaerobic conditions produce hydrogen using Pt/TiO<sub>2</sub> photocatalyst in solar radiation. With the incorporation of platinum metal onto TiO<sub>2</sub> the band gap energy lowered by 0.09 eV, but no photocatalytic activity was observed for hydrogen generation in visible light ( $\lambda > 420$  nm). Formaldehyde in solution act as electron donor and  $h^+/O_2$  scavenger, thereby suppress the  $e^-/h^+$  recombination and  $H_2/O_2$  backward reaction. Therefore, degradation of formaldehyde and hydrogen production takes place simultaneously with high apparent quantum yield (10.91%). Photocatalytic hydrogen generation from formaldehyde was very much influenced by solution pH, platinum content (wt%) on TiO<sub>2</sub>, catalyst concentration, light intensity, and initial formaldehyde concentration. The optimum conditions achieved for our study are: i)  $I_{\text{solar}} - 1$  sun, ii) platinum content – 0.25 wt %, iii) catalyst concentration – 1 g L<sup>-1</sup>, and iv) pH- neutral to alkaline. The proposed Langmuir-type model fits well with the experimental data for hydrogen generation at different initial concentration of formaldehyde.

### 3.8 References

- (1) Ni, M.; Leung, M. K. H.; Leung, D. Y. C.; Sumathy, K., A review and recent developments in photocatalytic water-splitting using  $\text{TiO}_2$  for hydrogen production. *Renew.Sust. Energ. Rev.* **2007**, 11 (3), 401.
- (2) Yoshida, M.; Takanabe, K.; Maeda, K.; Ishikawa, A.; Kubota, J.; Sakata, Y.; Ikezawa, Y.; Domen, K., Role and function of noble-metal/Cr-layer core/shell structure cocatalysts for photocatalytic overall water splitting studied by model electrodes. *J. Phys. Chem. C.* 2009, 113 (**23** ), 10151.
- (3) Maeda, K.; Domen, K., Photocatalytic water splitting: recent progress and future challenges. *J. Phys. Chem. Lett.* 2010, 1 (**18**), 2655.
- (4) Maeda, K., Photocatalytic water splitting using semiconductor particles: history and recent developments. *Journal of Photochemistry and Photobiology C: Photochemistry Reviews.* 2011, 12 (**4**), 237.
- (5) Townsend, T. K.; Browning, N. D.; Osterloh, F. E., Overall photocatalytic water splitting with  $\text{NiO}_x$  -  $\text{SrTiO}_3$  - a revised mechanism. *Energy Environ. Sci.* 2012, 5 (**11** ), 9543.
- (6) Garcia-Esparza, A. T.; Cha, D.; Ou, Y.; Kubota, J.; Domen, K.; Takanabe, K., Tungsten carbide nanoparticles as efficient cocatalysts for photocatalytic overall water splitting. *ChemSusChem.* 2013, 6 (**1** ), 168.
- (7) Wu, N. L.; Lee, M. S., Enhanced  $\text{TiO}_2$  photocatalysis by Cu in hydrogen production from aqueous methanol solution. *Int. J. Hydrogen Energy* **2004**, 29 (15), 1601.
- (8) Yasushi, T., Thermodynamics of water splitting, in energy carriers and conversion systems. In *Encyclopedia of Life Support Systems (EOLSS)*, Ohta., T., Ed. **2006**; pp 1-5.
- (9) Li, Y.; Lu, G.; Li, S., Photocatalytic hydrogen generation and decomposition of oxalic acid over platinized  $\text{TiO}_2$ . *Appl. Catal., A* **2001**, 214 (2), 179.



- (10) Primo, A.; Marino, T.; Corma, A.; Molinari, R.; Garcia, H., Efficient visible-light photocatalytic water splitting minute amounts of gold supported on nanoparticulate CeO<sub>2</sub> obtained by a biopolymer templating method. *J. Am. Chem. Soc.* 2011, 133, (18), 6930.
- (11) Gartner, F.; Losse, S.; Boddien, A.; Pohl, M-M.; Denurra, S.; Junge, H.; Beller, M., Hydrogen evolution from water/alcohol mixtures: effective in situ generation of an active Au/TiO<sub>2</sub> catalyst. *Chem Sub Chem.* 2012, 5 (3), 530.
- (12) Dang, H.; Dong, X.; Dong, Y.; Zhang, Y.; Hampshire, S., TiO<sub>2</sub> nanotubes coupled with nano-Cu(OH)<sub>2</sub> for highly efficient photocatalytic hydrogen production. *Int. J. Hydrogen Energy* 2013, 38 (5), 2126.
- (13) Liu, J.; Wen, S.; Zou, X.; Zuo, F.; Berau, G. J. O.; Feng, P., Visible-light responsive copper (II) borate photocatalysts with intrinsic midgap states for water splitting. *J. Mater. Chem. A.* 2013, 1 (5), 1553.
- (14) Sun, Y.; Sun, J.; Long, J. R.; Yong, P.; Chang, C. J., Photocatalytic generation of hydrogen from water using a cobalt pentapyridine complex in combination with molecular and semiconductor nanowire photosensitizers. *Chem. sci.* 2013, 4 ( ), 118.
- (15) Fan, X.; Lin, B.; Liu, H.; he, Li.; Chen, Y.; Gao, B., Remarkable promotion of photocatalytic hydrogen evolution from water on TiO<sub>2</sub>-pillared titanoniobate. *Int. J. Hydrogen Energy.* 2013, 38 (2), 832.
- (16) Badawy, M. I.; Ghaly, M. Y.; Ali, M. E. M., Photocatalytic hydrogen production over nanostructured mesoporous titania from olive mill wastewater. *Desalination* **2011**, 267 (2), 250.
- (17) Patsoura, A.; Kondarides, D. I.; Verykios, X. E., Photocatalytic degradation of organic pollutants with simultaneous production of hydrogen. *Catal. Today* **2007**, 124 (3), 94.
- (18) Patsoura, A.; Kondarides, D. I.; Verykios, X. E., Enhancement of photoinduced hydrogen production from irradiated Pt/TiO<sub>2</sub> suspensions with simultaneous degradation of azo-dyes. *Appl. Catal., B* **2006**, 64 (3), 171.

- (19) Hashimoto, K.; Kawai, T.; Sakata, T., Photocatalytic reactions of hydrocarbons and fossil fuels with water. Hydrogen production and oxidation. *J. Phys. Chem.* **1984**, 88 (18), 4083.
- (20) Li, Y.; Xie, Y.; Peng, S.; Lu, G.; Li, S., Photocatalytic hydrogen generation in the presence of chloroacetic acids over Pt/TiO<sub>2</sub>. *Chemosphere* **2006**, 63 (8), 1312.
- (21) Sakata, T., Photocatalysis of irradiated semiconductor surfaces: its application to water splitting and some organic reactions. *J. Photochem.* 1985, 29(1-2), 205.
- (22) Lin, W-C.; Yang, W-D.; Huang, I-L.; Wu, T-S.; Chung, Z-J., Hydrogen production from methanol/water photocatalytic decomposition using Pt/TiO<sub>2-x</sub>N<sub>x</sub> catalyst. *Energy & Fuels*, 2009, 23 (**4**), 2192.
- (23) Choi, H-J.; Kang, M., Hydrogen production from methanol/water decomposition in a liquid photosystem using the anatase structure of Cu loaded TiO<sub>2</sub>. *Int. J. Hydrogen Energy*, 2007, 32 (**16**), 3841.
- (24) Wu, N-L.; Lee, M-S., Enhanced TiO<sub>2</sub> photocatalysis by Cu in hydrogen production from aqueous methanol solution. *Int. J. Hydrogen Energy*, 2004, 29 (**15**), 1601.
- (25) Noguchi, T.; Fujishima, A.; Sawunyama, P.; Hashimoto, K., Photocatalytic degradation of gaseous formaldehyde using TiO<sub>2</sub> film. *Environ. Sci. Technol.* **1998**, 32 (23), 3831.
- (26) Lam, R. C. W.; Leung, M. K. H.; Leung, D. Y. C.; Vrijmoed, L. L. P.; Yam, W. C.; Ng, S. P., Visible-light-assisted photocatalytic degradation of gaseous formaldehyde by parallel-plate reactor coated with Cr ion-implanted TiO<sub>2</sub> thin film. *Sol. Energ. Mat. Sol. C.* **2007**, 91 (1), 54.
- (27) Ching, W. H.; Leung, M.; Leung, D. Y. C., Solar photocatalytic degradation of gaseous formaldehyde by sol-gel TiO<sub>2</sub> thin film for enhancement of indoor air quality. *Sol. Energy* **2004**, 77 (2), 129.

- (28) Zhang, X.; Liu, Q., Visible-light-induced degradation of formaldehyde over titania photocatalyst co-doped with nitrogen and nickel. *Appl. Surf. Sci.* **2008**, 254 (15), 4780.
- (29) Jarusutthirak, C.; Sangsawang, K.; Mattaraj, S.; Jiraratananon, R., Treatment of Formaldehyde-Containing Wastewater Using Membrane Bioreactor. *J. Environ. Eng.* 2012, 138 (3 ), 265.
- (30) Hidalgo, A.; Lopategi, A.; Prieto, M.; Serra, J. L.; Llama, M.J., Formaldehyde removal in synthetic and industrial wastewater by *Rhodococcus erythropolis* UPV-1. *Appl Microbiol Biotechnol* 2002, 58 (2 ), 260.
- (31) Glancer-Soljan, M.; Soljan, V.; Dragicevic, T. L.; Cacic, L., Aerobic degradation of formaldehyde in wastewater from the production of melamine resins. *Food Technol. Biotech.* 2001, 39 (3), 197.
- (32) Moussavi, G.; Yazdanbakhsh, A.; Heidarizad, M., The removal of formaldehyde from concentrated synthetic wastewater using  $O_3/MgO/H_2O_2$  process integrated with the biological treatment. *J. Hazard. Mater.* **2009**, 171 (1-3), 907.
- (33) Oliveira, S. V. W. B.; Moraes, E. M.; Adorno, M. A. T.; Varesche, M. B. A.; Foresti, E.; Zaiat, M., Formaldehyde degradation in an anaerobic packed-bed bioreactor. *Water Research* 2004, 38 (7), 1685.
- (34) Campos, J. L.; Sanchez, M.; Mosquera-Corral, A.; Mendez, R.; Lema, J.M., Coupled BAS and anoxic USB system to remove urea and formaldehyde from wastewater. *Water Research* 2003, 37 (14 ), 3445.
- (35) Zoutberg, G.R.; De Been, P., The Biobed® EGSB (Expanded Granular Sludge Bed) system covers shortcomings of the Upflow Anaerobic Sludge Blanket reactor in the chemical industry. *Wat. Sci. Tech.* 1997, 35 (10), 183.
- (36) Chen, D.; Ray, A. K., Photodegradation kinetics of 4-nitrophenol in  $TiO_2$  suspension. *Water Res.* **1998**, 32 (11), 3223.
- (37) Chowdhury, P.; Moreira, J.; Gomaa, H.; Ray, A. K., Visible Solar Light Driven Photocatalytic Degradation of Phenol with Dye-sensitized  $TiO_2$ : Parametric and Kinetic Study. *Ind. Eng. Chem. Res.* **2012**, 51 (12), 4523.

- (38) Li, Y.; Lu, G.; Li, S., Photocatalytic production of hydrogen in single component and mixture systems of electron donors and monitoring adsorption of donors by in situ infrared spectroscopy. *Chemosphere* **2003**, 52 (5), 843.
- (39) Chowdhury, P.; Gomaa, H.; Ray, A. K., Factorial design analysis for dye-sensitized hydrogen generation from water. *Int. J. Hydrogen Energ.* **2011**, 36 (21), 13442.
- (40) Linsebigler, A. L.; Lu, G.; Yates Jr, J. T., Photocatalysis on TiO<sub>2</sub> surfaces: principles, mechanisms, and selected results. *Chem. Rev.* 1995, 95 (3), 735.
- (41) Duonghong, D.; Borgarello, E.; Graetzel, M., Dynamics of light-induced water cleavage in colloidal systems. *J. Am. Chem. Soc.* 1981, 103 (16), 4685.
- (42) Bard, A. J., Design of semiconductor photoelectrochemical systems for solar energy conversion. *J. Phys. Chem.* 1982, 86 (2), 172.
- (43) Daskalaki, V. M.; Kondarides, D. I., Efficient production of hydrogen by photo-induced reforming of glycerol at ambient conditions. *Catal. Today* 2009, 144 (1-2), 75.
- (44) Karakitsou., K. E.; Verykios., X. E., Influence of Catalyst Parameters and Operational Variables on the Photocatalytic Cleavage of Water. *J. Catal.* 1992, 134(2), 629.
- (45) Lu, M. C.; Roam, G. D.; Chen, J. N.; Huang, C. P., Factors affecting the photocatalytic degradation of dichlorvos over titanium dioxide supported on glass. *J. Photoche. Photobio. A* 1993, 76 (1), 103.
- (46) Pichat, P., Surface properties, activity and selectivity of bifunctional powder photocatalysts. *New J. Chem.* 1987, 11, 135.
- (47) Sun, S.; Ding, J.; Bao, J.; Gao, C.; Qi, Z.; Li, C., Photocatalytic oxidation of gaseous formaldehyde on TiO<sub>2</sub>: an in situ DRIFTS study. *Catal. Lett.* 2010, 137 (3), 239.

(48) Fan, W; Lai, Q; Zhang, Q, Wang, Y., Nanocomposites of  $\text{TiO}_2$  and reduced graphene oxide as efficient photocatalysts for hydrogen evolution. J. Phys. Chem.C 2011, 115 (21), 10694.

(49) Miwa, T.; Kaneco, S.; Katsumata, H.; Suzuki, T.; Ohta, K.; Chand Verma, S.; Sugihara, K., Photocatalytic hydrogen production from aqueous methanol solution with  $\text{CuO}/\text{Al}_2\text{O}_3/\text{TiO}_2$  nanocomposite. Int. J. Hydrogen Energ. 2010, 35 (13), 6554.

(50) Shimidzu, T.; Iyoda, T.; Koide, Y., An advanced visible-light-induced water reduction with dye-sensitized semiconductor powder catalyst. J. Am. Chem. Soc. 1985, 107 (1), 35.

## Chapter 4

### 4 In-situ Grown Molybdenum Sulfide on $\text{TiO}_2$ for Solar Photocatalytic Hydrogen Generation

#### 4.1 Introduction

The increasing global energy demand, the depletion of fossil fuels and the significant environmental pollution caused by burning of fossil fuels have been known as various energy challenges worldwide.<sup>1</sup> Thus, developing clean, renewable and low-carbon containing alternative energy sources is extremely important in overcoming these challenges.<sup>2,3</sup> Solar energy is the most abundant, available and renewable energy source. Conversion of solar energy into chemical energy has been recognized to be a promising way to store solar energy for long-term energy demands and thereby, effectively address the world's energy problems.<sup>4</sup> Moreover, Hydrogen is known to be a good substitute for fossil fuels as it has high energy capacity and water is the only by-product of its combustion.<sup>1,3</sup> Hence, It is highly desirable to produce hydrogen through an environmental friendly pathway, in which renewable sources such as solar energy are being utilized. Photocatalytic hydrogen production from water using a semiconductor photocatalyst has attracted remarkable attention in recent years.<sup>1,5-7</sup>

However, Photocatalytic processes currently suffer from significant barriers associated with the available semiconductors used as a photocatalyst. Poor activation of the semiconductor and rapid recombination of photo-generated electron-hole pairs are the two main challenges that decrease the efficiency of the photocatalytic hydrogen generation.<sup>8</sup> To date, there have been significant efforts to address these issues by developing an effective photocatalyst.<sup>9,10</sup> It is been proved that co-catalyst is a vital element to accelerate the photocatalytic hydrogen generation, particularly by enhancing the separation of the photo-generated charges and by providing highly active sites with the low activation potentials for  $\text{H}_2$  generation.<sup>7,11</sup>

Noble metals such as Pt and Pd are known to be effective co-catalysts.<sup>6,12</sup> However, their scarcity and high cost prevent their application to be viable in large scale process

application.<sup>2,5,13</sup> Therefore, it is vital to exploit noble-metal free co-catalysts other than noble-metals that are inexpensive and earth-abundant.<sup>5,13</sup> Molybdenum sulfide ( $\text{MoS}_2$ ) has been recently proved to be a promising alternative for precious metals. It has been reported to be an active co-catalyst for  $\text{H}_2$  generation while it is environmental friendly, cheap and abundant.<sup>4,6,13,14</sup>

Zong et al.<sup>7</sup> reported that  $\text{MoS}_2$  loaded on CdS could significantly enhance the photocatalytic performance of CdS and its activity is even higher than Pt loaded CdS. Gao et al.<sup>15</sup> could fabricate a  $\text{MoS}_2$  quantum dots-graphene- $\text{TiO}_2$  with improved photocatalytic properties. The solvo-thermal method was used in their study. However, the synthesis methods in these reports mostly require high temperature process, long-term hydrothermal process and also presence of  $\text{H}_2\text{S}$ , which prevent these methods to be simply applicable.<sup>16–18</sup>

Recently, photo-deposition method has been proposed to load  $\text{MoS}_2$  on semiconductors.<sup>3,5,11</sup> Zong et al.<sup>19</sup> reported an in-situ photo-reduction process in a noble metal-free organic dye (EB) sensitized system to obtain  $\text{MoS}_x$ . This simple method exhibited high efficiency for photocatalytic hydrogen generation. Xu et al.<sup>20</sup> in their recent work loaded  $\text{MoS}_x$  on g- $\text{C}_3\text{N}_4$  with an in-situ approach during the photocatalytic hydrogen production.  $(\text{NH}_4)_2\text{MoS}_4$  and EB were used as precursor and sensitizer, respectively. EB-sensitized  $\text{MoS}_x$ -g- $\text{C}_3\text{N}_4$  (EB- $\text{MoS}_x$ -g- $\text{C}_3\text{N}_4$ ) exhibited the higher activity and stability than both EB-sensitized g- $\text{C}_3\text{N}_4$  (EB-g- $\text{C}_3\text{N}_4$ ) and EB-sensitized  $\text{MoS}_x$  (EB- $\text{MoS}_x$ ).<sup>20</sup> Kanda et al.<sup>13</sup> applied a photo-deposition technique to form  $\text{MoS}_2$  nano-crystals on  $\text{TiO}_2$  and ethanol was used as a reducing agent. In aqueous solution of formic acid the  $\text{MoS}_2/\text{TiO}_2$  system exhibited a high photocatalytic activity for hydrogen generation. In that study, UV light irradiation was used for the photocatalytic reaction to take place. To the best of our knowledge, dye-sensitized photo-deposition approach has not been studied to load  $\text{MoS}_x$  on  $\text{TiO}_2$  under solar light irradiation.

Developing new materials for photocatalytic processes, in particular, hydrogen generation has been extensively investigated. There are, however, only a few systematic studies based on robust experimental design and statistical analysis to determine the

effect of the process factors and to optimize them.<sup>21–24</sup> Factorial design is an experimental design methodology which enables us to screen the effect of selected operating factors, to evaluate the interaction effects of two or more factors and to determine the significant factors that affect the response with minimum number of experiments. Moreover, optimal conditions can be obtained by central composite design (CCD), known as a powerful statistical method of optimization. This approach is quicker and more reliable compared to the ‘single-variable-at-a-time’ (SVAT) approach, which varies one of the factors while keeping others constant and also suffers from ignoring the interaction effect of the various factors.<sup>23,25</sup>

Herein, in-situ photo-deposition method was applied using  $(\text{NH}_4)_2\text{MoS}_4$  as a precursor. Molybdenum sulfide was loaded on  $\text{TiO}_2$  by an in-situ photocatalytic hydrogen production over a dye synthesized photocatalytic process using Eosin Y (EY) as a photosensitizer and tri-ethanolamine (TEOA) as an electron donor. The proposed noble metal-free photocatalytic system exhibited high efficiency for  $\text{H}_2$  evolution. Furthermore, a factorial design of experiments was used to conduct the experiments in order to explore the impact of various operating parameters, i.e., TEOA, EY,  $(\text{NH}_4)_2\text{MoS}_4$  concentrations and solution pH on the response factor, which is hydrogen production after 3h of solar irradiation. Moreover, a central composite matrix was used to explore the response surfaces and determine the optimal values for the process parameters to achieve the highest amount of hydrogen. To the best of our knowledge, the statistical analysis has not been applied to in-situ photo-deposition of  $\text{MoS}_x$  on  $\text{TiO}_2$  for photocatalytic hydrogen generation. The possible mechanism for  $\text{H}_2$  generation in the applied reaction system was also proposed.

## 4.2 Materials and Methods

### 4.2.1 Photocatalyst Preparation

All reagents were analytical grade and were used without further treatment. Aeroxide  $\text{TiO}_2$  P25 from Evonik Degussa Corporation was used as semiconductor. Eosin Y dye (99.0%), tri-ethanolamine (98.0%) and  $(\text{NH}_4)_2\text{MoS}_4$  were purchased from Sigma Aldrich Canada Ltd.



TiO<sub>2</sub>-MoS<sub>x</sub> was prepared by an in situ photo-deposition method under solar light. The photocatalytic reaction was carried out for 3 h as described in section 2.3. The solid was recovered by centrifuge and washed with distilled water and anhydrous ethanol. Then, it was dried at 60 °C for 7 h and milled to obtain the product, TiO<sub>2</sub>-MoS<sub>x</sub>.

#### 4.2.2 Photocatalyst Characterizations

Structural analyses of the samples were carried out by X-ray powder diffractometer (Rigaku-Ultima IV ,XRD) with a scintillation counter detector, using a Cu K $\alpha$  source of X-rays ( $\lambda$ = 1.54 Å) over the desired 2 $\theta$  range with step width of 0.02 degree. UV spectra of the samples were recorded by a UV-Vis-NIR spectrophotometer (Shimadzu UV-3600) equipped with an integrating sphere using BaSO<sub>4</sub> as reference. The X-ray photoelectron spectroscopic (XPS) analyses were carried out with a Kratos Axis Ultra spectrometer using a monochromatic Al K $\alpha$  source (15mA, 14kV).

#### 4.2.3 Photocatalytic Reaction

Photocatalytic reactions were performed in a gas tight Pyrex reactor (5.5 cm in diameter, 6.3 cm in height) with a transparent window at the top for illumination. The reactions were carried out under simulated solar light. Solar simulator (model SS1KW, Sciencetech, Ontario, Canada, with a 1000 W Xe arc lamp and an AM 1.5G filter) was used to generate simulated solar light. It produces identical simulated 1-sun irradiance of 100 mW/cm<sup>2</sup> at full power that matches the global solar spectrum at sea level, as reported by the supplier. Spectral analysis of the irradiation from the solar simulator with a Stellar Net EPP2000C-25LT16 spectrometer for UV–vis–near-IR spectroscopy showed 6.5% UV, 64.5% visible, and the rest near-IR light. Typically, 0.1g TiO<sub>2</sub> was suspended in 100 mL solution containing tri-ethanolamine (TEOA, 10 v %) as an electron donor, EY (7.8× 10<sup>-4</sup> M) as a sensitizer and (NH<sub>4</sub>)<sub>2</sub>MoS<sub>4</sub> (2.27× 10<sup>-4</sup> M) as a precursor. The solution pH was adjusted with either 1:1 HCl or 0.1M NaOH. pH measurement was performed using the 780-Metrohm Ltd. pH meter. The catalyst was dispersed for 5min in an ultrasonic bath. The suspension was then degassed by bubbling ultra-pure nitrogen gas for 30 min. The photocatalytic reaction was carried out for 3h under solar light illumination. Continuous stirring was performed using a magnetic stirrer (500 rpm) during the reaction. The gas sampling port in the reactor was sealed with a silicone rubber septum, and

sampling was made intermittently through the septum during the experiments. Hydrogen was analyzed by gas chromatography (Shimadzu GC 2014, HeyeSep D packed column: 10 m length, 2 mm ID, 2 mm film thickness and thermal conductivity detector (TCD)).

## 4.2.4 Experimental Design and Statistical Analysis

### 4.2.4.1 Full Factorial Design

A  $2^4$  full factorial design matrix was defined for four independent variables with their values and coded levels given in Table 4.1. In statistical analysis, the real values of the independent variables are converted to dimensionless values known as coded values. In this work, the Design-Expert® software (Trial version 9.0.3 Stat-Ease, Inc. Minneapolis, USA), was used to generate the design matrix, to perform the statistical analysis and to obtain ANOVA (Analysis of variance) table for further interpretation. Full factorial design matrix, and the corresponding response factor are given in Table 4.2. An empirical model and its coefficients were obtained by regression analysis. Analysis of variance (ANOVA) was used to evaluate the significance of the terms in the model at a 95% confidence interval using their corresponding p-values. The adequacy of fitting to the regression model was also examined by evaluating determination coefficient ( $R^2$ ) and adjusted coefficient ( $R_{adj}^2$ ) of the model. These two values indicate the variability in the response that can be explained by the fitted model.

**Table 4.1** Independent variables and their levels chosen for full factorial design

Variable (unit, factor)	Coded Levels	
	Low value(-1)	High value(+1)
TEOA Concentration (v%, A)	1	10
Eosin Y Concentration (M, B)	$4 \times 10^{-4}$	$4 \times 10^{-3}$
(NH <sub>4</sub> ) <sub>2</sub> MoS <sub>4</sub> Concentration (M, C)	$1 \times 10^{-4}$	$1 \times 10^{-3}$
Initial Solution pH (D)	4	11

#### 4.2.4.2 The path of steepest ascent

The next step in statistical analysis to move towards the optimum response is using the method of steepest ascent. In this method, the value and sign of the main effects are used to find the right path along which the response value increases. Usually, the center of the design region in factorial design is considered as the origin of the path of steepest ascent.<sup>26–28</sup> A set of experiments is performed along this direction until the location corresponding to the maximum response value is reached, where no more increase in response is observed afterward. This maximum point is in the optimum region.

#### 4.2.4.3 Central Composite Design

RSM (Response surface methodology) was used to describe the behaviour of the response in the optimum region. Central composite design (CCD) as one of the methods of RSM was applied to optimize the response factor (Hydrogen produced after 3h solar irradiation). The results obtained from full factorial design and the path of steepest ascent confirmed that the concentration of TEOA and Eosin Y have the negative effect on the response; therefore, these two variables were kept at their lowest level in this section. Solution pH and concentration of  $(\text{NH}_4)_2\text{MoS}_4$  are the two independent variables that are considered in CCD. The levels of independent variables were coded as shown in Table 4.5. The obtained experimental results shown in Table 4.6 were fitted to an empirical quadratic model used for optimum prediction.

### 4.3 Results and Discussion

#### 4.3.1 Characterization

The XRD patterns of  $\text{TiO}_2$  and  $\text{TiO}_2\text{-MoS}_x$  are displayed in Figure 4.1. All diffraction peaks related to anatase and rutile phase of  $\text{TiO}_2$  are present in the both XRD patterns. There is no significant difference between the two curves indicating that growing  $\text{MoS}_x$  on  $\text{TiO}_2$  did not alter the phase composition of  $\text{TiO}_2$ . However, no diffraction peaks ascribed to  $\text{MoS}_x$  were detected in  $\text{TiO}_2\text{-MoS}_x$  curve, due to its low content.<sup>4,29</sup>

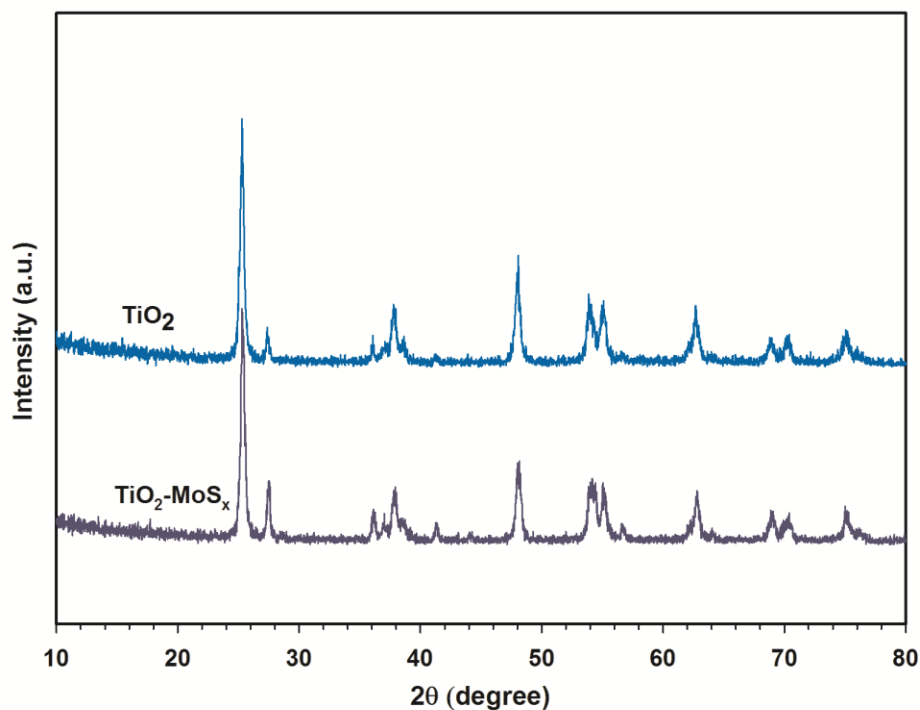


**Figure 4.1** XRD Patterns of  $\text{TiO}_2$  and  $\text{TiO}_2\text{-MoS}_x$

The chemical states of Mo and S in  $\text{TiO}_2\text{-MoS}_x$  sample were determined by XPS analysis. The survey scan of  $\text{TiO}_2\text{-MoS}_x$  confirms the presence of Mo, S, Ti and O in the sample, as shown in Figure 4.2(a). The high resolution XPS spectrum in Figure 4.2(b) shows the characteristic peaks at 233.13 and 230 eV, which are attributed to the binding energy of Mo 3d<sub>3/2</sub> and Mo 3d<sub>5/2</sub> for the +4 oxidation state. There are also two other peaks at 235.13 and 232 eV, corresponding to the binding energy of the Mo 3d<sub>3/2</sub> and Mo 3d<sub>5/2</sub> orbits in the +6 oxidation state. The presence of Mo<sup>+6</sup> can be explained by the possible formation of  $\text{MoO}_3$  on the surface of the  $\text{TiO}_2$ .<sup>5</sup> The XPS spectrum of S 2p is also displayed in Figure 4.2(c). Two peaks for S 2p<sub>3/2</sub> and S 2p<sub>1/2</sub> are observed at 162.79 and 163.97 eV, indicating the existence of  $\text{S}^{2-}$ , while the binding energies of 162.32 and 161.14 eV for S 2p<sub>1/2</sub> and 2p<sub>3/2</sub> reveal the existence of bridging  $\text{S}_2^{2-}$  or apical  $\text{S}_2^{2-}$ .<sup>5,20</sup> XPS results indicate that  $\text{MoS}_4^{2-}$  is reduced to  $\text{MoS}_x$  ( $x > 2$ ), which is in good agreement with the previous reports.<sup>19,20</sup>

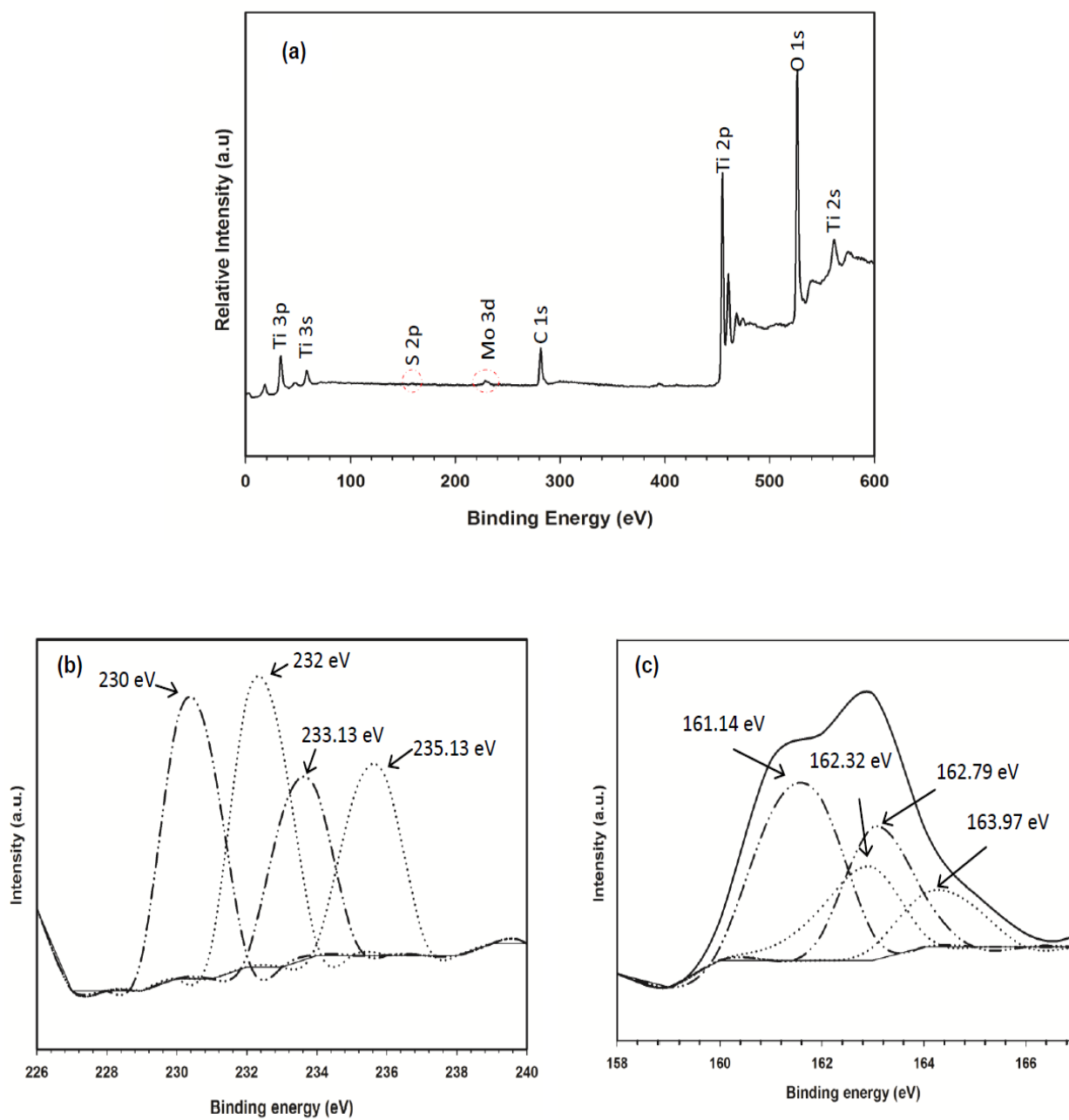


**Figure 4.2** XPS Spectrum of  $\text{TiO}_2\text{-MoS}_x$  (a), High resolution XPS spectra of Mo (b) and S 2p (c)

UV-vis diffuse reflectance absorption spectra of samples  $\text{TiO}_2$  and  $\text{TiO}_2\text{-MoS}_x$  are depicted in Figure 4.3. By incorporation of  $\text{MoS}_x$ , the absorption edge of the sample shifts toward the longer wavelength in visible range, which is beneficial for photocatalytic process. This shift is due to strong optical absorption of black  $\text{MoS}_x$  and its narrow band gap.<sup>30,31</sup>

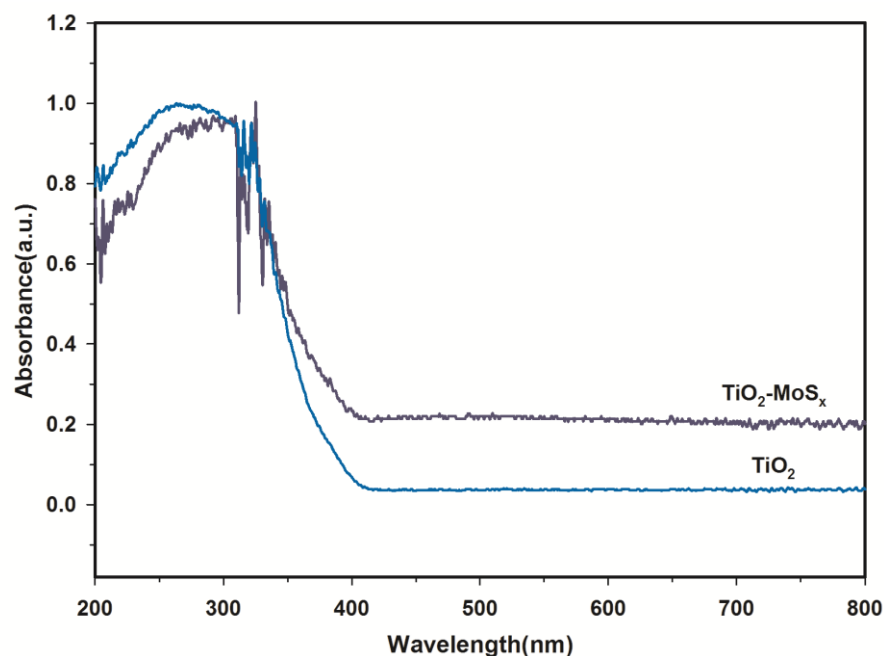


**Figure 4.3** UV- Vis absorption spectra of  $\text{TiO}_2$  and  $\text{TiO}_2\text{-MoS}_x$

#### 4.3.2 Photocatalytic Performance of $\text{TiO}_2\text{-MoS}_x\text{-EY-TEOA}$ reaction system

In-situ Photocatalytic hydrogen generation reaction was performed in a four-component system containing  $\text{TiO}_2$ , Eosin-Y(EY) as the photo-sensitizer, tri-ethanolamine as electron donor, and  $(\text{NH}_4)_2\text{MoS}_4$  as the precursor for molybdenum sulfide. Time course of in-situ photocatalytic hydrogen generation from this reaction system is shown in Figure 4.4. The control experiments were also performed to confirm the significance of each component in this reaction system. The system exhibits very low activity during 3h solar irradiation, with only eliminating a single component from the reaction system. The

activity for hydrogen generation in  $\text{TiO}_2\text{-MoS}_x\text{-EY-TEOA}$  system is approximately 10 times as high as that in other reaction systems. This indicates that the presence of co-catalyst is essential for increasing the activity of  $\text{TiO}_2$ . In addition, dye sensitization enhances the solar photo-activity of  $\text{TiO}_2$  to the great extent.

After in-situ photo-deposition reaction completed, the solid powder was recovered by centrifuge and was dispersed in a reaction solution containing fresh EY and TEOA. The photocatalytic reaction was again performed for 3h under solar irradiation to measure the photo-activity of the obtained material. Figure 4.4(f) illustrates that the recovered  $\text{TiO}_2\text{-MoS}_x$  is an active catalyst for solar  $\text{H}_2$  generation and  $\text{MoS}_x$  can play as a co-catalyst to enhance the electron-hole separation resulting in improved photocatalytic  $\text{H}_2$  generation. However, the activity observed for the solution containing the recovered catalyst is less than that of containing the  $(\text{NH}_4)_2\text{MoS}_4$  precursor. The similar result was reported previously in a different reaction system.<sup>19</sup>

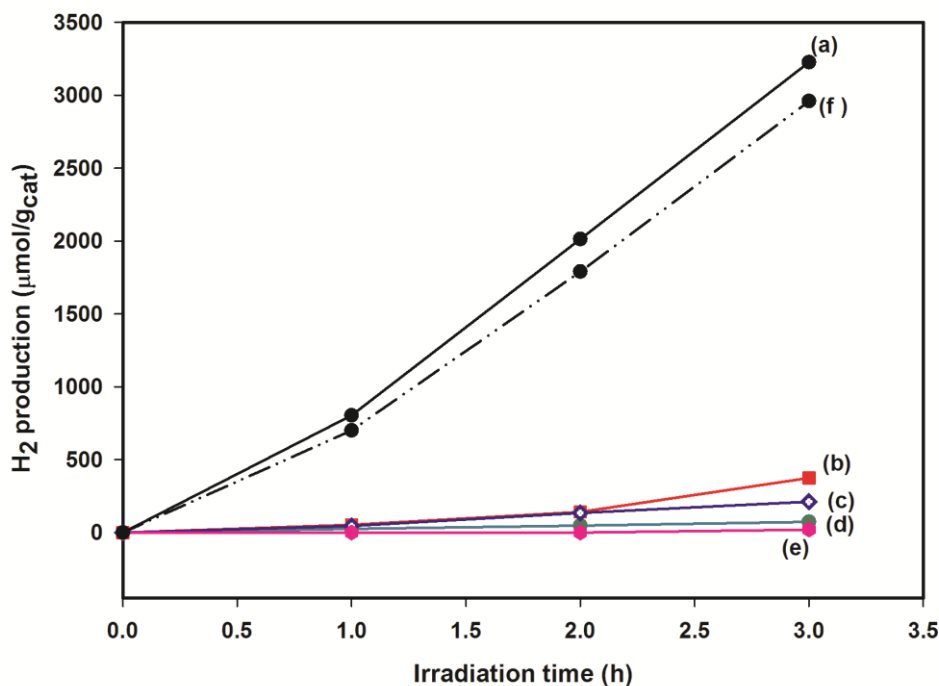


**Figure 4.4** Time course of hydrogen generation from (a) four components system:  $\text{TiO}_2$ (100 mg), EY( $7.8 \times 10^{-4}$  M), TEOA( 10 v%),  $(\text{NH}_4)_2\text{MoS}_4$  ( $2.27 \times 10^{-4}$  M),  $I_{\text{solar}}=100 \text{ mW/cm}^2$  (b) without EY , (c) without  $(\text{NH}_4)_2\text{MoS}_4$  , (d) without EY and  $(\text{NH}_4)_2\text{MoS}_4$ , (e) without TEOA, (f) Recovered  $\text{TiO}_2\text{-MoS}_x$  obtained by in situ photo-deposition

In order to investigate the effect of various experimental parameters such as concentration of EY, TEOA,  $(\text{NH}_4)_2\text{MoS}_4$  and solution pH, a systematic statistical analysis including full factorial design for screening, the path of steepest ascent and central composite design for optimization were performed that are discussed in detail in next section.

### 4.3.3 Statistical Analysis

#### 4.3.3.1 Full Factorial Design Analysis

A set of sixteen experiments was conducted using a two levels four factors full factorial design. Table 4.1 and 4.2 list the levels of the independent variables and the design matrix for all the experiments conducted. In addition, the actual responses with their replicates are collected in Table 4.2. The regression analysis based on the least square method was applied to obtain an empirical model. The model predicts the response variable as a function of the four independent factors.

The coefficients of the model represent the weight of the contribution of the factors on the response. In other words, each coefficient corresponds to the mean change in the response for one unit of change in one factor while keeping other factors constant. The significance of each variable was assessed using a Student t-test. The regression coefficients and their corresponding F-value and P-value are provided in Table 4.3. The large F-value and Low p-values ( $p < 0.05$ ) suggest that the corresponding model term is significant and has great contribution toward the response variable at the 95% confidence level.<sup>25,26</sup> Therefore, results shown in Table 4.3 reveal that all the four variables and their interaction terms have a significant impact on the produced hydrogen amount as the response, with the solution pH (term D) to have the highest contribution among all other terms.



**Table 4.2** Full factorial design matrix for four factors

and the corresponding responses

Run	Design Matrix				Response	
	A	B	C	D	H <sub>2</sub> ( $\mu\text{mol} / \text{g}_{\text{cat}}$ )	
					Replicate1	Replicate2
1	–	–	–	–	68	74
2	+	–	–	–	401	410
3	–	+	–	–	558	566
4	+	+	–	–	296	286
5	–	–	+	–	0	40
6	+	–	+	–	218	130
7	–	+	+	–	0	70
8	+	+	+	–	0	38
9	–	–	–	+	435	429
10	+	–	–	+	82	94
11	–	+	–	+	44	70
12	+	+	–	+	27	26
13	–	–	+	+	4200	4216
14	+	–	+	+	462	460
15	–	+	+	+	1350	998
16	+	+	+	+	295	306

**Table 4.3** ANOVA for the proposed model (Full Factorial)

Source	Coefficient Estimate	Sum of Squares(SS)	F-Value	P-Value
Model		7189.93	80.97	< 0.0001
Constant	17.10			
A	-3.75	450.99	71.11	< 0.0001
B	-3.07	302.00	47.62	< 0.0001
C	3.07	302.35	47.67	< 0.0001
D	5.49	964.54	152.08	< 0.0001
AB	0.39	4.90	0.77	0.3916
AC	-2.67	228.26	35.99	< 0.0001
AD	-5.49	963.75	151.95	< 0.0001
BC	-2.41	185.11	29.19	< 0.0001
BD	-3.47	385.73	60.82	< 0.0001
CD	8.80	2478.97	390.85	< 0.0001
ABC	1.55	77.14	12.16	0.0028
ABD	4.06	528.43	83.32	< 0.0001
ACD	-3.14	315.91	49.81	< 0.0001
BCD	0.24	1.84	0.29	0.5973
Lack of Fit		12.94	2.18	0.1591

\*R-Squared= 0.98, Adj R-Squared= 0.97, Pred R-Squared=0.95

A, B, C, D are as defined in Table 4.1.

Furthermore, a Pareto plot was used to identify the importance of the factors as shown in Figure 4.5. This plot is a useful tool that displays the absolute values of the effects of all the terms involved in the fitted model. A reference line is also drawn in this plot that represents the border to identify the significant terms past this line.<sup>32</sup> In this study, A, B, C, D, AC, AD, BC, BD, CD, ABC, ABD and ACD are significant model terms.

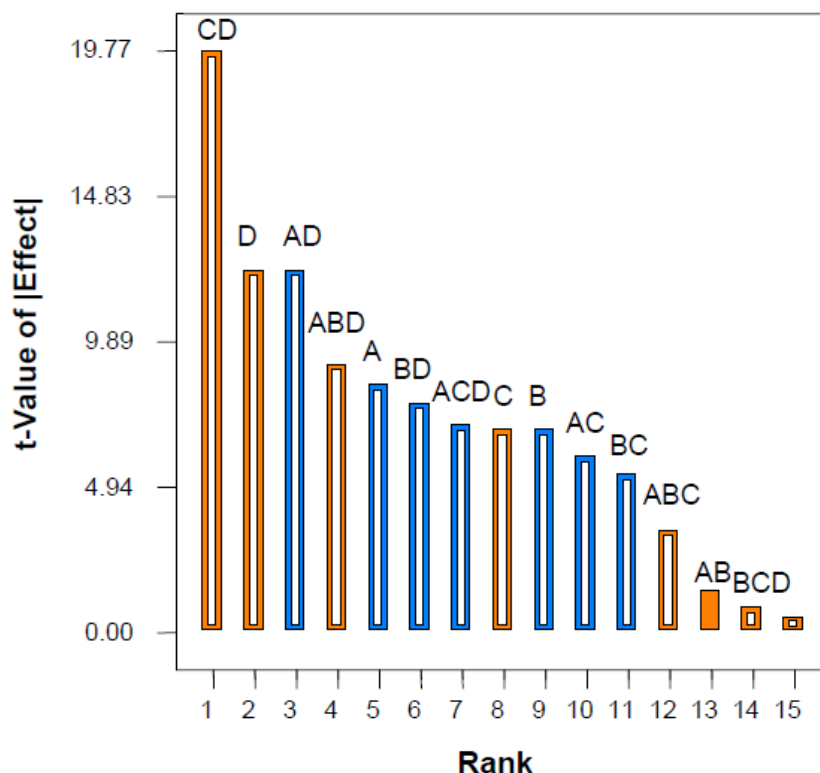


**Figure 4.5** Pareto Chart for full factorial design

The ANOVA of the model implies that the model is statistically significant for the observed data in the design space. The model F-value is 80.97 and its P-value is  $<0.0001$ , which translate that there is only 0.01% chance for the model F-value to occur due to noise. The lack of fit (LOF) test was also performed to determine if the model can successfully describe the observed data.<sup>33</sup> The P-value of the LOF is  $>0.05$ , which confirms that the LOF is not statistically significant at a 95% confidence interval. This is desirable as it can affirm the good fit of the model. Furthermore, the coefficient of determination ( $R^2$ ) is high,  $R^2=0.98$ , indicating the adequacy of the model and that the

fitted model can successfully predict the response within the experimental range. It is also in good agreement with the adjusted  $R^2$ ,  $R^2_{adj}=0.97$  and predicted  $R^2$ ,  $R^2_{pred}=0.95$ . Figure 4.6 shows the predicted values of the response versus the actual values that were observed in the experiments.

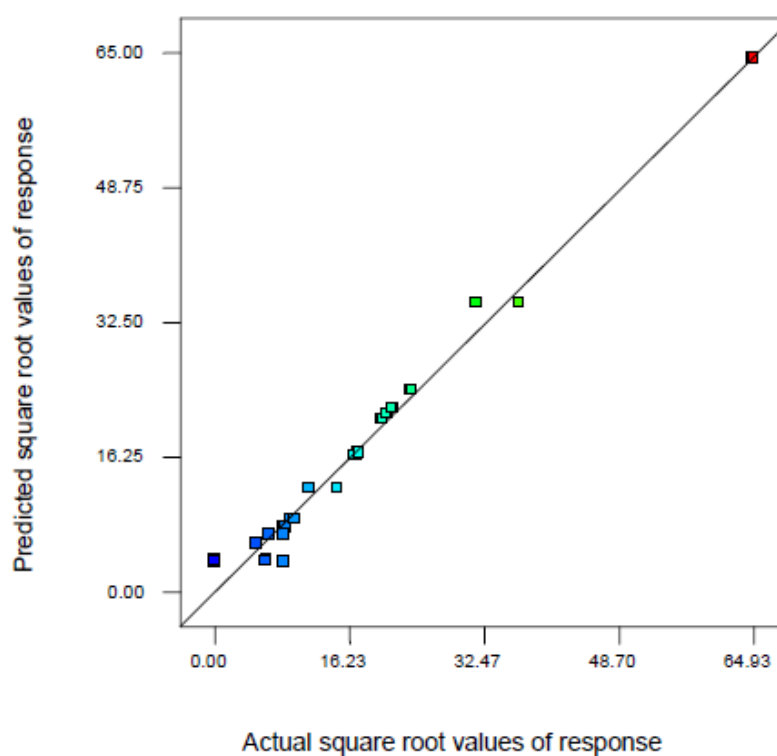


**Figure 4.6** Predicted vs. Actual square root values of response ( $H_2$ :  $\mu\text{mol/g}_{\text{cat}}$ )

(Full Factorial Design)

One of the important assumptions for the statistical analysis is that the data of the experiments follow a normal distribution.<sup>32</sup> The normal probability plot of the residuals, as depicted in Figure 4.7, is a tool to determine if the model satisfies this assumption. As it is clear from Figure 4.7, all the data points are close to a straight line, indicating the errors are normally distributed.

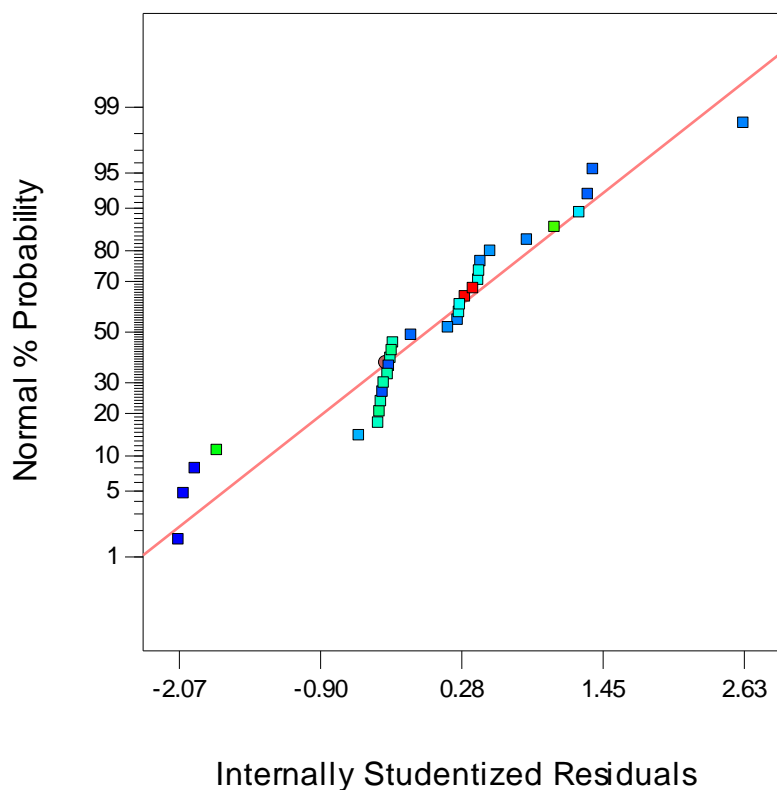


**Figure 4.7** Normal probability plot of the studentized residuals  
(full factorial design)

However, in cases where this assumption is not satisfied, one possible option is to apply a proper transformation to the data, thereby design a new model that has main aspects of the original model and also satisfies all the assumptions.<sup>34,35</sup> Figure 4.8 provides box-cox plot which can be helpful to calculate the best power law transformation. “Lambda” is a symbol of the power applied to the response values. The red lines indicate the 95% confidence interval surrounding the Lambda value. If this interval includes the current Lambda, then no transformation is required or the current transformation is satisfactory.<sup>34</sup> In this particular case, root square transformation (Lambda=0.5) was required for the model to satisfy the normality assumption. All the reported results and figures in this section are related to the model after applying power transformation.

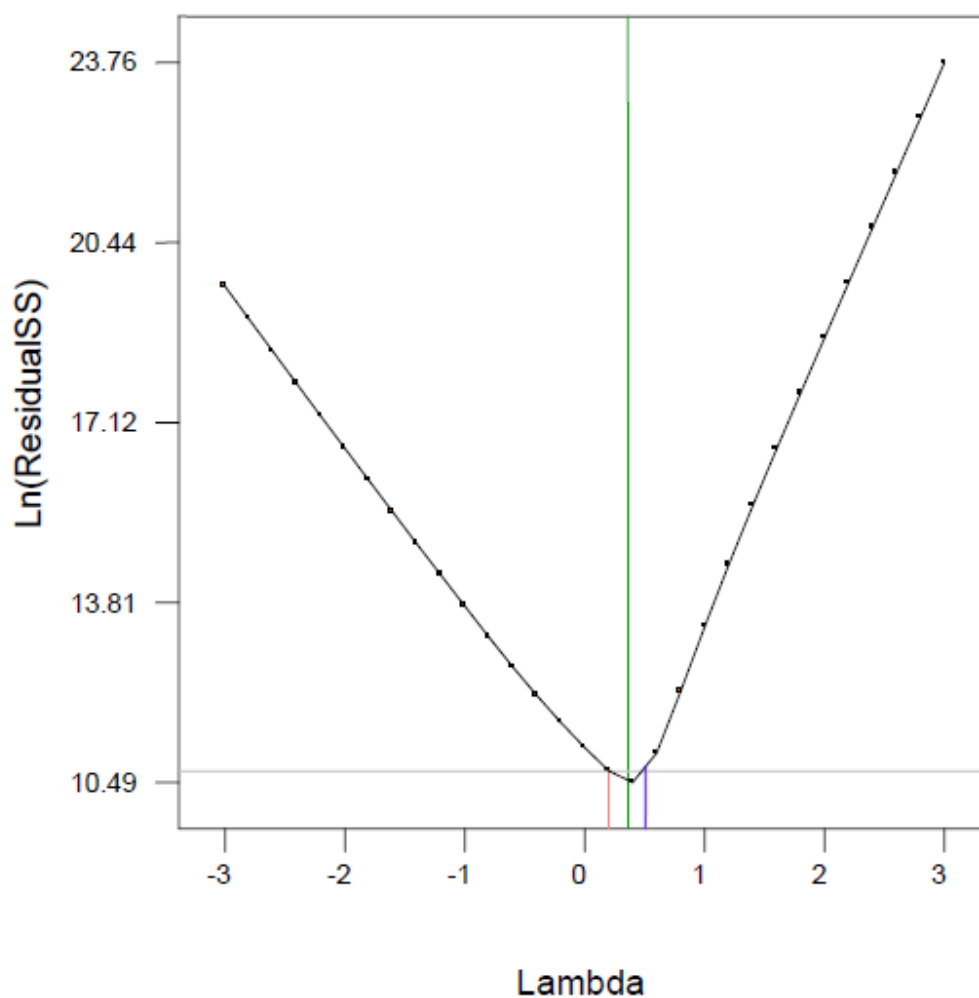


**Figure 4.8** Box-Cox plot for power transform

#### 4.3.3.2 The Path of Steepest Ascent Analysis

The steepest ascent was used to determine the next set of experiments toward the optimum point. (Details are explained in experimental methods). Table 4.4 provides the directions and the increments that the variables were changed as well as the results of the experiments. The results clearly show that the hydrogen production increases when the TEOA concentration as well as Eosin-Y concentration decrease, while  $(\text{NH}_4)_2\text{MoS}_4$  concentration and pH increase. After the third experiment along the path, further changes

of the parameters cannot provide higher value of the response. The highest response value is achieved in the third location; therefore, this point is in the vicinity of the optimum and is chosen for further optimization.

**Table 4.4** Experimental design of the steepest ascent and the results

Run	Coded variables				Real variables			Response	
	A	B	C	D	TEOA (v%)	EY(M)	(NH <sub>4</sub> ) <sub>2</sub> MoS <sub>4</sub> (M)	pH	H <sub>2</sub> ( μmol /gcat )
Center	0	0	0	0	5.5	0.0022	0.0006	7.5	929
S-1	-0.25	-0.20	0.20	0.27	4.4	0.0018	0.0006	8.5	1449
S-2	-0.5	-0.41	0.41	0.55	3.3	0.0015	0.0007	9.4	2743
S-3	-1	-0.82	0.82	1.10	1.0	0.0007	0.0009	11.3	4279
S-4	-1.1	-0.90	0.90	1.21	0.6	0.0006	0.0010	11.7	4098

#### 4.3.3.3 Central Composite Design and Response Surface Analysis

Central composite design for the two factors was performed. This design includes a full 2<sup>2</sup> full factorial design with 4 cubic points, 4 axial points and augmented with 5 replicates of the center point. The experimental design and results are depicted in Table 4.5 and 4.6.

**Table 4.5** Independent variables and their levels chosen for central composite design

Variable (unit, factor)	Coded Levels				
	-1.4	-1	0	+1	+1.4
(NH <sub>4</sub> ) <sub>2</sub> MoS <sub>4</sub> Concentration (M, C)	4.94× 10 <sup>-4</sup>	6.53× 10 <sup>-4</sup>	1.04× 10 <sup>-3</sup>	1.42× 10 <sup>-3</sup>	1.58× 10 <sup>-3</sup>
Initial Solution pH (D)	10.3	10.5	11	11.5	11.7

\*EY= 4 × 10<sup>-4</sup>, TEOA= 1v%

**Table 4.6** CCD matrix for two factors and the corresponding responses

Run	Design Matrix		Response $H_2(\mu\text{mol/g}_{\text{cat}})$
	C	D	Actual
1	-1	-1	3134.96
2	1	-1	4069.83
3	-1	1	1010.34
4	1	1	2792.47
5	-1.4	0	1962.96
6	1.4	0	3894.72
7	0	-1.4	4347.32
8	0	1.4	544.124
9	0	0	4199.99
10	0	0	4216.66
11	0	0	4286.42
12	0	0	5142.36
13	0	0	3931.4

The experimental results were fitted with a quadratic equation, expressed as follow in terms of actual variables.

$$H_2(\mu\text{mol/g}_{\text{cat}}) = -4.2 \times 10^5 - 21.4 [(\text{NH}_4)_2\text{MoS}_4] + 79263.76\text{pH} - 6.97 [(\text{NH}_4)_2\text{MoS}_4]^2 - 3754.67 \text{pH}^2$$

(Eq 4.1)



The results for statistical analysis of the model are given in table 4.7. The low P-value (0.0003) and high F-value (22.91) of the model suggest that the model is a significant fit. In addition, the lack of fit of the F-value is not significant, which translates that the model can be successfully used for prediction. The high value of coefficient of determination ( $R^2=0.94$ ) expresses the goodness of the fit. In addition,  $R^2$  is in close agreement with the corresponding adjusted  $R^2$  ( $R^2_{adj}=0.90$ ), which confirms that the model is sufficient to describe the observed data within the experimental range. Figure 4.9 shows the predicted values of the response versus the corresponding observed data. Figure 4.10 illustrates the normal probability of the residuals, indicating that the errors are normally distributed.

**Table 4.7** ANOVA for Quadratic Model (CCD)

Source	Coefficient Estimate	F-Value	P-Value
Model		22.91	0.0003
Constant	4355.37		
C	681.12	19.33	0.0032
D	-1097.56	50.19	0.0002
CD	211.81	0.93	0.3659
$C^2$	-697.11	17.61	0.0041
$D^2$	-938.67	31.92	0.0008
Lack of Fit		0.78	0.5628

\*R-Squared= 0.94, Adj R-Squared= 0.90, Pred R-Squared=0.79

C, D are as defined in Table 4.5.

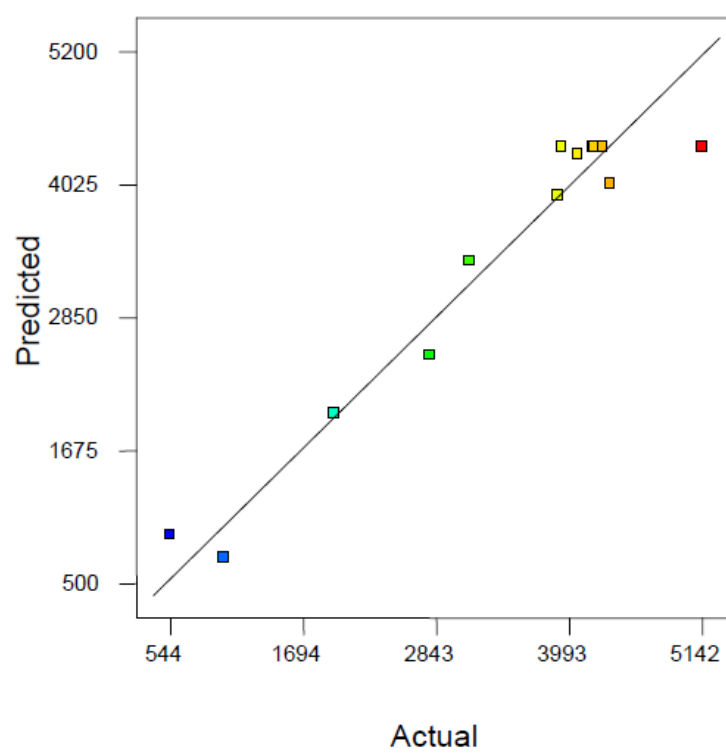


**Figure 4.9** Predicted vs. Actual values of response for CCD ( $H_2$ :  $\mu\text{mol/g}_{\text{cat}}$ )

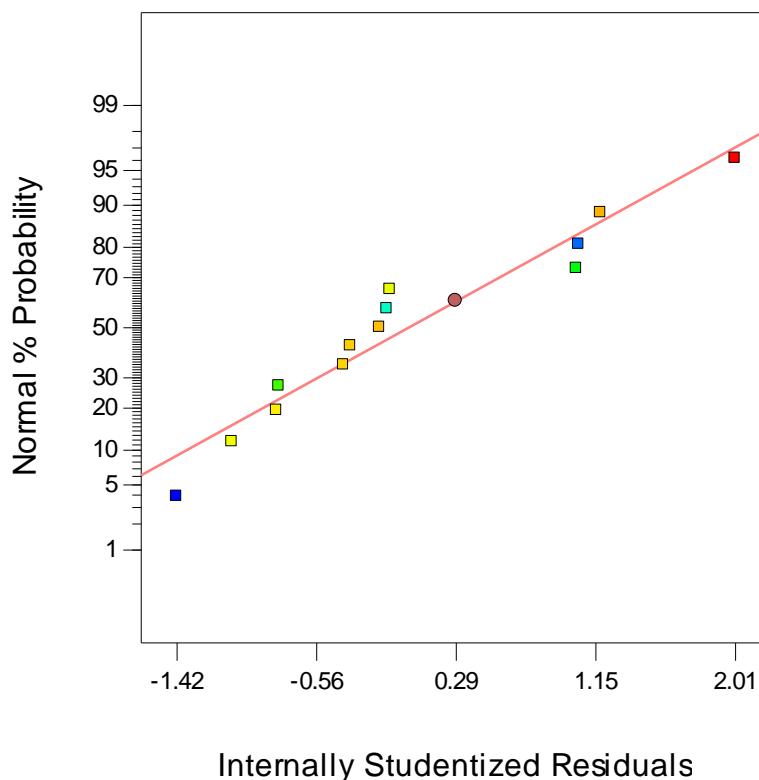


**Figure 4.10** Normal probability plot of the studentized residuals (CCD)

Response surface plot and the corresponding contour plot for the factors are shown in Figure 4.11. According to this figure, increasing both factors; the solution pH and  $(\text{NH}_4)_2\text{MoS}_4$  concentration has a positive effect on the response up to a certain point. After reaching the maximum point, further raise in both factors has an adverse effect on the response. Therefore, an optimum point within this experimental range exists and will be found in the next section.

#### 4.3.3.4 Optimization

Numerical optimization was applied to obtain the optimal values of the selected variables. The goal of the optimization was to maximize the hydrogen production after 3h solar light irradiation. The optimum values for solution pH and  $(\text{NH}_4)_2\text{MoS}_4$  concentration were found to be at 10.7 and  $1.19 \times 10^{-3}$  M, respectively, in order to

maximize the hydrogen production. Based on the empirical model the maximum amount of hydrogen at the optimal condition will be 4790  $\mu\text{mol/gcat}$ . In order to verify the accuracy of this optimization, three experiments at the obtained condition were carried out. The average hydrogen production after 3h of the solar irradiation was found to be  $4890 \pm 151$   $\mu\text{mol/gcat}$ , which is in reasonable agreement with the predicted value. This confirms that the obtained model is valid.

## 4.4 Mechanism

Figure 4.12 illustrates the proposed two steps mechanism for charge transfer and hydrogen production using in-situ photo-deposition method to grow  $\text{MoS}_x$  on  $\text{TiO}_2$ . In this multi-component system, reactions are initiated by excitation of  $\text{TiO}_2$  and EY to their excited states upon solar light irradiation. Both UV and visible spectrum are present in solar light irradiation. Under UV light irradiation,  $\text{TiO}_2$  can be excited and generate electron-hole pairs. At the same time, EY dye will be excited with visible photons and then injects electrons to the conduction band of  $\text{TiO}_2$ . Following this electron injection, EY will be converted to its oxidized form,  $\text{EY}^+$ .<sup>8</sup>

In general, photo-generated electrons and holes will follow two opposite paths; they can either participate in redox reaction on the surface of the photocatalyst or they can recombine.<sup>31</sup> The rate of recombination process is fast in pure  $\text{TiO}_2$  without loading any co-catalyst and thereby, the efficiency of the photocatalytic process will be declined. In the first step of this proposed reaction system, the electrons following their excitation are transferred to  $(\text{NH}_4)_2\text{MoS}_4$  resulting in its reduction to  $\text{MoS}_x$ . It is known that  $\text{MoS}_x$  can accept electrons and act as active sites for hydrogen production due to its quantum-confinement effect.<sup>4,31</sup> In the second step, as hydrogen evolution co-catalyst,  $\text{MoS}_x$ , is present in the system, the electron transfer to the in situ formed  $\text{MoS}_x$  will reduce the recombination of electron and hole pairs and the electron on the surface of  $\text{MoS}_x$  will react with  $\text{H}^+$  ions leading to the formation of  $\text{H}_2$ .

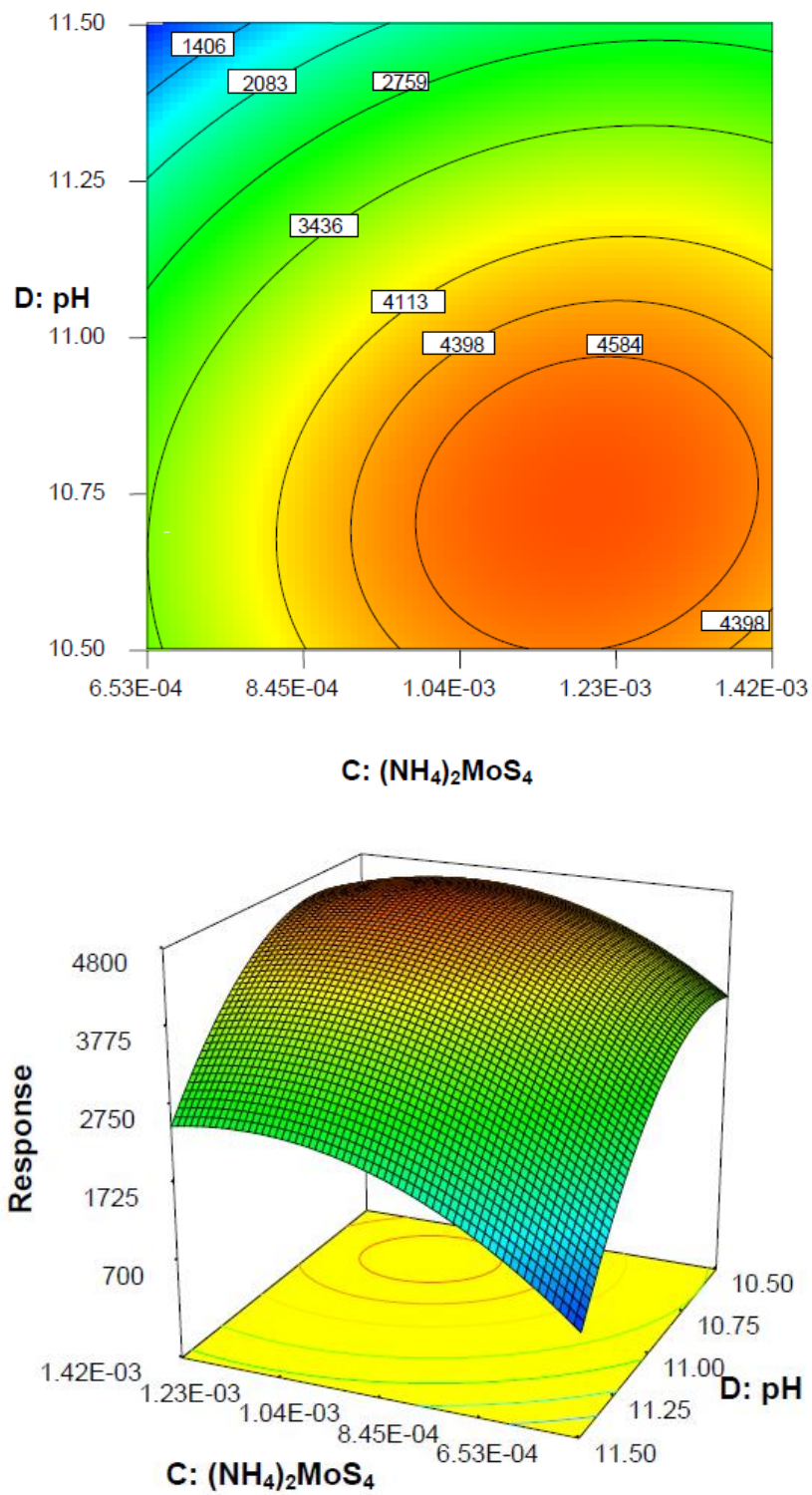


**Figure 4.11** Response Surface and Contour plot of the quadratic model

In another study from our group<sup>8</sup>, it was shown that in a similar dye-sensitized photocatalytic process under solar irradiation, TEOA is oxidized in presence of  $h^+$  and/or  $HO^\cdot$ . It was confirmed by the formation of formaldehyde as an intermediate. Under visible light TEOA is oxidized only by  $EY^+$  species, however, in the case of solar light, the hole ( $h^+$ ) will also oxidize TEOA. In addition, it was shown that formaldehyde molecule was further oxidized to hydrogen under solar light.<sup>8</sup> The same mechanism can be proposed here for TEOA.

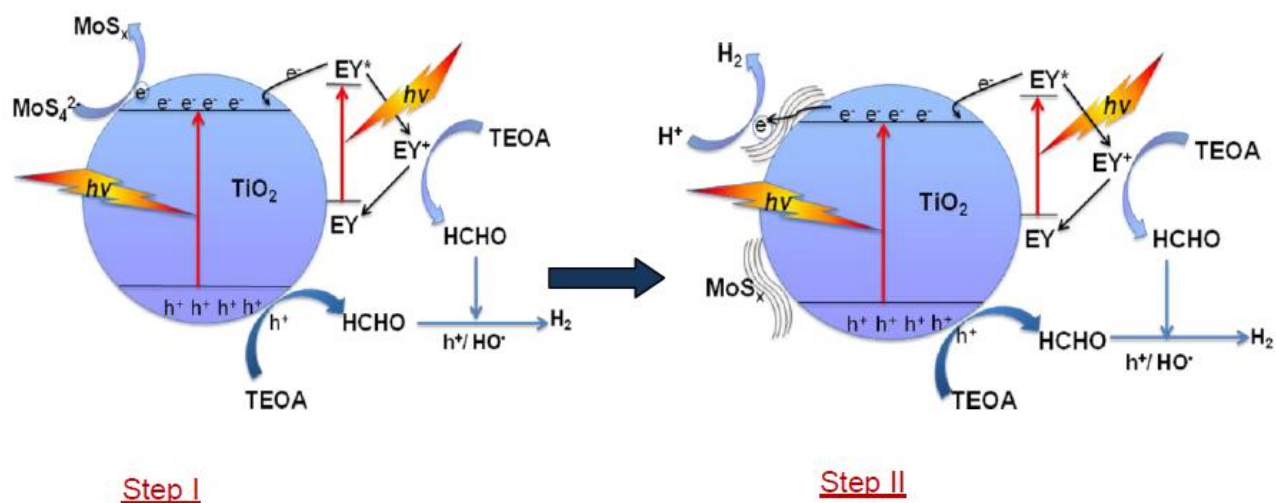


**Figure 4.12** Proposed mechanism for  $H_2$  generation in an in-situ photo-deposition method to grow  $MoS_x$  as a co-catalyst

## 4.5 Apparent Quantum Yield

Apparent quantum yield for hydrogen generation using in-situ grown  $MoS_x$  on  $TiO_2$  can be calculated by the formula shown in Eq.2.<sup>36</sup>

$$\begin{aligned} \text{Apparent Quantum Yield, } \phi_{H_2} (\%) &= \frac{(\text{number of reacted } e^- \text{ or } h^+)}{(\text{number of incident photons})} \times 100 \\ &= \frac{(\text{number of } H_2 \text{ molecules evolved}) \times 2}{(\text{number of incident photons})} \times 100 \quad (\text{Eq.4.2}) \end{aligned}$$

Incident light intensities were measured with StelerNET instrument. The quantum yield will certainly be higher than the apparent quantum yield, as the adsorbed photons are a certain fraction of the incident photons.

Considering full solar spectrum, 300-650nm, the apparent quantum yield at the optimum point for hydrogen generation that was obtained in section 4.3.3.4 found to be 2%. However, as EY could utilize photons up to wavelength of 520 nm, the apparent quantum yield was recalculated using the wavelength range of 300-520 nm and a higher value of 4% was found for the apparent quantum yield. These values are comparable with those that were reported in another study<sup>8</sup>, which was performed in the same reaction system under 100 mW/cm<sup>2</sup> intensity of solar irradiation, using Pt as a co-catalyst. This confirms the promising potential of molybdenum sulfide to react as an active co-catalyst and to be a reliable alternative for noble metals.

## 4.6 Conclusion

In-situ solar photo-deposition method in a dye-sensitized photocatalytic system was applied to grow molybdenum sulfide on TiO<sub>2</sub> resulting in an active photocatalyst for hydrogen generation. The process was performed at ambient conditions without using toxic precursors, which is beneficial for large-scale processes. The synthesis process as well as the obtained material, both demonstrated high efficiency for photocatalytic hydrogen generation. Full factorial design analysis was performed in order to investigate the effect of different reaction parameters as well as their interaction effects. In addition, central composite design was applied to maximize the hydrogen generation after 3h solar light irradiation. ANOVA confirmed the adequacy of the obtained model for the response. Based on the proposed model, the optimum values for solution pH and (NH<sub>4</sub>)<sub>2</sub>MoS<sub>4</sub> concentration were found to be at 10.7 and  $1.19 \times 10^{-3}$  M, respectively, in order to maximize the hydrogen production. It was predicted that 4790  $\mu\text{mol/g}_{\text{cat}}$  will be produce at the optimal conditions. A two steps mechanism was also proposed for this noble metal-free photocatalytic process.

## 4.7 References

- (1) Li, X.; Yu, J.; Low, J.; Fang, Y.; Xiao, J.; Chen, X. Engineering Heterogeneous Semiconductors for Solar Water Splitting. *J. Mater. Chem. A* **2015**, 3 (6), 2485.
- (2) Nguyen, M.; Tran, P. D.; Pramana, S. S.; Lee, R. L.; Batabyal, S. K.; Mathews, N.; Wong, L. H.; Graetzel, M. In Situ Photo-Assisted Deposition of MoS<sub>2</sub> Electrocatalyst onto Zinc Cadmium Sulphide Nanoparticle Surfaces to Construct an Efficient Photocatalyst for Hydrogen Generation. *Nanoscale* **2013**, 5 (4), 1479.
- (3) Reza Gholipour, M.; Dinh, T. C.; Béland, F.; Do, T.-O. Nanocomposites as Sunlight-Driven Photocatalysts for Hydrogen Production from Water Splitting. *Nanoscale* **2015**.
- (4) Xiang, Q.; Yu, J.; Jaroniec, M. Synergetic Effect of MoS<sub>2</sub> and Graphene as Cocatalysts for Enhanced Photocatalytic H<sub>2</sub> Production Activity of TiO<sub>2</sub> Nanoparticles. *J. Am. Chem. Soc.* **2012**, 134 (15), 6575.
- (5) Zong, X.; Yan, H.; Wu, G.; Ma, G.; Wen, F.; Wang, L.; Li, C. Enhancement of Photocatalytic H<sub>2</sub> Evolution on CdS by Loading MoS<sub>2</sub> as Cocatalyst under Visible Light Irradiation. *J. Am. Chem. Soc.* **2008**, 130 (23), 7176.
- (6) Meng, C.; Liu, Z.; Zhang, T.; Zhai, J. Layered MoS<sub>2</sub> Nanoparticles on TiO<sub>2</sub> Nanotubes by Photocatalytic Strategy as High-Performance Electrocatalysts for Hydrogen Evolution Reaction. *Green Chem.* **2015**.
- (7) Meng, F.; Li, J.; Cushing, S. K.; Zhi, M.; Wu, N. (Nick). SI- Solar Hydrogen Generation by Nanoscale P - N Junction of P -Type Molybdenum Disulfide/ N - Type Nitrogen-Doped Reduced Graphene Oxide. *J. Am. Chem. Soc.* **2013**, 135 (28), 130628121322008.
- (8) Chowdhury, P.; Gomaa, H.; Ray, A. K. Sacrificial Hydrogen Generation from Aqueous Triethanolamine with Eosin Y-Sensitized Pt/TiO<sub>2</sub> Photocatalyst in UV, Visible and Solar Light Irradiation. *Chemosphere* **2015**, 121, 54.



- (9) Chen, X.; Shen, S.; Guo, L.; Mao, S. S. Semiconductor-Based Photocatalytic Hydrogen Generation. *Chem. Rev.* **2010**, *110* (11), 6503.
- (10) Al-Azri, Z. H. N.; Chen, W.-T.; Chan, A.; Jovic, V.; Ina, T.; Idriss, H.; Waterhouse, G. I. N. The Roles of Metal Co-Catalysts and Reaction Media in Photocatalytic Hydrogen Production: Performance Evaluation of M/TiO<sub>2</sub> Photocatalysts (M=Pd, Pt, Au) in Different Alcohol–water Mixtures. *J. Catal.* **2015**, 329, 355.
- (11) Li, Y.; Wang, H.; Peng, S. Tunable Photodeposition of MoS<sub>2</sub> onto a Composite of Reduced Graphene Oxide and CdS for Synergic Photocatalytic Hydrogen Generation. *J. Phys. Chem. C* **2014**, *118* (34), 19842.
- (12) Chowdhury, P.; Malekshoar, G.; Ray, M. B.; Zhu, J.; Ray, A. K. Sacrificial Hydrogen Generation from Formaldehyde with Pt/TiO<sub>2</sub> Photocatalyst in Solar Radiation. *Ind. Eng. Chem. Res.* **2013**, *52* (14), 5023.
- (13) Kanda, S.; Akita, T.; Fujishima, M.; Tada, H. Facile Synthesis and Catalytic Activity of MoS<sub>2</sub>/TiO<sub>2</sub> by a Photodeposition-Based Technique and Its Oxidized Derivative MoO<sub>3</sub>/TiO<sub>2</sub> with a Unique Photochromism. *J. Colloid Interface Sci.* **2011**, *354* (2), 607.
- (14) Min, S.; Lu, G. Sites for High Efficient Photocatalytic Hydrogen Evolution on a Limited-Layered MoS<sub>2</sub> Cocatalyst Confined on Graphene Sheets — The Role of Graphene. *J. Phys. Chem. C* **2012**, *116*, 25415–25424.
- (15) Gao, W.; Wang, M.; Ran, C.; Li, L. Facile One-Pot Synthesis of MoS<sub>2</sub> Quantum dots–graphene–TiO<sub>2</sub> Composites for Highly Enhanced Photocatalytic Properties. *Chem. Commun.* **2015**, *51* (9), 1709.
- (16) Pourabbas, B.; Jamshidi, B. Preparation of MoS<sub>2</sub> Nanoparticles by a Modified Hydrothermal Method and the Photo-Catalytic Activity of MoS<sub>2</sub>/TiO<sub>2</sub> Hybrids in Photo-Oxidation of Phenol. *Chem. Eng. J.* **2008**, *138* (1-3), 55.

- (17) Zhu, B.; Lin, B.; Zhou, Y.; Sun, P.; Yao, Q.; Chen, Y.; Gao, B. Enhanced Photocatalytic H<sub>2</sub> Evolution on ZnS Loaded with Graphene and MoS<sub>2</sub> Nanosheets as Cocatalysts. *J. Mater. Chem. A* **2014**, 2 (11), 3819.
- (18) Deng, Z. H.; Li, L.; Ding, W.; Xiong, K.; Wei, Z. D. Synthesized Ultrathin MoS<sub>2</sub> Nanosheets Perpendicular to Graphene for Catalysis of Hydrogen Evolution Reaction. *Chem. Commun.* **2015**, 51 (10), 1893.
- (19) Zong, X.; Xing, Z.; Yu, H.; Bai, Y.; Lu, G. Q.; Wang, L. Photocatalytic Hydrogen Production in a Noble-Metal-Free System Catalyzed by in Situ Grown Molybdenum Sulfide Catalyst. *J. Catal.* **2014**, 310, 51.
- (20) Xu, J.; Li, Y.; Peng, S. Photocatalytic Hydrogen Evolution over Erythrosin B-Sensitized Graphitic Carbon Nitride with in Situ Grown Molybdenum Sulfide Cocatalyst. *Int. J. Hydrogen Energy* **2015**, 40 (1), 353.
- (21) Chowdhury, P.; Gomaa, H.; Ray, A. K. Factorial Design Analysis for Dye-Sensitized Hydrogen Generation from Water. *Int. J. Hydrogen Energy* **2011**, 36 (21), 13442.
- (22) Hou, D.; Goei, R.; Wang, X.; Wang, P.; Lim, T. T. Preparation of Carbon-Sensitized and Fe-Er Codoped TiO<sub>2</sub> with Response Surface Methodology for Bisphenol A Photocatalytic Degradation under Visible-Light Irradiation. *Appl. Catal. B Environ.* **2012**, 126, 121.
- (23) Chen, J.; Luo, H.; Shi, H.; Li, G.; An, T. Anatase TiO<sub>2</sub> Nanoparticles–carbon Nanotubes Composite: Optimization Synthesis and the Relationship of Photocatalytic Degradation Activity of Acyclovir in Water. *Appl. Catal. A Gen.* **2014**, 485, 188.
- (24) Chen, J.; Li, G.; Huang, Y.; Zhang, H.; Zhao, H.; An, T. Optimization Synthesis of Carbon Nanotubes-Anatase TiO<sub>2</sub> Composite Photocatalyst by Response Surface Methodology for Photocatalytic Degradation of Gaseous Styrene. *Appl. Catal. B Environ.* **2012**, 123-124, 69.

- (25) Feilizadeh, M.; Mul, G.; Vossoughi, M. E. Coli Inactivation by Visible Light Irradiation Using a Fe–Cd/TiO<sub>2</sub> Photocatalyst: Statistical Analysis and Optimization of Operating Parameters. *Appl. Catal. B Environ.* **2015**, 168-169, 441.
- (26) Douglas C. Montgomery, G. C. R. *Applied Statistics and Probability for Engineers*, 3rd ed.; John Wiley & Sons, Inc., 2003.
- (27) Gheshlaghi, R.; Scharer, J. M.; Moo-Young, M.; Douglas, P. L. Medium Optimization for Hen Egg White Lysozyme Production by Recombinant *Aspergillus Niger* Using Statistical Methods. *Biotechnol. Bioeng.* **2005**, 90 (6), 754.
- (28) Chen, Q. H.; He, G. Q.; Ali, M. a M. Optimization of Medium Composition for the Production of Elastase by *Bacillus* Sp. EL31410 with Response Surface Methodology. *Enzyme Microb. Technol.* **2002**, 30 (5), 667.
- (29) Li, Q.; Zhang, N.; Yang, Y.; Wang, G.; Ng, D. H. L. High Efficiency Photocatalysis for Pollutant Degradation with MoS<sub>2</sub>/C<sub>3</sub>N<sub>4</sub> Heterostructures. *Langmuir* **2014**, 30 (29), 8965.
- (30) Chang, K.; Mei, Z.; Wang, T.; Kang, Q.; Ouyang, S. MoS<sub>2</sub> / Graphene Cocatalyst for Efficient Photocatalytic H<sub>2</sub> Evolution under Visible Light Irradiation. *ACS Nano* **2014**, No. 7, 1.
- (31) Zhu, Y.; Ling, Q.; Liu, Y.; Wang, H.; Zhu, Y. Photocatalytic H<sub>2</sub> Evolution on MoS<sub>2</sub>–TiO<sub>2</sub> Catalysts Synthesized via Mechanochemistry. *Phys. Chem. Chem. Phys.* **2015**, 17 (2), 933.
- (32) Antony, J. *Design of Experiments for Engineers and Scientists*; Butterworth-Heinemann: New York, 2003.
- (33) Jollet, V.; Gissane, C.; Schlaf, M. Optimization of the Neutralization of Red Mud by Pyrolysis Bio-Oil Using a Design of Experiments Approach. *Energy Environ. Sci.* **2014**, 7 (3), 1125.

- (34) Montgomery, D. C. *Design and Analysis of Experiments*; John Wiley & Sons, Inc.: New York, 2009.
- (35) Sakia, R. M. The Box-Cox Transformation Technique : A Review. *Stat.* **1992**, *41*, 169.
- (36) Shimidzu, T.; Iyoda, T.; Koide, Y. An Advanced VisibleLight Induced Water Reduct Ion with Dye-Sensitized Semiconductor Powder Catalyst. *J. Am. Chem. Soc.* **1985**, *107* (2), 35.

## Chapter 5

### 5 Enhanced Solar Photocatalytic Degradation of Phenol with Coupled Graphene-based Titanium Dioxide and Zinc Oxide

#### 5.1 Introduction

Advanced Oxidation Processes (AOPs) have received remarkable attention for degradation of organic pollutants in wastewater.<sup>1</sup> Among them heterogeneous photocatalysis has been widely employed due to its promising potential for environmental remediation. This technique makes use of solid semiconductors, which can be activated with different light sources providing sufficient energy corresponding to their band-gap. Activated semiconductor particles generate electrons and holes that act as powerful reductants and oxidants respectively.<sup>2,3</sup>

The efficiency of photocatalytic reaction is primarily influenced by two competitive processes, the migration rate of electrons and holes to the semiconductor's surface and the recombination rate of photo-excited charges.<sup>4</sup> To enhance quantum efficiency of photocatalytic process, the inhibition of rapid recombination rate of active species is crucial.<sup>4,5</sup>

Titanium dioxide ( $\text{TiO}_2$ ) has been widely used in photocatalytic processes due to being highly stable, non-toxic and inexpensive. Another semiconductor material with similar properties to  $\text{TiO}_2$  is Zinc Oxide ( $\text{ZnO}$ ) that has received the most application after  $\text{TiO}_2$ .  $\text{ZnO}$  has been reported in some cases to have better performance than  $\text{TiO}_2$  for degradation of organic compounds.<sup>6,7</sup> However, efficacy of the photocatalytic activity of pure  $\text{TiO}_2$  or  $\text{ZnO}$  is still low as the photo-generated charges have a high tendency to recombine. Consequently, in order to improve the practical application for high-rate photocatalytic treatment of wastewater, development of the semiconductors with enhanced photocatalytic activity is essential.<sup>8,5</sup> Recently, many strategies have been proposed in order to achieve higher efficiency. Coupling two semiconductors<sup>9,10</sup> and

utilizing carbon-based materials<sup>11</sup> are the two possible promising approaches reported in literature to accomplish this goal.

Utilization of coupled semiconductors that increases the separation of photo-excited charges has been proposed as a possible technique to enhance the performance of the photocatalysts.<sup>2,12</sup> ZnO/SnO<sub>2</sub> has been reported to be more active than pure ZnO or SnO<sub>2</sub> for decolorization of methyl orange.<sup>2,13-15</sup> Serpone et al.<sup>16</sup> explained this improvement by proposing an inter-particle electron transfer process (IPET) within the coupled semiconductors due to their different redox energy levels corresponding to their conduction and valence bands.

Wu<sup>17</sup> compared the photo-degradation efficiency of single semiconductor and coupled semiconductor systems using TiO<sub>2</sub>, ZnO and SnO<sub>2</sub> to degrade two azo dyes. The reaction rate constant of Procion Red MX-5B was reported to be larger for TiO<sub>2</sub>/ZnO couple than that of pure ones at pH 7. However, no significant increase was observed for the mixture at pH 10. In these studies, the weight ratio of the photocatalysts in the coupled system was kept at 1:1. Therefore, the effect of the different mixing ratio on the photocatalytic performance of the coupled system should still be investigated.

In order to further improve the photocatalytic efficiency, composites consisting of carbonaceous materials have been studied. In particular, many efforts have been devoted to take the advantage of graphene's superior properties through coupling it with semiconductors. Graphene has a two-dimensional sp<sup>2</sup> hybridized carbon network.<sup>18,19</sup> It possesses unique properties such as a large theoretical specific surface area (2600 m<sup>2</sup>/g), high thermal conductivity (3000 W/m·K) and high intrinsic electron mobility (15,000 m<sup>2</sup>/V.s).<sup>20</sup>

Therefore, it is highly desirable to explore its potential to form hybrid structure with different nanomaterials for photocatalytic applications. Several graphene-semiconductor composites have been reported<sup>21, 23-24</sup>, using either surfactant assisted growth or simple physical mixing of pre-synthesized nanoparticles and graphene.

Although some progress has been achieved for the application of graphene in photocatalysis, the studies in this field are at the primary stage and further investigations are required. So far, majority of the researches focused on graphene-based  $\text{TiO}_2$ . But, very few studies have been performed on graphene-based zinc oxide.<sup>25</sup> Thus, more investigation is essential on incorporation of graphene on  $\text{ZnO}$ , which is another important semiconductor material.

Moreover, majority of the photocatalytic evaluations have been performed under UV light, therefore, the studies under solar light are still missing. Furthermore, as of our knowledge, organic dyes have been mostly selected as a model compound to evaluate the photocatalytic activity of graphene-based composites.<sup>21,25-27</sup> It is important to apply a wider choice of model compounds to further authenticate success of graphene- $\text{ZnO}/\text{TiO}_2$  composite in photocatalysis applications.

Among the hazardous organic contaminants found in industrial effluents, phenol and phenolic compounds are very important.<sup>28,29</sup> The discharge amount of phenol in water must be maintained at 0.1-1 mg/L (ppm) based on the environmental protection rules of Central Pollution Control Board (1992).<sup>29,30</sup> Therefore, phenol was chosen as the model compound in this study.

In this work, one-step hydrothermal method was employed on  $\text{TiO}_2$  and  $\text{ZnO}$  to obtain the graphene-based composites. The synthesized materials were characterized and exhibited improved photocatalytic degradation of phenol under simulated solar irradiation after incorporation of graphene. The photocatalytic activity of the coupled semiconductors,  $\text{ZnO}/\text{TiO}_2$  and  $\text{ZnO-G}/\text{TiO}_2\text{-G}$ , were investigated by mixing the different stoichiometric amount of the components. The ratio of the two components in the coupled system was optimized. The rate for phenol degradation under solar irradiation was increased by coupling the two semiconductors. Parametric studies of (i) catalyst amount, (ii) Initial phenol concentration, (iii) solution pH, and (iv) light intensity were carried out. By using coupled  $\text{ZnO-G}/\text{TiO}_2\text{-G}$  system, complete photocatalytic degradation of 40 ppm phenol could be achieved, after 1 h solar light illumination at the optimum experimental conditions.

## 5.2 Materials and Methods

### 5.2.1 Photocatalyst Preparation

Commercial zinc oxide nano powder (Inframat® Advanced Materials™) and titanium dioxide (Aeroxide® P25) were used. Phenol (99.0 %) and Ethanol (99.5 %) were purchased from sigma-Aldrich Canada Ltd. Graphite Powder (natural, microcrystal grade, product number 14736) was purchased from Alfa Aesar. All reagents were used as received without further treatment.

Modified Hummers method was applied to obtain graphite oxide (GO) from graphite powder as described previously.<sup>31,32</sup> In a typical procedure to obtain graphene based composites, 2 mg GO was dissolved in a solution of water and ethanol (2:1) followed by one hour ultrasonic treatment. The solution was stirred for 2 more hours after adding 200 mg TiO<sub>2</sub> or ZnO. The mixture was transferred to a Teflon-lined autoclave and then the hydrothermal process was performed at 120 °C for 3 hours. During this process, GO could be reduced to graphene and concurrently the deposition of TiO<sub>2</sub> or ZnO was achieved. The obtained composites were centrifuged, rinsed with de-ionized water and vacuum dried at 60 °C. The prepared samples are denoted as TiO<sub>2</sub>-G and ZnO-G. Different stoichiometric amount of the prepared composites were mixed to obtain coupled ZnO-G/TiO<sub>2</sub>-G system. Similarly, different mixtures of the coupled ZnO/TiO<sub>2</sub> were also provided for more comparison.

### 5.2.2 Photocatalyst Characterizations

Structural analyses of the samples were carried out by X-ray powder diffractometer (Rigaku-Ultima IV ,XRD) with a scintillation counter detector, using a Cu K $\alpha$  source of X-rays ( $\lambda = 1.54 \text{ \AA}$ ) over the desired  $2\theta$  range with step width of 0.02 degree. UV spectra of the samples were recorded by a UV-Vis-NIR spectrophotometer (Shimadzu UV-3600) equipped with an integrating sphere using BaSO<sub>4</sub> as reference. Raman spectroscopy was performed on a Renishaw Raman spectrometer Model 2000 using a 632.8 nm laser at 100% power.



The X-ray photoelectron spectroscopic (XPS) analyses were carried out with a Kratos Axis Ultra spectrometer using a monochromatic Al K $\alpha$  source (15mA, 14kV). The morphologies of the samples were determined using scanning electron microscopy (SEM, Hitachi S-4500), and transmission electron microscopy (TEM, JEOL 2010F).

### 5.2.3 Photocatalytic Reaction

Photo-degradation of phenol as a model compound was investigated under simulated solar light using the prepared composites. The photocatalytic experiments were performed as described in previous work.<sup>33</sup> The catalyst powder was suspended in 100 mL of phenol solution after pH adjustment with either 1:1 HCl or 0.1 M NaOH solution. A pH meter (780-Metrohm Ltd.) was used to measure the solution pH. The catalyst suspension was dispersed for 5 min in an ultrasonic bath, and then it was kept in dark for 1 hour to achieve adsorption equilibrium. The mixture was then transferred to a Pyrex glass reactor (6.5 cm in diameter, 6.3 cm in height) to conduct the photocatalytic experiments. Simulated air mass (AM) 1.5 solar light was generated using a solar simulator (model SS1KW, Sciencetech, Ontario, Canada, with a 1000-W Xe arc lamp and an AM 1.5G filter). It produced identical simulated 1-sun irradiance of 100 mW/cm<sup>2</sup> at full power that matches the global solar spectrum at sea level, as reported by the supplier. All experiments were performed by continuously bubbling air through the liquid phase.

Liquid samples were collected at regular intervals and the quantification analyses of phenol in the samples were performed in a Shimadzu high-performance liquid chromatography (HPLC) prominence LC 20AB instrument with an SIL-20AC.HT auto sampler and CTO-0AC column oven with an SPD-M20A diode array detector. An Altima HP C18 column (5  $\mu$ m  $\times$  150 mm  $\times$  4.6 mm) and a mobile phase of methanol and water (MiliQ water) 67/33% v/v at a flow rate of 0.5 mL/min were used. The injection volume of the samples was 5  $\mu$ L. The temperature of the column oven was kept at 25  $^{\circ}$ C throughout the analysis. The wavelength of analysis for phenol was 270 nm.

## 5.3 Results and Discussion

### 5.3.1 Characterization

The structural characterizations of the  $\text{TiO}_2\text{-G}$ ,  $\text{ZnO-G}$ , and  $\text{GO}$  were performed. The XRD pattern of  $\text{GO}$  exhibits the diffraction peak at  $2\theta = 11.3^\circ$ , which is in close agreement with the previous reports.<sup>23, 34</sup> Figure 5.1 shows the highly crystalline nature of  $\text{TiO}_2\text{-G}$  and both anatase and rutile crystalline phases are observed.

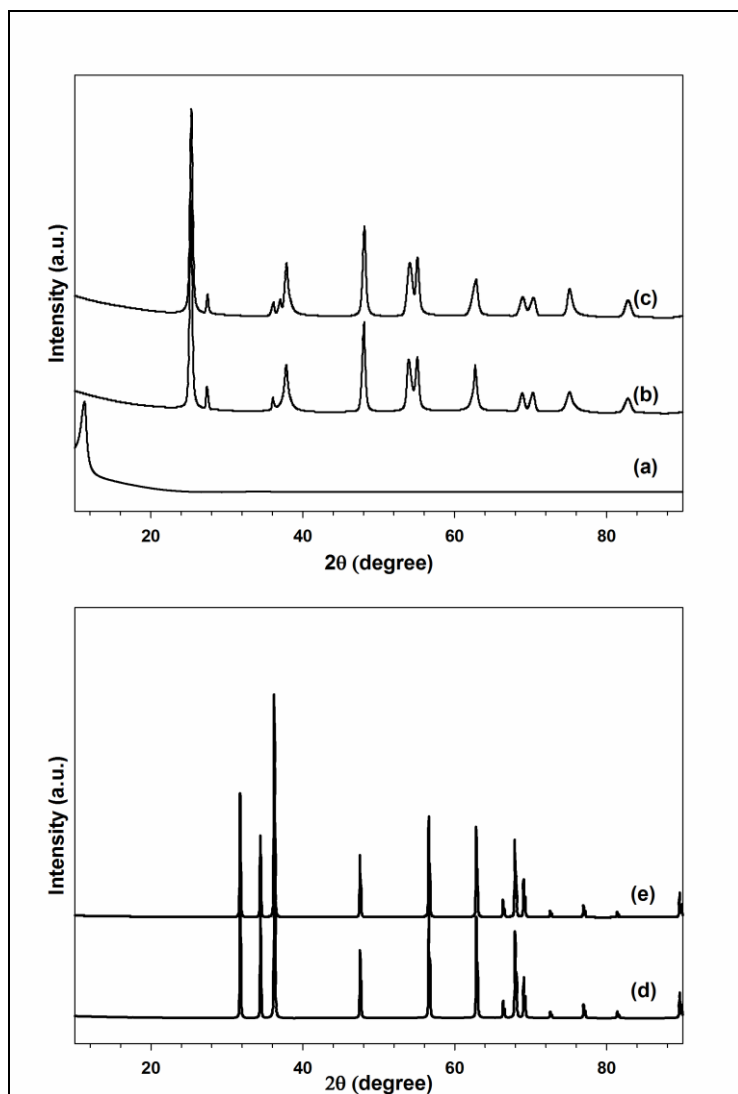


**Figure 5.1** XRD patterns of (a)  $\text{GO}$ , (b)  $\text{TiO}_2$ , (c)  $\text{TiO}_2\text{-G}$ , (d)  $\text{ZnO}$  and (e)  $\text{ZnO-G}$ .

However, peaks associated only with  $\text{TiO}_2$  are observed and no peak is assigned to GO, indicating that it was reduced to graphene during the hydrothermal process. Likewise, the XRD pattern of ZnO-G displays an excellent crystalline characteristic of the composite as shown in Figure 5.1. The peaks at  $2\theta = 31.7^\circ, 34.4^\circ, 36.2^\circ, 47.5^\circ, 56.5^\circ, 62.8^\circ$  and  $67.9^\circ$  are corresponded to the crystal faces  $[1\ 0\ 0]$ ,  $[0\ 0\ 2]$ ,  $[1\ 0\ 1]$ ,  $[1\ 0\ 2]$ ,  $[1\ 1\ 0]$ ,  $[1\ 0\ 3]$  and  $[1\ 1\ 2]$  of ZnO respectively.<sup>35, 36</sup> Similar to  $\text{TiO}_2$ -G no peak for GO is observed in XRD pattern of ZnO-G.

The optical properties of the samples were investigated by UV-Vis spectroscopy. The absorption spectra of  $\text{TiO}_2$ ,  $\text{TiO}_2$ -G, ZnO and ZnO-G are compared in Figure 5.2. It can be observed that after graphene introduction into the bare  $\text{TiO}_2$ , the absorption edge is noticeably shifted into the visible region, whereas the small shift is observed for ZnO-G.

In order to estimate the band gap of the samples, Tauc plot can be generated by Kubelka-Munk transformation on the adsorption data.<sup>37</sup> The Kubelka-Munk function,  $[F(R_\infty)h\nu]^{1/2}$  is approximated by  $(\alpha h\nu)^{1/2}$  where  $\alpha$  is the absorption coefficient and  $h\nu$  is the photon energy.<sup>26</sup> A Tauc plot is  $(\alpha h\nu)^{1/2}$  versus  $h\nu$ . Band gap can be found by passing a tangential line through the edge of the curve to the x-axis as shown in Figure 5.2B. By adding graphene to  $\text{TiO}_2$ , the band-gap is noticeably decreased from 3.1 eV to 2.2 eV, which can be associated with the enhanced chemical bonding between  $\text{TiO}_2$  and graphene.<sup>21</sup> However, the corresponding band-gap to ZnO-G is 2.9 eV, which is slightly decreased compared to that of pure ZnO. Therefore, the degree of band gap narrowing is higher for  $\text{TiO}_2$ -G than ZnO-G, implying that the interaction of  $\text{TiO}_2$  and graphene was stronger. This may also suggest that the graphene mainly act as a substrate for immobilization of ZnO particles.<sup>35</sup> As a result of this extension in photo-response range, the solar spectrum could be utilized more efficiently and the solar degradation rate of phenol was improved by applying graphene into  $\text{TiO}_2$  and ZnO.

The high-resolution C1s XPS spectra of the GO,  $\text{TiO}_2$ -G and ZnO-G are shown in Figure 5.3. It is observed that the peaks for GO are located at the binding energies of 284.5, 286.59, 288.11 eV. (Figure 5.3c) The peak at 284.8 is typically assigned to the C=C, C-C and C-H bonds, while the other two at higher binding energies are attributed to C-O-C, C-

OH and C=O respectively.<sup>23,38</sup> In fact, these peaks indicate the remarkable contribution of the oxygenated carbon species on GO, which provides the active sites for the deposition of TiO<sub>2</sub> nanoparticles or ZnO nanoparticles.<sup>34</sup>

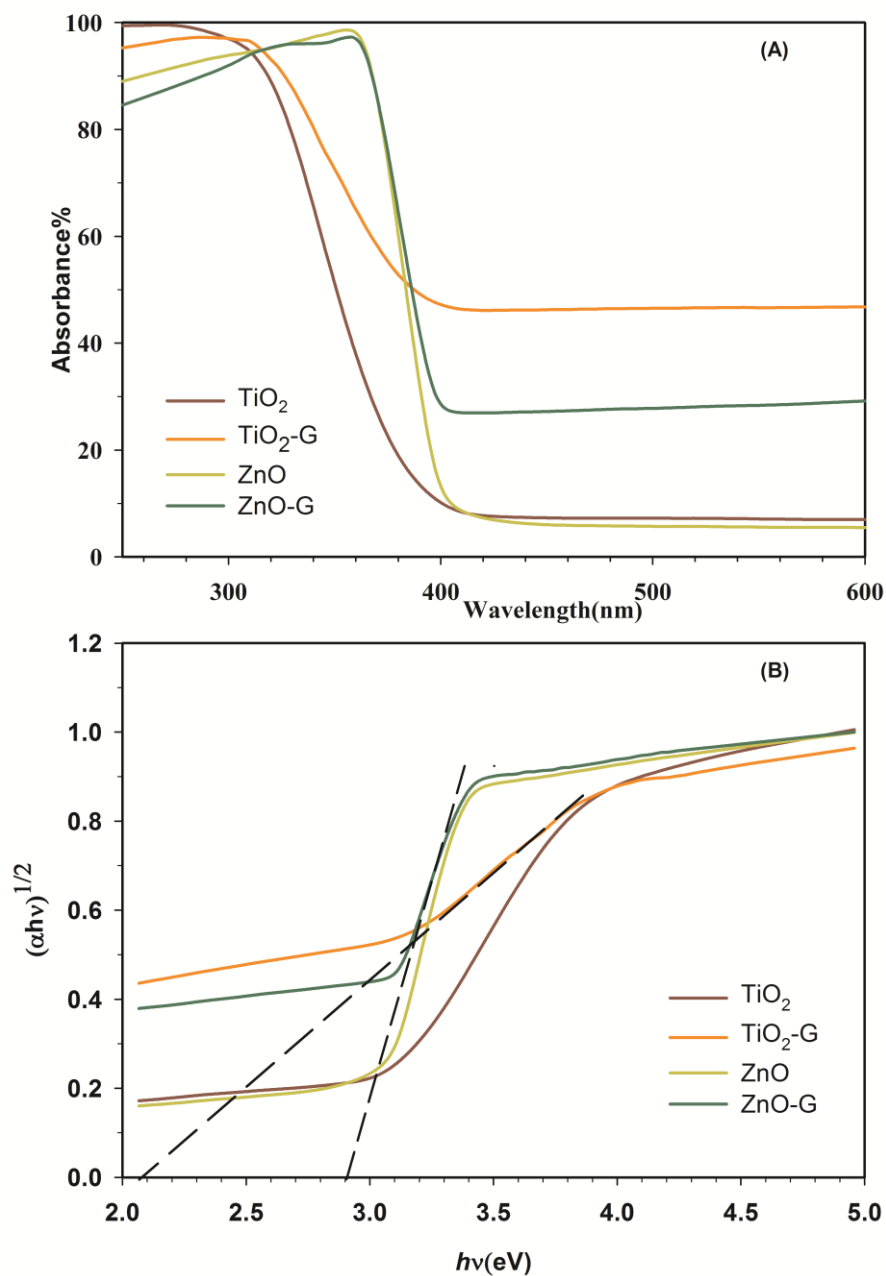


**Figure 5.2** (A) Absorbance spectra, (B) Tauc plot for band gap estimation.

According to C1s XPS spectra of TiO<sub>2</sub>-G and ZnO-G (Figure 5.3a and 5.3b respectively), the considerable reduction of oxygen-containing functional groups could be confirmed. Table 5.1 provides the peak area ratio of different functional groups to that of the sp<sup>2</sup> carbon species. During the hydrothermal process, the concentration of oxygenated carbon species in TiO<sub>2</sub>-G and ZnO-G was decreased. Therefore, the effective reduction of GO to graphene sheets in the TiO<sub>2</sub>-G and ZnO-G composites by hydrothermal method can be concluded.

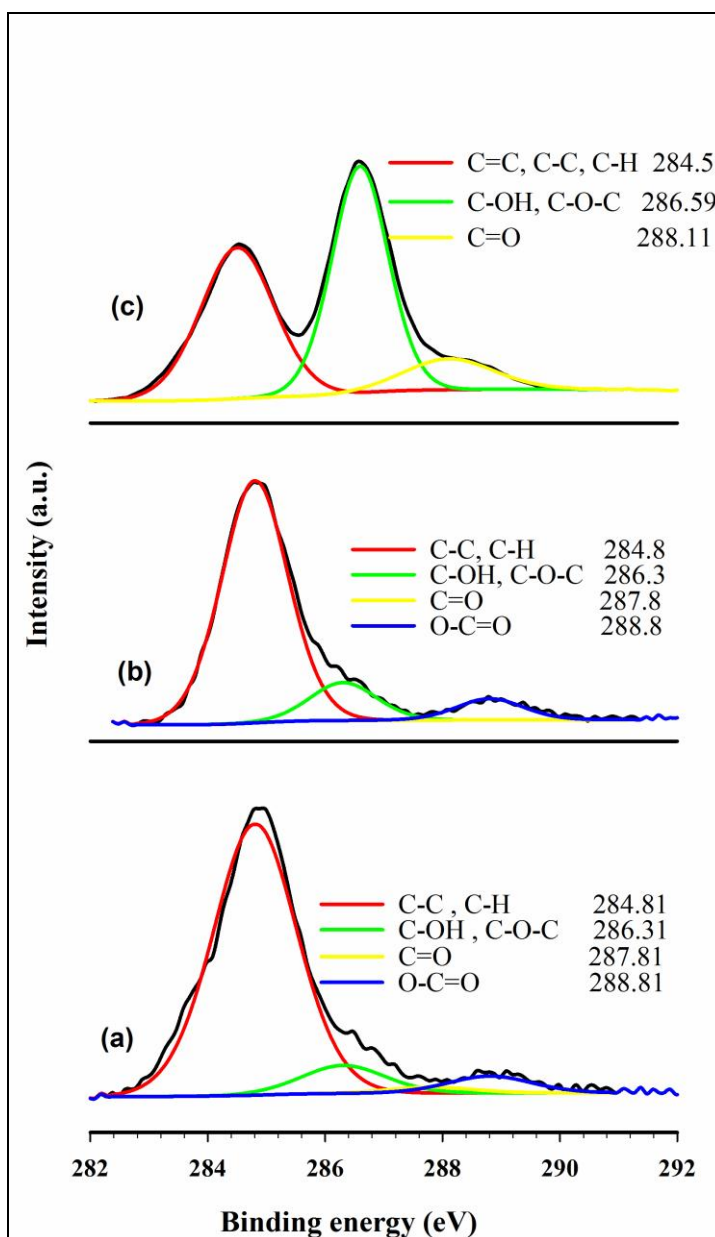


**Figure 5.3** High-resolution XPS spectra of C 1s for (a) ZnO-G, (b) TiO<sub>2</sub>-G, (c) GO

**Table 5.1** The peak area (A) ratios of the oxygen-containing bonds to the CC bonds of the TiO<sub>2</sub>-G and ZnO-G samples reduced by hydrothermal method.

Composite	$A_{\text{COH}} / A_{\text{CC}}$	$A_{\text{CO}} / A_{\text{CC}}$	$A_{\text{OCO}} / A_{\text{CC}}$
TiO <sub>2</sub> -G	0.15	0.01	0.08
ZnO-G	0.11	0.02	0.06

Raman spectroscopy is a reliable technique to characterize carbonaceous materials. It is widely applied in order to determine the crystalline ordered/disordered and defects in carbon structure.<sup>38,39</sup> In particular, the structural changes during the reduction of GO to graphene can be observed in the Raman Spectra.<sup>34</sup>

The Raman spectra for the TiO<sub>2</sub>-G, ZnO-G and GO are provided in Figure 5.4. In general two characteristic peaks are assigned to carbon materials in their Raman spectra, known as the D band and the G band. The GO spectrum in Figure 5.4A shows the D band around 1344 cm<sup>-1</sup> which is assigned to breathing mode of k-point phonons of A<sub>1g</sub> symmetry, and the G band is around 1599 cm<sup>-1</sup> corresponds to the first order scattering of the E<sub>1g</sub> phonon mode of the sp<sup>2</sup> carbon atoms.<sup>38</sup> The D/G ratio indicates the degree of functionalization.<sup>40</sup> According to Figure 5.4A the D/G intensity ratio of TiO<sub>2</sub>-G and ZnO-G are increased to 0.95 and 1.1 respectively, compared to that of GO which is 0.86.

Therefore, the good attachment of the TiO<sub>2</sub> and ZnO with the graphene sheets is confirmed in both composites, TiO<sub>2</sub>-G and ZnO-G. Moreover, the Raman spectrum of TiO<sub>2</sub>-G (Figure 5.4B) displays different vibration peaks at 146 cm<sup>-1</sup>, 395 cm<sup>-1</sup>, 510.2 cm<sup>-1</sup> and 634.4 cm<sup>-1</sup>, which again confirms the presence of crystalline TiO<sub>2</sub> in the composite. Similarly, in addition to G and D bands the Raman Spectrum of ZnO-G exhibits the typical peaks, the low intensity peak at 329.3 cm<sup>-1</sup> and the peak at 436.2 cm<sup>-1</sup> related to ZnO (Figure 5.4C). The latter is attributed to the optical phonon E<sub>2</sub> mode of wurtzite hexagonal phase, and the former indicates the multiple phonon scattering process in ZnO.<sup>39,41</sup>

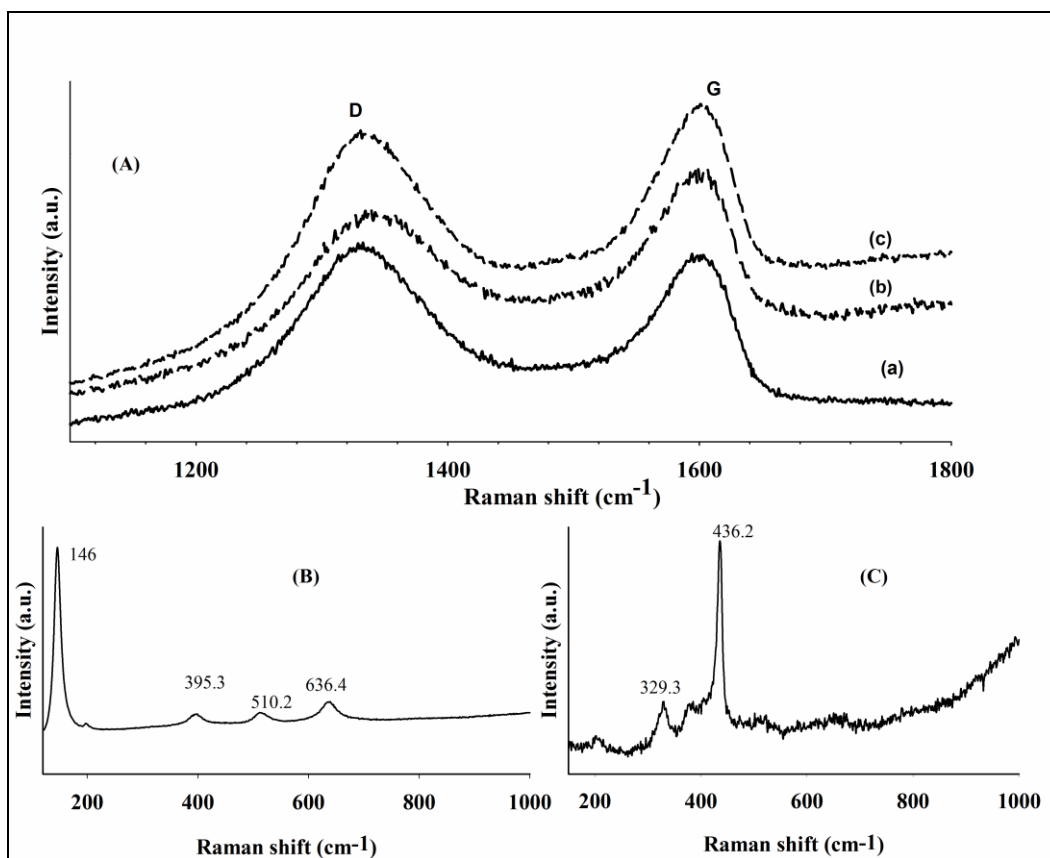


**Figure 5.4** Raman Spectra of (A) TiO<sub>2</sub>-G (a), GO (b) and ZnO-G (c), (B) TiO<sub>2</sub>-G, (C) ZnO-G

Typical SEM and TEM images of ZnO-G and TiO<sub>2</sub>-G are shown in Figure 5.5. These images verify TiO<sub>2</sub> or ZnO loading on the graphene sheet. The interaction of the –OH and –COOH functional groups of GO with the surface of the semiconductors facilitates this loading. The functional groups are reduced during the hydrothermal process, and thereby unpaired  $\pi$  electrons are more available to bind to the surface atoms of the semiconductor.<sup>26</sup>

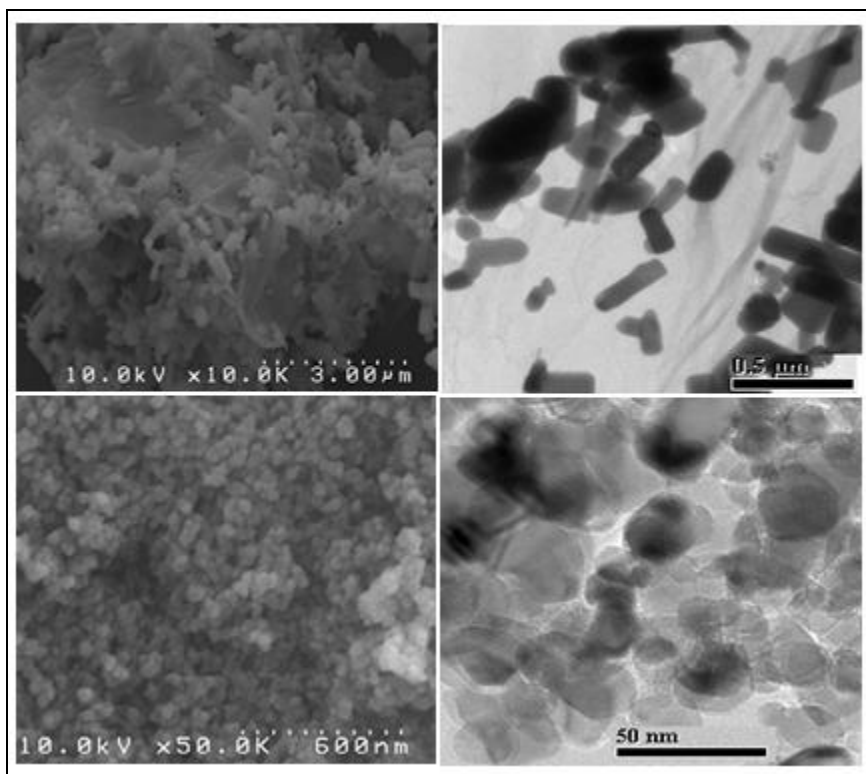


**Figure 5.5** SEM images for ZnO-G, TiO<sub>2</sub>-G (a, c), TEM images for ZnO-G, TiO<sub>2</sub>-G (b, d).

### 5.3.2 Photocatalytic Performance

Photo-degradation of phenol as a model compound under simulated solar light was studied by using different photocatalysts including, TiO<sub>2</sub>, ZnO, TiO<sub>2</sub>-G and ZnO-G. Figure 6 exhibits that incorporation of graphene on TiO<sub>2</sub> and ZnO enhances their photo-activity for the degradation of phenol. The apparent reaction rate constant ( $k$ ) of TiO<sub>2</sub>-G is increased to 0.0069 min<sup>-1</sup>, which indicates about 33% improvement over that of pure TiO<sub>2</sub> ( $k=0.0052$  min<sup>-1</sup>). Likewise, the same trend is observed by using ZnO-G. In this case,  $k$  value is increased to 0.0221 min<sup>-1</sup> from 0.0163 min<sup>-1</sup> for that of pure ZnO. ZnO-G can effectively decompose phenol under solar light within three hours, as shown in Figure 5.6.



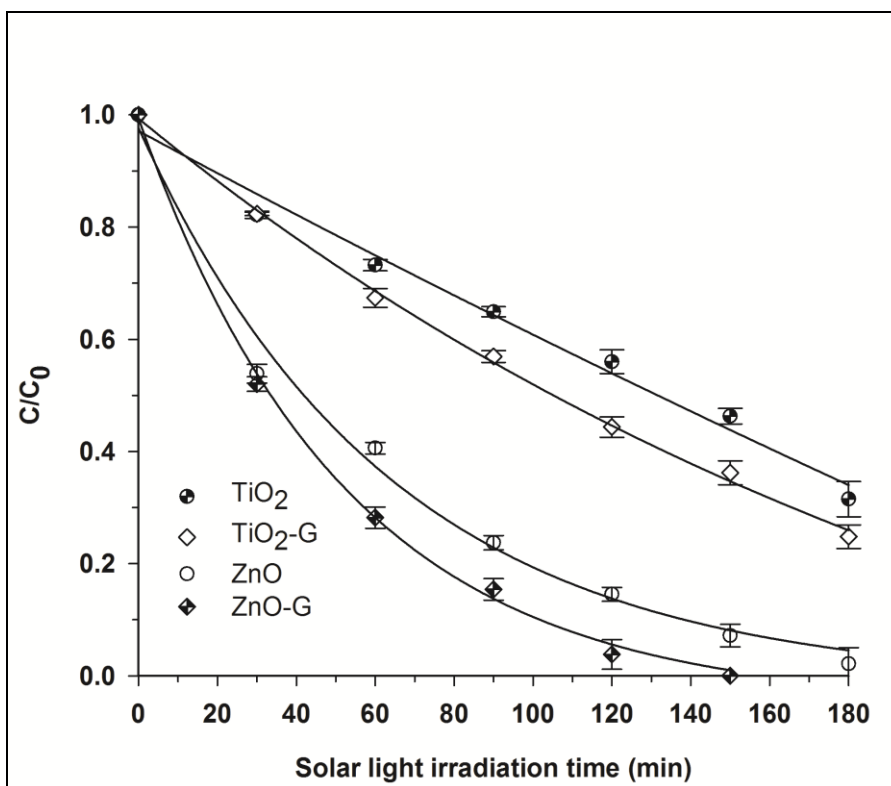


**Figure 5.6** Photocatalytic degradation of phenol using different photocatalysts.

Experimental conditions: [photocatalyst] = 1 g/L, [phenol] = 40 ppm,  $I_{\text{solar}} = 100$  mW/cm<sup>2</sup>, pH = 7, O<sub>2</sub> saturated.

This improvement on the performance of TiO<sub>2</sub>-G and ZnO-G are ascribed to optical and structural properties of the composites, which were discussed in previous section. The band-gap energy reduction and extended absorption range after introduction of graphene allowed utilization of solar spectrum more effectively, and thereby, improving the photo-activity of the catalyst for phenol degradation.

Moreover, graphene has a high conductivity level and been known as an excellent electron acceptor, owing to its two-dimensional  $\pi$ -conjugation structure.<sup>42</sup> Therefore, in TiO<sub>2</sub>-G or ZnO-G, the photo-excited electrons are transferred to the graphene from the conduction band of the semiconductors, and consequently, let effective suppression of charge recombination. Thus, more reactive species are provided due to the presence of more photo-generated charges, resulting in the enhancement of the photo-activity of the catalyst.

In this study, the photocatalytic activity of the coupled semiconductor composites instead of a single one was also explored for solar photocatalytic phenol degradation. The ZnO/TiO<sub>2</sub> (or ZnO-G/TiO<sub>2</sub>-G) mixtures were prepared by mixing different stoichiometric amount of each components. The total amount of the catalyst was kept at 1 g/L in the slurry. Figure 5.7 shows the apparent rate constant for phenol degradation by using the coupled semiconductors at different stoichiometric ratio.

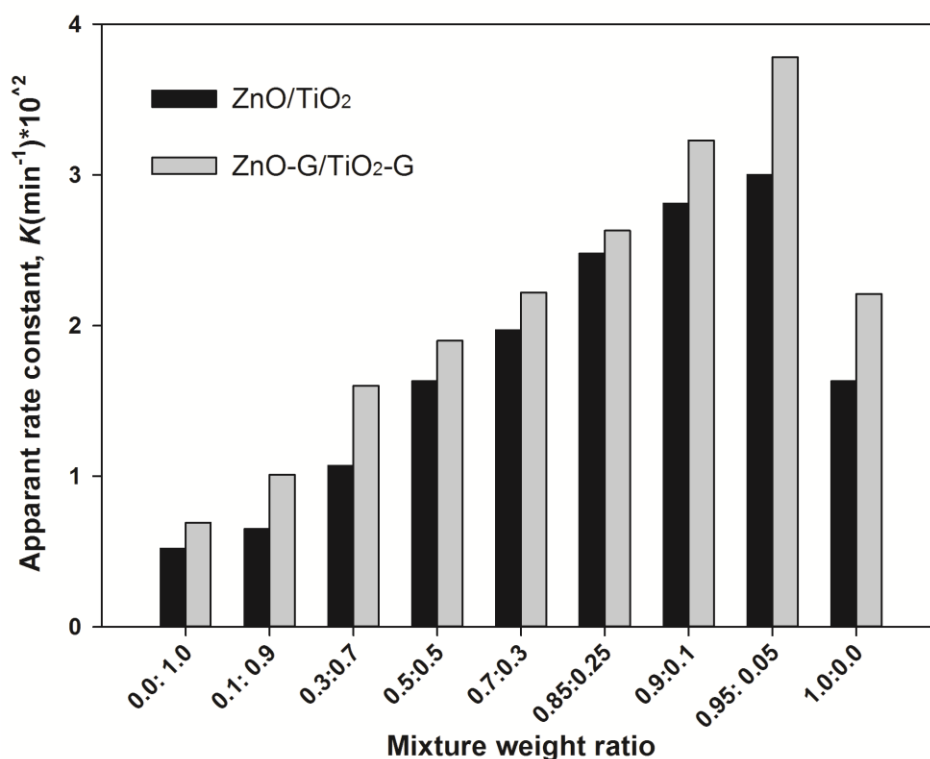


**Figure 5.7** Phenol degradation rate constants using coupled system at different weight ratio Experimental conditions: [photocatalyst] = 1 g/L, [phenol] = 40 ppm,  $I_{\text{solar}} = 100 \text{ mW/cm}^2$ , pH = 7, O<sub>2</sub> saturated.

The results clearly demonstrate that by increasing the mixture ratio of ZnO to TiO<sub>2</sub> (or ZnO-G to TiO<sub>2</sub>-G) from 0.0:1.0 up to 0.95:0.05, the photocatalytic rate progressively increased. After this point, further increment in the ratio has an adverse effect on the degradation reaction rate of phenol. This steady improvement in photocatalytic degradation rate can be explained by the enhancement of the charge separation by

coupling two semiconductors with different energy levels. Serpone et al.<sup>16</sup> proposed the application of inter-particle electron transfer process (IPET) in this phenomenon. In the coupled semiconductors system, more efficient charge separation and longer life time of the charge carriers can be realized due to the difference in the redox energy levels of the semiconductors at their conduction and valence bands. For instance, in the coupled system of ZnO/TiO<sub>2</sub>, the electron (e<sup>-</sup>) transfers from conduction band of the light-activated ZnO to the corresponding band of TiO<sub>2</sub>, and the hole (h<sup>+</sup>) transfer occurs from the valence band of TiO<sub>2</sub> to that of ZnO. Therefore, the recombination of photo-generated electrons and holes are suppressed allowing higher degradation rate to be achieved.

Herein, the best result is achieved for the ZnO-G/TiO<sub>2</sub>-G coupled system, where the ratio is kept at 0.95:0.05. At this point, the apparent rate constant (k) is 0.0378 min<sup>-1</sup> and 40 ppm phenol could be degraded completely in one hour under 100 mW/cm<sup>2</sup> of simulated solar irradiation. Therefore, it was chosen as the best performed catalyst for further parametric studies.

### 5.3.3 Parametric Study

#### 5.3.3.1 Effect of Catalyst Loading

Figure 5.8 represents the significant effect of the catalyst loading on the photo-degradation of phenol. The catalyst loading was varied between 0.25 g/L and 1.75 g/L, while all other parameters were kept constant. The results reveal that the degradation rate (mg/min per unit volume (L) of the reaction liquid,  $r_1$ ) is increased with the increasing amount of the catalyst loading up to 1.25 g/L and then reaches a plateau.

This enhancement at low catalyst loading can be attributed to the increased number of available active sites for phenol adsorption and light absorption, which leads to higher number of hydroxyl and/or superoxide radicals.<sup>33</sup> Beyond the optimum point (1.25 g/L), the adverse effect of higher catalyst concentration on the degradation rate is observed. In fact, particle agglomeration at higher concentration limits the light penetration (light limiting) as well as phenol adsorption on the available surface of the catalyst. Furthermore, with gradual increment of the catalyst concentration, the opacity in the slurry and also light scattering by the particles prevent efficient light-harvesting<sup>43</sup>, which

results in less illuminated active sites on the catalyst surface.<sup>36,44-45</sup> Therefore,  $r_2$ , the rate of degradation per unit mass of catalyst is decreased gradually with increase in catalyst loading, as shown in Figure 5.8. The rate profiles of  $r_1$  and  $r_2$  clearly show that apparent degradation rate is affected due to mutual influence of internal mass-transfer resistance due to particle agglomeration obstructing phenol to reach the catalyst surface and the ability of photons to make a way through the agglomerates and activate the inner surfaces (light limiting due to shielding effect). These two factors counteract each other for catalyst loading between 0.25 and 1.25 g/L resulting in a region of optimal catalyst loading at around 1.25 g/L. When catalyst loading is increased further, the shielding effect completely dominates and addition of catalyst loading beyond 1.25 g/L is equivalent to addition of inert to the system.

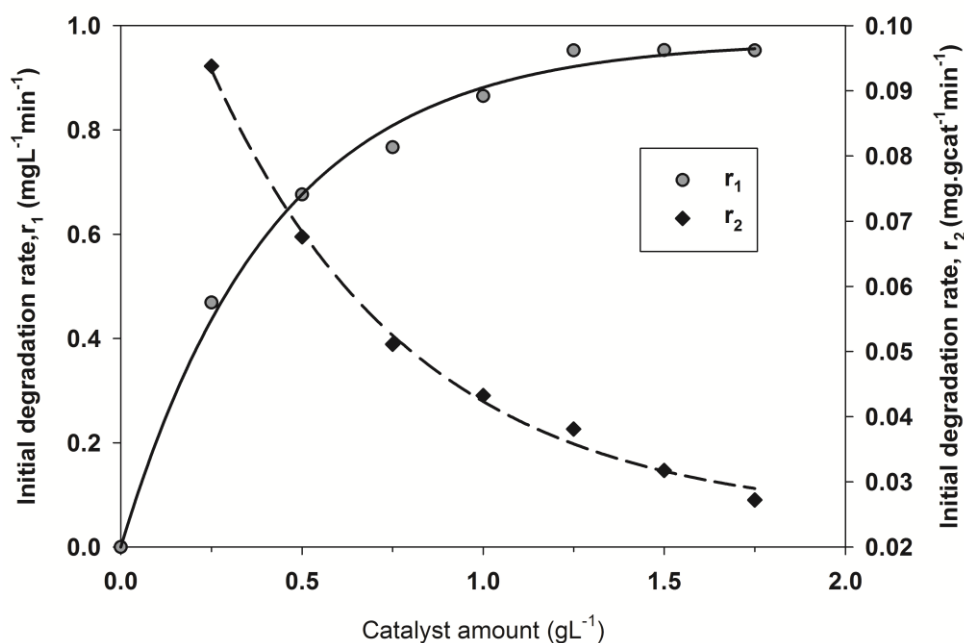


**Figure 5.8** Effect of catalyst loading.

Experimental conditions: [ZnO-G/TiO<sub>2</sub>-G] = 0.25-1.75 g/L, [phenol] = 40 ppm,  $I_{\text{solar}}$  = 100 mW/cm<sup>2</sup>, pH = 7, O<sub>2</sub> saturated.

The photocatalytic degradation of phenol at different concentration between 20 and 100 ppm was investigated. Figure 5.9 shows that the required time for complete degradation is increased by increasing the initial phenol concentration. Approximately, half an hour is required for 20 ppm phenol to achieve complete degradation, compared with more than 3 hours for 100 ppm phenol. The exponential function shown below can be applied to correlate all the concentration profiles.<sup>43</sup>

$$C = C_0 \exp(-kt) \quad (\text{Eq 5.1})$$

Keeping all other parameters unchanged, the apparent rate constant  $k$  ( $\text{min}^{-1}$ ) is decreased by increasing the initial phenol concentration. Therefore, the degradation rate is considered as pseudo-first-order with respect to the phenol concentration in experimental range. At higher initial phenol concentration, adsorbed amount of phenol on the surface of the catalyst is more, which requires more  $\cdot\text{OH}$  and  $\cdot\text{O}_2^-$  to degrade. Having all other operating parameters constant, the sufficient  $\cdot\text{OH}$  and  $\cdot\text{O}_2^-$  cannot be provided<sup>44</sup>, leading to a remarkable decline in degradation rate.

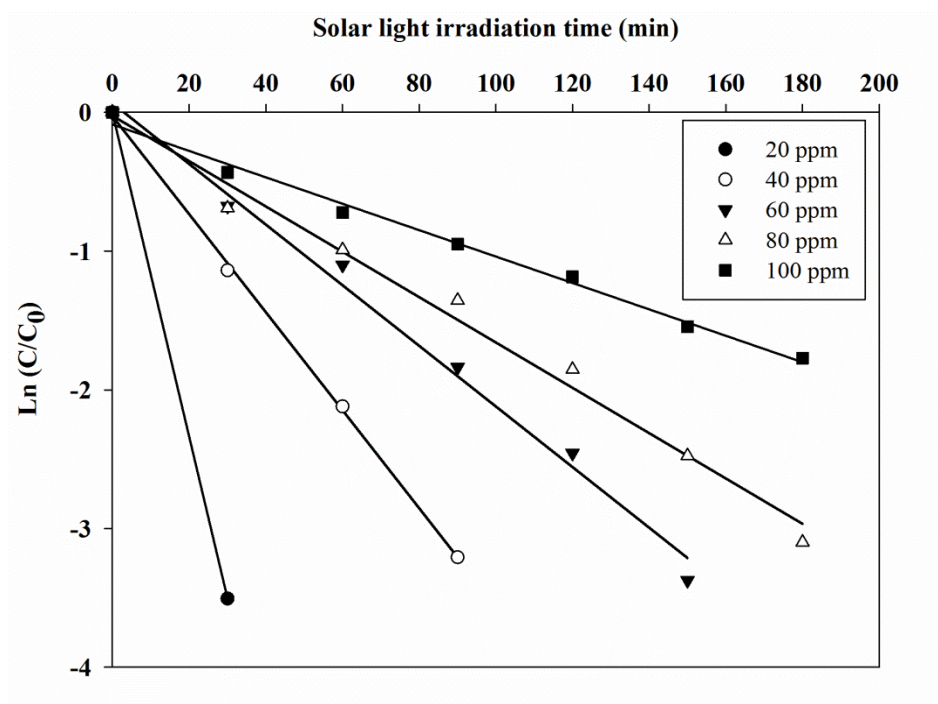


**Figure 5.9** Effect of initial concentration of phenol. Experimental conditions:  $[\text{ZnO-G/TiO}_2\text{-G}] = 1.25 \text{ g/L}$ ,  $[\text{phenol}] = 20\text{-}100 \text{ ppm}$ ,  $I_{\text{solar}} = 100 \text{ mW/cm}^2$ ,  $\text{pH} = 7$ ,  $\text{O}_2$  saturated.

In heterogeneous photocatalysis reaction takes place on the surface of the photocatalyst, and hence surface property of the semiconductors plays a significant role. Therefore, acid-base condition of the metal oxide surfaces can have large impact on the adsorption-desorption characteristic at the surface and consequently on their photocatalytic degradation performance.<sup>43, 46</sup> This signifies the necessity of effect of pH study on any photocatalytic degradation processes.

In this study, the effect of solution pH was examined in the range of 3 to 9, as shown in Figure 5.10. By increasing pH from 3 to 5, the rate of degradation enhanced, but by further increase in pH the degradation rate declined slightly up to pH 6-7, and significantly beyond pH 9. Hence, the phenol degradation is favored at slightly acidic conditions within the experimental parameters used in our study. This is in good agreement with reported previous studies.<sup>43, 44</sup>

This can be explained based on the point of zero charge (pzc) of the semiconductors. The point of zero charge ( $\text{pH}_{\text{pzc}}$ ) for  $\text{TiO}_2$  and  $\text{ZnO}$  are found to be 6.8 and 9 respectively, from zeta potential analysis.<sup>36</sup> Therefore,  $\text{TiO}_2$  surface is positively charged in acidic condition ( $\text{pH} < 6.8$ ), whereas it is negatively charged under alkaline condition ( $\text{pH} > 6.8$ ).  $\text{ZnO}$  surface is positively charged below pH 9.<sup>36</sup>

However, the point of zero charge for  $\text{TiO}_2\text{-G}$  and  $\text{ZnO-G}$  might be different compared with that of pure semiconductors, as the surface chemistry is changed after incorporation of graphene. Morales-Torres et al.<sup>47</sup> reported that the prepared Graphene Oxide-P25 composites presented more acidic properties due to the addition of GO with oxygenated groups. They showed that the  $\text{pH}_{\text{PZC}}$  decreased with the increase of the GO content, but increased with increasing temperature of the post-treatment due to the partial removal of acid groups and formation of RGO. The  $\text{pH}_{\text{PZC}}$  for Graphene Oxide-P25 (1%, 200 °C) was reported as 4.1 compared with 6.3 for that of P25 based on their measurement.<sup>47</sup>

In slightly acidic condition, more phenol molecules are favored to be adsorbed on the positively charged surface of the catalyst, thereby enhancing degradation rate. In contrast, in alkaline condition less surface interaction is possible between the negatively charged surface and the negatively charged phenolic compounds, impeding adsorption of phenol

molecules on the catalyst surface.<sup>44, 46</sup> Hence, photo-degradation of phenol in high pH range is not favorable.

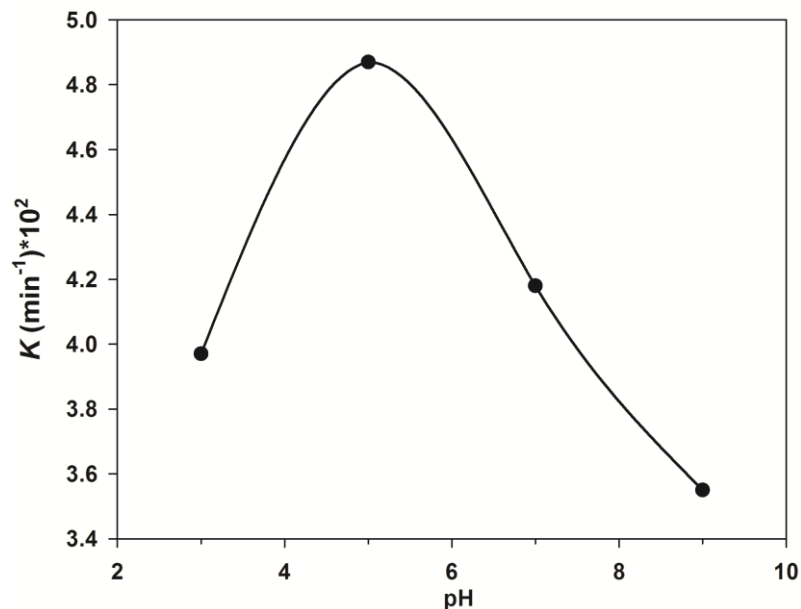


**Figure 5.10** Effect of solution pH on degradation rate of phenol. Experimental conditions: [ZnO-G/TiO<sub>2</sub>-G] = 1.25 g/L, [phenol] = 40 ppm,  $I_{\text{solar}} = 100 \text{ mW/cm}^2$ , O<sub>2</sub> saturated.

Understanding the impact of light intensity is of major importance from the design and operational points of view. It is an important parameter to be optimized in every photocatalytic set-up in order to utilize the light energy effectively, and to avoid the fraction of photons to be wasted.

Effect of light intensity has been studied by numerous researchers. In general reported results show three regions of the light intensities. At low light intensities the rate generally increases linearly with increasing light intensity. At intermediate light intensities, the rate follows power-law dependence with of the light intensity with exponent varying between 0.5-0.8, and the rate dependence found to be independent at high light intensities. For example, Chen<sup>43</sup> reported that this effect can be correlated with the power law equation as  $k \propto I^\beta$ , where  $\beta$  found to be 0.84 for degradation of 4-NP. Herein, to determine the relationship between the light intensity, and the reaction rate

constant, experiments were conducted by varying the light intensity between 20 mW/cm<sup>2</sup> and 100 mW/cm<sup>2</sup>. The apparent rate constants were plotted for different values of light intensity as shown in Figure 5.11. The data was fitted with an empirical equation as below:

$$k = \frac{\alpha I_{\text{solar}}^{\beta}}{1 + \gamma I_{\text{solar}}^{\beta}} \quad (\text{Eq 5.2})$$

Where the three constants  $\alpha$ ,  $\beta$ , and  $\gamma$  were found as 0.001, 2.085,  $1.875 \times 10^{-4}$ , respectively. The linear dependence of the degradation rate vs intensity is noticeable at the intensities less than 50 mW/cm<sup>2</sup>, whereas the reaction rate increases approximately with the power of 0.7 at higher intensities.

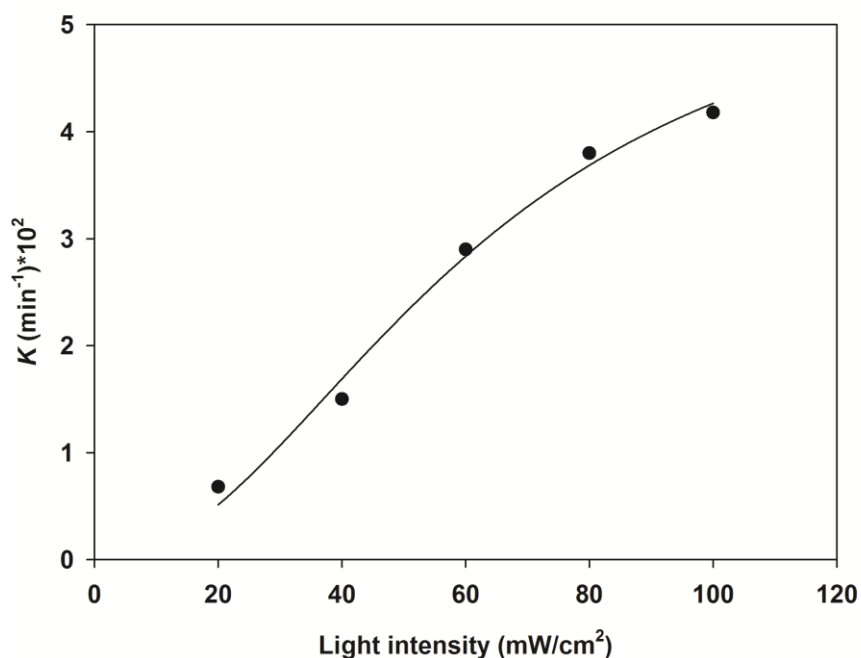


**Figure 5.11** Apparent degradation rate constant at different light intensities.

Experimental conditions: [ZnO-G/TiO<sub>2</sub>-G] = 1.25 g/L, [phenol] = 40 ppm,  $I_{\text{solar}}$  = 20-100 mW/cm<sup>2</sup>, pH = 7, O<sub>2</sub> saturated.



## 5.4 Conclusion

TiO<sub>2</sub>-G and ZnO-G composites were prepared by simple hydrothermal method. Optical and structural properties of the composites were obtained using XRD, XPS, Raman spectroscopy, UV-Vis Spectroscopy, TEM, and SEM. The two composites showed improved performance in photocatalytic degradation of phenol under simulated solar illumination. Incorporation of graphene facilitates more adsorption sites for phenol, electron-hole pairs' separation, and extension of light absorption wave-length range. In addition, the photocatalytic performance of the coupled ZnO-G/TiO<sub>2</sub>-G with an optimized ratio of the components was investigated. The results reveal that the coupled composites (ZnO-G/TiO<sub>2</sub>-G with 0.95:0.05 ratio) outperformed when compared to single composite by a factor of two. In addition, the parametric study was carried out to optimize the reaction conditions. Experimental results showed that one hour of 100 mW/cm<sup>2</sup> solar irradiation was required to degrade 40 ppm phenol at neutral pH, when 1.25 g/L of coupled ZnO-G/TiO<sub>2</sub>-G composites were used. When the results found in this study are further compared with published results for photocatalytic phenol degradation, it can be concluded that there is great potential for graphene-based composites as well as coupling of the composites for higher photocatalytic activity.

## 5.5 References

- (1) Kansal, S.K.; Singh, M.; Sud, D. Studies on photodegradation of two commercial dyes in aqueous phase using different photocatalysts. *J. Hazard. Mater.* **2007**, 141, 581.
- (2) Chiang, Y.J.; Lin, C.C. Photocatalytic decolorization of methylene blue in aqueous solutions using coupled ZnO/SnO<sub>2</sub> photocatalysts. *Powder Technol.* **2013**, 246, 137.
- (3) Shafaei, A.; Nikazar, M.; Arami, M. Photocatalytic degradation of terephthalic acid using titania and zinc oxide photocatalysts: Comparative study. *Desalination.* **2010**, 252, 8.
- (4) Jamil, T.S.; Gad-Allah, T.A.; Ghaly, M.Y. Parametric study on phenol photocatalytic degradation under pure visible and solar irradiations by Fe-doped TiO<sub>2</sub>. *Desalin. Water. Treat.* **2012**, 50, 264.
- (5) Xu, T.; Zhang, L.; Cheng, H.; Zhu, Y. Significantly enhanced photocatalytic performance of ZnO via graphene hybridization and the mechanism study. *Appl. Catal., B.* **2011**, 101, 382.
- (6) Khatamian, M.; Alaji, Z. Efficient adsorption-photodegradation of 4-nitrophenol in aqueous solution by using ZnO/HZSM-5 nanocomposites. *Desalination.* **2012**, 286, 248.
- (7) Marcy, G.; Augugliaro, V.; Lopez-Munoz, M.J.; Martyn, C.; Palmisano, L.; Rives, V.; Schiavello, M.; Tilley, R. J.D.; Venezia, A.M. Preparation characterization and photocatalytic activity of polycrystalline ZnO/TiO<sub>2</sub> systems. 2. Surface and bulk characterization, and 4-Nitrophenol photodegradation in liquid-solid regime. *J. Phys. Chem. B.* **2001**, 105, 1033.
- (8) Wang, C.; Xu, B.Q.; Wang, X.; Zhao, J. Preparation and photocatalytic activity of ZnO/TiO<sub>2</sub>/SnO<sub>2</sub> mixture. *J. Solid State Chem.* **2005**, 178, 3500.
- (9) Elder, S.H.; Cot, F.M.; Su, Y.; Heald, S.M.; Tyryshkin, A.M.; Bowman, M.K.; Gao, Y.; Joly, A.G.; Balmer, M.L.; Kolwaite, A.C.; Magrini, K.A.; Blake, D.M. The discovery and study of nanocrystalline TiO<sub>2</sub>-(MoO<sub>3</sub>) core-shell materials. *J. Am. Chem. Soc.* **2000**, 122, 5138.

- (10) Tatsuma, T.; Saitoh, S.; Ngatrakanwiwat, P.; Ohko, Y.; Fujishima, A. Energy storage of  $\text{TiO}_2\text{-WO}_3$  photocatalysis systems in the gas phase. *Langmuir*. **2002**, 18, 7777.
- (11) Woan, K.; Pyrgiotakis, G.; Sigmund, W. Photocatalytic carbon-nanotube- $\text{TiO}_2$  composites. *Adv. Mater.* **2009**, 21, 2223.
- (12) Liao, D.L.; Badour, C.A.; Liao, B.Q. Preparation of nanosized  $\text{TiO}_2/\text{ZnO}$  composite catalyst and its photocatalytic activity for degradation of methyl orange. *J. Photochem. Photobiol., A*. **2008**, 194, 11.
- (13) Cun, W.; Jincai, Z.; Xinming, W.; Bixian, M.; Guoying, S.; Ping, P.A.; Jiamo, F. Preparation, characterization and photocatalytic activity of nano-sized  $\text{ZnO/SnO}_2$  coupled photocatalysts. *Appl. Catal., B*. **2002**, 39, 269.
- (14) Wang, C.; Wang, X.; Xu, B.Q.; Zhao, J.; Mai, B.; Peng, P.A.; Sheng, G.; Fu, J. Enhanced photocatalytic performance of nanosized coupled  $\text{ZnO/SnO}_2$  photocatalysts for methyle orange degradation. *J. Photochem. Photobiol., A*. **2004**, 168, 47.
- (15) Zhang, M.; Sheng, G.; Fu, J.; An, T.; Wang, X.; Hu, X. Novel preparation of nanosized  $\text{ZnO-SnO}_2$  with high photocatalytic activity by homogeneous co-precipitation method. *Mater. Lett.* **2005**, 59, 3641.
- (16) Serpone, N.; Maruthamuthu, P.; Pichat, P.; Pelizzetti, E.; Hidaka, H. Exploiting the interparticle electron transfer process in the photocatalysed oxidation of phenol, 2-chlorophenol and pentachlorophenol: chemical evidence for electron and hole transfer between coupled semiconductors. *J. Photochem. Photobiol., A*. **1995**, 85, 247.
- (17) Wu, C.H. Comparison of azo dye degradation efficiency using UV/single and UV/coupled semiconductor systems. *Chemosphere*. **2004**, 57, 601.
- (18) Zhang, X.; Tang, Y.; Li, Y.; Wang, Y.; Liu, X.; Liu, C.; Luo, S. Reduced graphene oxide and PbS nanoparticles co-modified  $\text{TiO}_2$  nanotube arrays as a recyclable and stable photocatalyst for efficient degradation of pentachlorophenol. *Appl. Catal., A*. **2013**, 457, 78.

- (19) Liu, Y.; Hu, Y.; Zhou, M.; Qian, H.; Xiao, H. Microwave-assisted non-aqueous route to deposit well-dispersed ZnO nanocrystals on reduced graphene oxide sheets with improved photoactivity for the decolorization of dyes under visible light. *Appl. Catal., B.* **2012**, 125, 425.
- (20) Akhavan, O.; Ghaderi, E. photocatalytic reduction of graphene oxide nanosheets on TiO<sub>2</sub> thin film for photoinactivation of bacteria in solar light irradiation. *J. Phys. Chem. C.* **2009**, 113, 20214.
- (21) Zhang, H.; Lv, X.; Li, Y.; Wang, Y.; Li, J. P25-Graphene composite as a high performance photocatalyst. *ACS Nano.* **2010**, 4, 380.
- (22) Y. Liang, H. Wang, H. S.Casalongue, Z. Chen and H. Dai. TiO<sub>2</sub> nanocrystals grown on graphene as advanced photocatalytic hybrid materials. *Nano Res.* **2010**, 3, 701.
- (23) Fan, W.; Lai, Q.; Zhang, Q.; Wang, Y. Nanocomposites of TiO<sub>2</sub> and reduced graphene oxide as efficient photocatalysts for hydrogen evolution. *J. Phys. Chem. C.* **2011**, 115, 10694.
- (24) Zhang, J.; Xiong, Z.; Zhao, X.S. Graphene-metal-oxide composites for the degradation of dyes under visible light irradiation. *J. Mater. Chem.*, **2011**, 21, 3634.
- (25) Li, B.; Cao, H. ZnO@graphene composite with enhanced performance for the removal of dye from water. *J. Mater. Chem.* **2011**, 21, 3346.
- (26) Lui, G.; Liao, J.Y.; Duan, A; Zhang, Z.; Fowler, M.; Yu, A. Graphene-wrapped hierarchical TiO<sub>2</sub> nanoflower composites with enhanced photocatalytic performance. *J. Mater. Chem. A.* **2013**, 1, 12255.
- (27) Xiong, Z.; Zhang, L.; Ma, J.; Zhao, X.S. Photocatalytic degradation of dyes over graphene-gold nanocomposites under visible light irradiation. *Chem. Commun.*, **2010**, 46, 6099.
- (28) Khodja, A.A.; Sehili, T.; Pilichowski, J.F.; Boule, P. Photocatalytic degradation of 2-phenylphenol on TiO<sub>2</sub> and ZnO in aqueous suspensions. *J. Photochem. Photobiol., A.* **2001**, 141, 231.

- (29) Lathasree, S.; Rao, A.N; SivaSankar, B.; Sadasivam, V.; Rengaraj, K. Heterogeneous photocatalytic mineralisation of phenols in aqueous solutions. *J. Mol. Catal. A: Chem.* **2004**, 223, 101.
- (30) Kashif, N.; Ouyang, F. Parameters effect on heterogeneous photocatalysed degradation of phenol in aqueous dispersion of TiO<sub>2</sub>. *J Environ Sci.* **2009**, 21, 527.
- (31) Hassan, F.M.; Chabot, V.; Li, J.; Kim, B.K.; Ricardez-Sandoval, L.; Yu, A. Pyrrolic-structure enriched nitrogen doped graphene for highly efficient next generation supercapacitors. *J. Mater. Chem. A.* **2013**, 1, 2904.
- (32) Hummers, W.S.; Offeman, R. E. Preparation of graphitic oxide. *J. Am. Chem. Soc.* **1958**, 80, 1339.
- (33) Chowdhury, P.; Moreira, J.; Gomaa, H.; Ray, A.K. Visible-Solar-Light-Driven Photocatalytic Degradation of Phenol with Dye-Sensitized TiO<sub>2</sub>: Parametric and Kinetic Study. *Ind. Eng. Chem. Res.* **2012**, 51, 4523.
- (34) Xiang, Q.; Yu, J.; Jaroniec, M. Enhanced photocatalytic H<sub>2</sub>-production activity of graphene-modified titania nanosheets. *Nanoscale.* **2011**, 3, 3670.
- (35) Sun, H.; Liu, S.; Liu, S.; Wang, S. A comparative study of reduced graphene oxide modified TiO<sub>2</sub>, ZnO and Ta<sub>2</sub>O<sub>5</sub> in visible light photocatalytic/photochemical oxidation of methylene blue. *Appl. Catal., B.* **2014**, 146, 162.
- (36) Sakthivel, S.; Neppolian, B.; Shankar, M.V.; Arabindoo, B.; Palanichamy, M.; Murugesan, V. Solar photocatalytic degradation of azo dye: comparison of photocatalytic efficiency of ZnO and TiO<sub>2</sub>. *Sol. Energy Mater. Sol. Cells.* **2003**, 77, 65.
- (37) Lin, H.; Huang, C.P.; Li, W.; Ni, C.; Shah, S.I.; Tseng, Y.H. Size dependency of nanocrystalline TiO<sub>2</sub> on its optical property and photocatalytic reactivity exemplified by 2- chlorophenol. *Appl. Catal., B.* **2006**, 68, 1.
- (38) Akhavan, O. Photocatalytic reduction of graphene oxides hybridized by ZnO nanoparticles in ethanol. *Carbon.* **2011**, 49, 11.

- (39) Ramadoss, A.; Kim, S.J. Facile preparation and electrochemical characterization of graphene/ZnO nanocomposite for supercapacitor applications. *Mater. Chem. Phys.* **2013**, 140, 405.
- (40) Farhangi, N.; Chowdhury, R.R.; Gonzalez, Y.M.; Ray, M.B.; Charpentier, P.A. Visible light active Fe doped TiO<sub>2</sub> nanowires grown on graphene using supercritical CO<sub>2</sub>. *Appl. Catal., B.* **2011**, 110, 25.
- (41) Zheng, Q.; Fang, G.; Cheng, F.; Lei, H.; Wang, W.; Qin, P.; Zhou, H. Hybrid graphene–ZnO nanocomposites as electron acceptor in polymer-based bulk-heterojunction organic photovoltaics. *J. Phys. D: Appl. Phys.* **2012**, 45, 455103.
- (42) Liu, Q.; Liu, Z. F.; Zhang, X.Y.; Yang, L.Y.; Zhang, N.; Pan, G.L.; Yin, S.G.; Chen, Y.S.; Wei, J. Polymer photovoltaic cells based on solution-processable graphene and P3HT. *Adv. Funct. Mater.* **2009**, 19, 894.
- (43) Chen, D.; Ray, A.K. Photodegradation kinetics of 4-nitrophenol in TiO<sub>2</sub> suspension. *Wat. Res.* **1998**, 32, 3223.
- (44) Pardeshi, S.K.; Patil, A.B. A simple route for photocatalytic degradation of phenol in aqueous zinc oxide suspension using solar energy. *Solar Energy.* **2008**, 82, 700.
- (45) Chowdhury, P.; Malekshoar, G.; Ray, M.B.; Zhu, J.; Ray, A.K. Sacrificial hydrogen generation from formaldehyde with Pt/TiO<sub>2</sub> photocatalyst in solar radiation. *Ind. Eng. Chem. Res.* **2013**, 52, 5023.
- (46) Bahnemann, D.; Bockelmann, D.; Goslich, R. Mechanistic studies of water detoxification in illuminated TiO<sub>2</sub> suspensions. *Sol. Energ. Mater.* **1991**, 24, 564.
- (47) Morales-Torres et al. Graphene oxide-P25 photocatalysts for degradation of diphenhydramine pharmaceutical and methyl orange dye. *Appl. Surf. Sci.* **2013**, 275, 361.
- (48) Yuan, Z.; Jia, J.H.; Zhang, L.D. Influence of co-doping of Zn(II) and Fe(III) on the photocatalytic activity of TiO<sub>2</sub> for phenol degradation. *Mater. Chem. Phys.* **2002**, 73, 323.

- (49) Sonawane, R.S.; Dongare, M.K. Sol-gel synthesis of Au/TiO<sub>2</sub> thin films for photocatalytic degradation of phenol in sunlight. *J. Mol. Catal. A: Chem.* **2006**, 243, 68.
- (50) Naeem, K.; Ouyang, F. Preparation of Fe<sup>3+</sup>-doped TiO<sub>2</sub> nanoparticles and its photocatalytic activity. *Physica B: Condensed Matter.* **2009**, 405, 221.
- (51) Chiou, C.H.; Juang, R.S. Photocatalytic degradation of phenol in aqueous solutions by Pr-doped TiO<sub>2</sub> nanoparticles. *J. Hazard. Mater.* **2007**, 149, 1.
- (52) Liqiang, J.; Xiaojun, S.; Baifu, X.; Baiqi, W.; Weimin, C.; Honggang, F. The preparation and characterization of La doped TiO<sub>2</sub> nanoparticles and their photocatalytic activity, *J. Solid State Chem.*, **2004**, 177, 3375.

## Chapter 6

### 6 Conclusions and Recommendations

To date, many semiconductors have been reported as active photocatalysts for photocatalytic applications, including water splitting and water treatment. Despite significant investigations and progress in this field, overall efficiency of photocatalysis is still fairly low, particularly under solar light as the most favorable light source. Two dominant reasons cause this drawback. Firstly, most of the current materials have a quite large band gap leading to less light absorption in the visible region of solar spectrum. Secondly, the fast recombination of photo-generated charges, which is significantly faster than the redox reactions, results in low photocatalytic efficiency. One of the key approaches to overcome the aforementioned challenge is constructing hybrid photocatalysts composed of semiconductor hetero-junctions. The hybrid materials have been recognized to outperform single material in photocatalysis, not only due to their capability to absorb a wider range of solar light, but also by suppressing the charges recombination.<sup>1,2</sup>

The basic goal of this thesis was to investigate the application of solar photocatalysis for hydrogen generation as well as water treatment with the modified semiconductors used as active photocatalysts. The main focus was on development of efficient photocatalysts via simple and practical synthesis methods. Different hetero-structure photocatalysts including metal-semiconductor, semiconductor on 2-D nanomaterial, semiconductor-semiconductor, and noble metal-free co-catalyst-semiconductor were synthesized, characterized and their performance for photocatalytic reactions were evaluated and compared with single and unmodified semiconductors. The enhanced photocatalytic activity of pure semiconductors ( $\text{TiO}_2$  and  $\text{ZnO}$ ) via the specific hetero-structuring was confirmed and the merits of the hetero-structures over single semiconductors were verified. The main benefits of the developed material are ascribed to suppression of charge carriers recombination and extension of solar light absorption range. The significant contributions of this thesis are as follow.



## 6.1 Major Conclusions

Pt/TiO<sub>2</sub> as an example of metal-semiconductor hetero-structure for photocatalytic hydrogen generation was studied. Solar photo-deposition method was applied to load platinum on TiO<sub>2</sub>. The application of solar light instead of UV light has not been fairly studied for photo-deposition in literature. In this study, formaldehyde was used as sacrificial agent for solar photocatalytic hydrogen generation using Pt/TiO<sub>2</sub>, for the first time. Formaldehyde acts as electron donor, thereby suppress the  $e^-/h^+$  recombination reaction.

Photocatalytic activity increased significantly with the incorporation of platinum metal on TiO<sub>2</sub> catalyst via solar photo-deposition method. This improvement is due to a Schottky barrier formed at the metal/semiconductor interface, resulting in less electron/hole recombination rate. Furthermore, detailed parametric study was performed for photocatalytic hydrogen generation using Pt/TiO<sub>2</sub> and formaldehyde. It was found that the process was affected by solution pH, platinum content (wt%) on TiO<sub>2</sub>, catalyst concentration, light intensity, and initial formaldehyde concentration and the optimum conditions were obtained as follow: : a)  $I_{\text{solar}}$  - 100 mW/cm<sup>2</sup>, b) platinum content – 0.25 wt %, c) catalyst concentration – 1 g/l, and d) pH- neutral to alkaline. Hydrogen was generated with high apparent quantum yield (10.91%) at the optimum point.

Molybdenum sulfide was grown on TiO<sub>2</sub> and its performance as a noble metal-free co-catalyst-semiconductor hetero-structure was studied for photocatalytic hydrogen generation. For the first time, in-situ solar photo-deposition method in a dye-sensitized photocatalytic system was applied to grow molybdenum sulfide on TiO<sub>2</sub>. The synthesis process was performed at ambient conditions without using toxic precursors, which is beneficial for large-scale processes as opposed to the most of the current methods that require harsh conditions.

High efficiency for photocatalytic hydrogen generation was demonstrated during this process. In addition, Systematic statistical analysis, including full factorial design and central composite design was performed in order to investigate the effect of different reaction parameters as well as their interaction effects and to maximize the hydrogen

generation after 3h solar light irradiation. A two steps mechanism was also proposed for this noble metal-free photocatalytic process.

Moreover, from the obtained results in chapter 5, it can be concluded that there is a great potential for graphene-based composites as well as coupling of the composites for higher photocatalytic activity. Graphene-based  $\text{TiO}_2$  (and  $\text{ZnO}$ ) were synthesized and their performances for photocatalytic water treatment were investigated.  $\text{TiO}_2$ -G and  $\text{ZnO}$ -G composites were prepared by simple hydrothermal method. Optical and structural properties of the composites were obtained using XRD, XPS, Raman spectroscopy, UV-Vis Spectroscopy, TEM, and SEM.

The two composites (graphene-semiconductor) showed improved performance in solar photocatalytic degradation of phenol compared to single semiconductor. This enhancement is ascribed to the incorporation of graphene, which facilitates electron-hole separation, and extension of light absorption wave-length range. In addition, the coupled composites ( $\text{ZnO}$ -G/ $\text{TiO}_2$ -G) outperformed the single composite by a factor of two. The parametric study was carried out to optimize the reaction conditions. Experimental results showed that one hour of  $100 \text{ mW/cm}^2$  solar irradiation was required to degrade 40 ppm phenol at neutral pH, when 1.25 g/L of coupled  $\text{ZnO}$ -G/ $\text{TiO}_2$ -G composites were used.

## 6.2 Recommendations

- ✓ Further study and optimization of solar photo-deposition method for loading Pt on  $\text{TiO}_2$  to improve the photocatalyst.
- ✓ Incorporate other metals such as Pd, Cu, Au and Ni on  $\text{TiO}_2$  by solar photo-deposition process and explore their performance for different photocatalytic applications.
- ✓ Determine the performance of  $\text{TiO}_2$ -G,  $\text{ZnO}$ -G for hydrogen generation, and metal reduction to expand their application.
- ✓ Further optimization of the synthesis condition of  $\text{TiO}_2$ -G and  $\text{ZnO}$ -G.
- ✓ Grow molybdenum sulfide on other semiconductors by in-situ photo-deposition method and evaluate their photocatalytic activity.

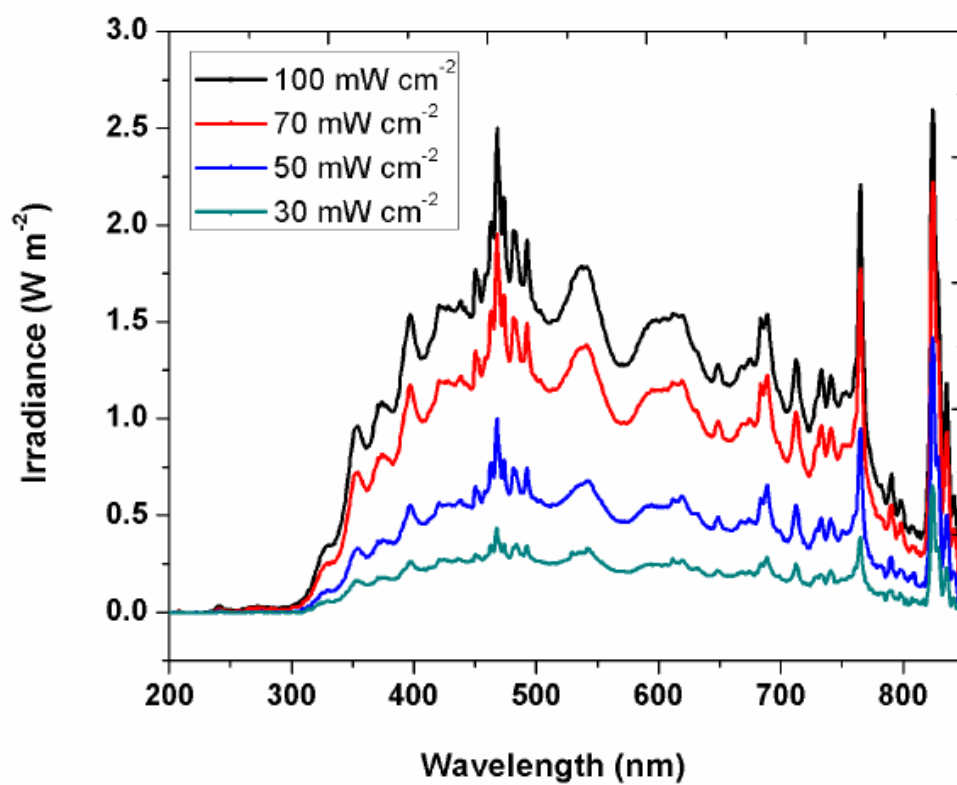
- ✓ Apply in-situ photo-deposition to modify semiconductors with the hybrid of molybdenum sulfide and graphene.

## 6.3 References

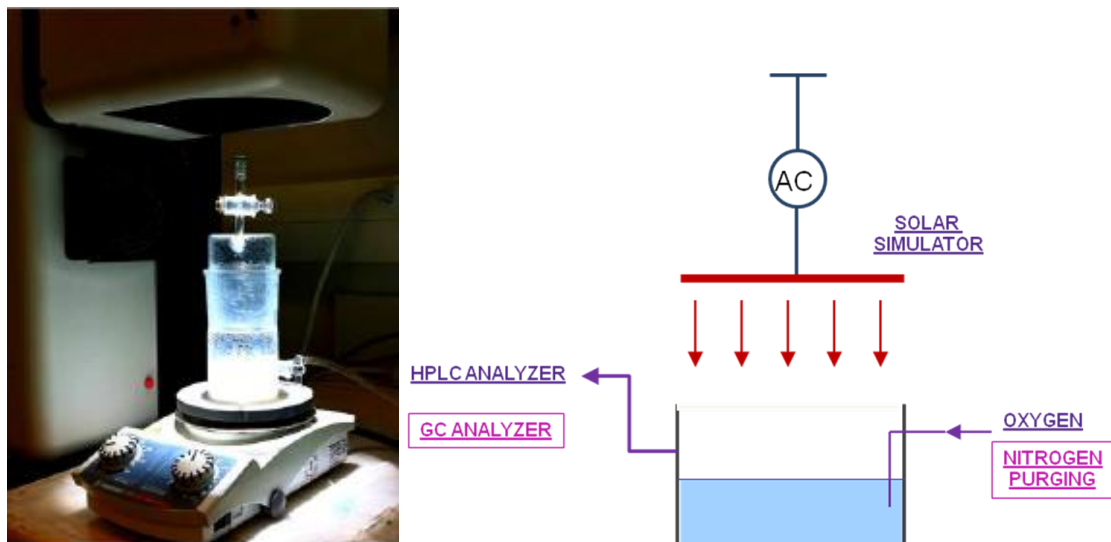
- (1) Yuan, Y.; Ruan, L.; Barber, J.; Chye, S.; Loo, J.; Xue, C. Hetero-Nanostructured Suspended Photocatalysts for Solar-to-Fuel Conversion. *Energy Environ. Sci.* **2014**, 7, 3934.
- (2) Liu, G.; Wang, L.; Yang, H. G.; Cheng, H.-M.; (Max) Lu, G. Q. Titania-Based Photocatalysts—crystal Growth, Doping and Heterostructuring. *J. Mater. Chem.* **2010**, 20 (5), 831.

## Appendices

### Appendix A: Light Spectra of Solar Simulator



## Appendix B: Photoreactor specifications



- ✓ Reactor's total volume= 530 ml
- ✓ Reaction mixture volume= 100 ml
- ✓ Illumination by solar simulator from the top through 6.5 cm diameter(5.5 cm in chapter 4)
- ✓ Under vigorous mixing
- ✓ System is purged by nitrogen gas (Chapters 3-4)
- ✓ System is saturated with oxygen (Chapter 5)

## Curriculum Vitae

<b>Name:</b>	Ghodsieh Malekshoar
<b>Post-secondary Education and Degrees:</b>	<p>Sharif University of Technology Tehran, Iran 2001-2005 B.Sc.</p> <p>Sharif University of Technology Tehran, Iran 2005- 2007 M.Sc.</p> <p>The University of Western Ontario London, Ontario, Canada 2011-2015 Ph.D.</p>
<b>Honours and Awards:</b>	<p>Province of Ontario Graduate Scholarship The University of Western Ontario 2014-2015</p> <p>1<sup>st</sup> Place Award at CBE Research Bridge Sarnia, Ontario, Canada June 2014</p> <p>Excellence in Teaching Award Chemical &amp; Biochemical Engineering The University of Western Ontario 2014</p> <p>Julie Lassonde Scholarship Faculty of Engineering, the University of Western Ontario 2013</p> <p>Nominated for the Graduate Teaching Assistant Award GTA, the University of Western Ontario 2013</p>
<b>Related Work Experience</b>	<p>Lecturer (Heat Transfer, full course) Chemical &amp; Biochemical engineering, The University of Western Ontario Sep-Dec 2014</p> <p>Teaching Assistant</p>

Chemical & Biochemical engineering,  
The University of Western Ontario  
2011-2015

Research Assistant  
Chemical & Biochemical engineering,  
The University of Western Ontario  
2011-2015

Process Engineer  
Pars Oil and Gas Company  
Tehran, Iran  
2007-2010

## **Publications**

- G. Malekshoar, K. Pal, Q. He, A. Yu, and A. K. Ray, “Enhanced solar photocatalytic degradation of phenol with coupled graphene-based titanium dioxide and zinc oxide,” *Ind. Eng. Chem. Res.*, 2014, 53 (49), pp 18824–18832.
- P. Chowdhury, G. Malekshoar, M. Ray, J. Zhu, and A. K. Ray, “Sacrificial hydrogen generation from formaldehyde with Pt/TiO<sub>2</sub> photocatalyst in solar radiation,” *Ind. Eng. Chem. Res.*, 2013, 52(14), pp 5023-5029
- G. Malekshoar and A.K. Ray, “In-situ grown molybdenum sulfide on TiO<sub>2</sub> for solar photocatalytic hydrogen generation,” Submitted to *Chemical Engineering Science*.
- G. Kumordzi, G. Malekshoar, E. K. Yanful, A. K. Ray, “Solar photocatalytic degradation of Zn<sup>2+</sup> using graphene-based TiO<sub>2</sub>,” Submitted to *Separation and Purification Technology*.
- V. Bhatia, G. Malekshoar, A. K. Ray, “Enhanced photocatalytic degradation of Atenolol using Graphene TiO<sub>2</sub> Composite ,” Submitted to *Journal of Photochemistry and Photobiology A: Chemistry*.

## **Conferences:**

- G. Malekshoar and A.K. Ray, “Solar Photocatalytic Hydrogen Generation over EY-sensitized TiO<sub>2</sub> using in-situ grown Molybdenum sulfide as a c-catalyst,” 65<sup>th</sup> Canadian Conference of Chemical Engineering(CSChE), Calgary, AB, October 2015(Oral)

- G. Malekshoar and A.K. Ray, “Solar photocatalytic application of graphene-based Nanocomposites,” Research Bridges Symposium, Research Park, Sarnia, ON , 2014 (Oral)
- G. Malekshoar and A.K. Ray, “TiO<sub>2</sub>-Graphene nanocomposite as an advanced photocatalyst: synthesize and application”, AIChE Annual Meeting, San Francisco, USA, November 2013(Oral)
- G. Malekshoar, P. Chowdhury, and A.K. Ray, “Solar hydrogen generation by using Pt/TiO<sub>2</sub> and formaldehyde,” 61<sup>st</sup> Canadian Conference of Chemical Engineering(CSChE), London, ON, October 2011(Oral)
- P. Chowdhury, G. Malekshoar, N. Hashim, and A.K. Ray, “Efficient use of solar energy for generation green hydrogen fuel and purifying water by band-engineered photocatalysis, “ Research Showcase, UWO, March 2011(Poster)